# PLA-PCL textile reinforced composites for connective tissues applications

by

Carolina Pereira Lobato Costa

A dissertation submitted in partial fulfillment of the requirements for the degree of Doctor of Philosophy in

Materials Science and Engineering

Universidad Carlos III de Madrid

Advisor(s):

Javier Llorca

Carlos González

Tutor:

Mónica Campos Gómez

January 2024

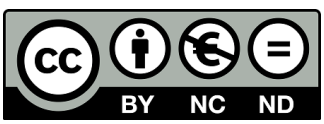

“Nothing that´s worthwhile is ever easy”- Indira Gandhi

# Acknowledgements

I thank the principal supervisors at IMDEA Materials Institute, Javier Llorca and Carlos Gonzalez, for their support, guidance and mentorship throughout the project. Thanks for your time, patience, and commitment to my academic and professional growth.

I also want to thank Khoa Do, who guided me at ITA GmBH. To Agnese and Flavia, my working colleagues who became my friends, thanks for listening, guiding me once I arrived, and "fighting alongside me". Being a microelectronics and nanotechnology engineer and able to deal with mechanical materials, polymers, and cells was impossible without Dr. Monica Echeverry, Dr. Cristina Pascual (my double), Dr Mario Rueda, Dr. JuanPe. They taught me so much that I will be forever grateful. I also acknowledge the help of Guillermo, Dr. Bruno Ribeiro, and Dr. Mafalda in biological tests. Bruno and Malfalda, "meus conterrâneos" with different accents, became good friends, very supportive, and I am happy to have met them.

I also would not have been able to accomplish even half of the work without the technicians: Jimena, who was so patient with me and the GPC; Vanesa and Jose Luis for helping me find a solution for all my problems; and even though I would always come to them with a suspicious face :/. Also, to Monica and Miguel, who were always ready to help me. To Amalia, to Manu for being so patient and always improving the quality of my SEM images, to Javi, for the many hours in the XRD and tomograph, for the good humour and the KitKat chocolate, I will never forget it. To my working colleagues Wahaaj, Cillian and Yuyao. Yuyao was always ready to help and the sweetest even when things are not so good with her; together, we are stronger!!!!!! Cillian, he became a good friend, puff; I don't even know where to start; I do not think it would be possible to conclude this PhD without him. Thanks, thanks, thanks, we know all the struggles, all the happy moments, all the fun.... People from the composites group..... Moises, my table mate, thanks for making

me laugh, lending me the charger almost every day, helping me, encouraging me and always trying to be fair with the hot press time slots :) Andrea, for always being positive and teaching me how to deal with Favimat. To Davide, for always being ready to help even after complaining and for showing me Napoli and the best pizza in the world ( at least according to him). To Sofia, I have no words for my strong connection with her since the beginning; some people shine in this world! And to Dr Keayvan Keramati, I also do not know from where to start: from work to personal life... We shared many things and have been through so many things... good, bad, sad, crazy... you marked my life!

I also want to mention other people who were not from my group, but in some way or another, our paths crossed. Josesito Hobson, el amiguito que todos deseamos, thanks a lot for helping me, listening to me, laughing with me, and taking care of me ... Saumya, the girl who became a sister from a different mom, even though she said I was the cutest Spanish girl. The person who understands me even without me speaking, the girl who reads my thoughts. You will come with me for my entire life. Venkatesh, thanks to Saumya, I got to know him more; I am happy that at the end of my journey, I annoyed him and disturbed him from his work with my stupidity and craziness, even though in the beginning, I would think he was very serious. To Maria, the best morning hugs, even though she is an amphibian and a very cute cactus (she picked me some times with her spontaneity), to Rafa, Cristian, Elena, and Miguel for sharing with me lunchtime and always being there to make me laugh.

Also, to the people on the 4th floor, the administrative staff of IMDEA materials, Mariana, for always with a smile and ready to help, to Ainhoa for doing so much in the beginning when I started the PhD, and COVID came into our lives. To Vanessa, she would always clarify my doubts about the project processes, even if I would ask more than once.

Also, thank you to long-standing friends and those I got to know in this beautiful way. To Ana Luisa, to Catarina, to Sara, to Cassia, to Prafull and many more. Thanks for always being there.

I will take you all in my heart.... and my heart is overwhelmed with so much love and companionship. This journey has been incredible because of all of you; I am not the same Carolina of 2020 but a better Carolina in all aspects because of All OF YOU. Some way or another, you taught me so much and made me grow.

I have also to mention my family... My parents ( Eduarda e Paulo, eles vivem

para mim), my sister Carlota, and my grandparents are not here anymore, but they have always influenced my behaviour and my thinking. And all my aunts, uncles, and cousins. We are unique, and I am lucky to have grown up in a family like this. Open, receptive, comprehensive and efussive!

Lastly, I want to acknowledge financial support from the European Union's Horizon 2020 research and innovation programme under the European Training Network BioImpant (Development of improved bioresorbable materials for orthopaedic and vascular implant applications), Marie Skłodowska-Curie grant agreement No 813869.

*Carolina Pereira Lobato Costa*
*Madrid,*

# Published and submitted content

- Journal articles
  - Pereira-Lobato C, Echeverry-Rendón M, Fernández-Blázquez JP, González C, LLorca J. Mechanical properties, in vitro degradation and cytocompatibility of woven textiles manufactured from PLA/PCL commingled yarns. Journal of Mechanical Behavior of Biomedical Materials. 2024;150:106340. $doi$ : 10.1016/$j.jmbbm$.2023.106340 ( The experimental part of this publication is included in chapter 2 and 3 and the results and discussion on the chapter 4 of the thesis )
- Conference presentations
  - $7^{th}$ Seminario de Jóvenes Investigadores en Polímeros, October 2023, Mechanical properties, in vitro degradation and cytocompatibility of woven textiles manufactured from PLA/PCL commingled yarns, Madrid, Spain (Oral presentation)
  - $32^{th}$ Annual Conference of the European Society for Biomaterials, September 2022, Woven PLA-PLA and PLA-PCL composites for biomedical applications, Bordeaux, France (Poster presentation)
  - Bioengineering in Ireland[27], May 2022, Mechanical and strutural analysis of woven PLA-PLA and PLA-PCL composites for biomedical applications, Galway, Ireland (Oral Presentation)

# Contents

# List of Figures

# List of Tables

# Abstract

Tissue engineering presents a promising frontier in addressing injuries and degenerative conditions within the human body. This doctoral thesis focuses on developing biodegradable textile polymer composite materials, specifically woven from commingling yarns, to gain insights into their long-term performance for connective tissue engineering applications. This interdisciplinary project aims to advance the creation of robust materials for connective tissues, utilizing hybrid PLA/PCL and PLA/PLA commingled yarns to manufacture woven materials and composites. The unique combination of different grades of PLA and PCL characteristics in hybrid yarns enables the production of fabrics and composites with high strength and ductility.

The mechanical, thermal, and biological performance of these materials is analyzed in the thesis, exploring the advantages of commingled hybrid yarns. Different degradation rates of PLA and PCL allow for tailoring this property. Materials undergo degradation in phosphate-buffered saline solution for up to 160 days at 37°C and accelerated degradation at 50°C.

Observations reveal different degradation patterns of the materials. The PLA-PCL woven textile shows minimal changes in thermal and mechanical properties after 80 days at 37°C, with slight degradation observed after 160 days, which is attributed to chain scission in PLA fibres. This trend is also observed in the PLA-PCL composite materials. Conversely, PLA-PLA weaves experience a notable decrease in elastic modulus after 40 days. Upon immersion at 50°C, the PLA-PCL weave undergoes a rapid strength reduction after 40 days, primarily due to PLA hydrolysis, and significant degradation after 160 days, attributed to PCL chain scission. The PLA-PLA composite experiences the fastest deterioration, rendering it impossible to test samples after 40 days of degradation.

The study concludes that all materials exhibit potential for connective tissue implants, assuming a six-month average regeneration time. Despite indirect tests did not ensured optimal biocompatibility, direct tests indicated a good cell/material

interaction, with the PLA-PLA composite showcasing superior performance. These findings underscore the potential of hybrid commingled yarns in manufacturing textile scaffolds and composites with tailored mechanical properties and good ductility for connective tissue engineering applications.

# Abbreviations

| | |
|---|---|
| **ACL** | **A**nterior **C**ruciate **L**igament |
| **BJL** | **B**one to **J**oint **L**igament |
| **$\beta$-TCP** | $\beta$- **t**ricalcium **p**hosphate |
| **CA** | **C**ontact **A**ngle |
| **CaP** | **C**alcium **P**hosphate |
| **CT** | **C**onnective **T**issue |
| **DAPI** | **4**,6-diamidino-2-phenylindole |
| **dECM** | **d**ecellularized **E**xtracellular **M**atrix |
| **DIC** | **D**igital **I**mage **C**orrelation |
| **DMSO** | **D**imethyl **S**ulfoxide |
| **DSC** | **D**ifferencial **S**canning **C**alorimeter |
| **ECM** | **E**xtracellular **M**atrix |
| **ES** | **E**lectro**s**pun |
| **FBS** | **F**etal **B**ovine **S**erum |
| **FDA** | **F**ood and **D**rug **A**dministration |
| **FFF** | **F**used **F**ilament **F**abrication |
| **GPC** | **G**el **P**ermiation **C**hromatography |
| **HA** | **H**ydroxy**a**patite |
| **HNT** | **H**olloysite **n**ano**T**ubes |
| **LARS** | **L**igament **A**ugmentation **R**econstruction **S**ystem |
| **LDH** | **L**actate **d**ehydrogenase |

| | |
|---|---|
| **MEM** | **M**inimum **E**ssential **M**edium |
| **MTT** | **3**-(4,5-dimethylthiazol-2-yl)-2,5-diphenyl **T**etrazolium **B**romide |
| **PBS** | **P**hosphate- **B**uffered **S**aline |
| **PCL** | **P**osterior **C**ruciate **L**igament |
| **PDLLA** | **P**oly- **d**- l- **L**actic **A**cid |
| **PE** | **P**olyethylene |
| **PET** | **P**olyethylene **T**erephthalate |
| **PLLA** | **P**oly- l- **L**actic **A**cid |
| **PMMA** | **P**oly(**M**ethyl **M**ethacrylate) |
| **PSN@EG** | **N**anostructured SN coated on PK fibers with EGCG |
| **PUUR** | **P**olycaprolactone **b**ased Polyurethane **U**rea |
| **RC** | **R**einforced **C**omposite |
| **SEM** | **S**canning **E**lectron **M**icroscopy |
| **SN** | **S**ilicon **N**itride |
| **SRC** | **S**elf- **R**einforced **C**omposite |
| **SS** | **S**tainless **S**teel |
| **TE** | **T**issue **E**ngeneering |
| **THF** | **T**etrahydrofuran |
| **T/L** | **T**endon **L**igaments |
| **TSC** | **T**issue **S**tem/progenitor **C**ells |
| **UHMWPE** | **U**ltra-high **M**olecular **W**eigth **P**olyethylene |

# Introduction and objectives 1

## 1.1 Tissue engineering for connective tissue

Tissue engineering (TE) is a highly interdisciplinary field that draws upon various scientific and engineering disciplines, including biology, physiology, mechanical engineering, and material science (1). The primary objective of TE is to develop functional biological tissues capable of maintaining, healing, and enhancing the functions of damaged tissues. This is achieved through the strategic use of cells, scaffolds, and biologically active chemicals. These three fundamental components, often called the ”triad”, encompass various aspects, including scaffold production, cell sourcing and signaling within tissue-engineered structures. As illustrated in Figure 1.1, these scaffolds can be manufactured with biomaterials like natural or synthetic materials, hydrogels, and meshes. These scaffolds can integrate autologous, heterologous, differentiated, or stem cells, and for the cells to differentiate or proliferate, growth factors, other molecules known for promoting differentiation, or even the mechanical forces that tissues provide should also be consider. Integrating all these elements is crucial for the successful practice of tissue engineering (2; 3). Moreover, the donor waiting list, which continues to grow faster than the number of organ donors, highlights the critical need for TE and regenerative medicine (3).

Connective tissues (CTs) represent one of the four primary types of animal tissue, and they play essential roles in the human body (4). These tissues provide structural support, connect various body components, and offer exceptional mechanical strength to withstand continuous mechanical stresses. CTs encompass a variety of structures such as ligaments, tendons, cartilage, meniscus, fascia, intervertebral discs, bones, the dermal layer of skin, adipose tissue, the iris, and more (4; 5; 6). They comprise tissue-specific cells, with examples including osteoblasts and osteoclasts in bones, fibroblasts

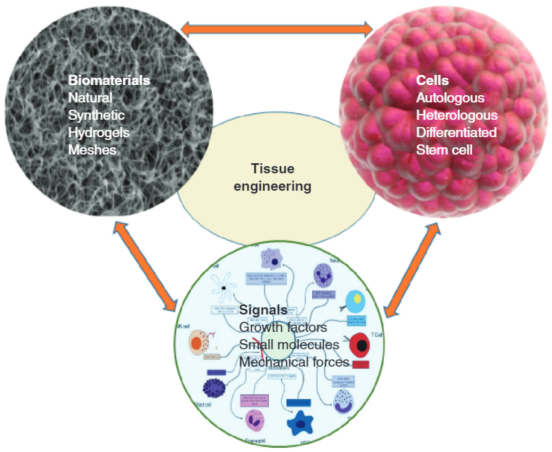


Figure 1.1: Tissue engineering main components to construct functional tissues: a combination of cells, scaffolds, and signals are employed (3).

in ligaments and tendons, and chondrocytes in cartilage. Their extracellular matrix (ECM) comprises a mixture of collagen and elastin fibrils, proteoglycans, and various glycoproteins, arranged in unique combinations and ratios (4; 6).

### 1.1.1 Tendon, Ligaments (T/L) and bone properties

Ligaments and tendons are collagenous connective tissues that connect bones to other bones and muscles, respectively (7; 8; 9). Tendons primarily consist of proteoglycans and collagen, with collagen type I molecules aligning in parallel, forming fibrils, fibres, and bundles (10). In contrast, ligaments have higher protein and lower collagen content, making them often more metabolically active than tendons. The structural hierarchy of tendons closely resembles that of ligaments, as depicted in Figure 1.2. However, collagen fibres are organized into discrete packages in tendons, which are further bundled together within fascicles. In the case of bones, the collagen in the extracellular matrix (ECM) becomes mineralized, resulting in stiff and rigid bone structures (6; 11).

Additionally, the rope-like structure and composition of the tendons and ligaments are responsible for their unique mechanical properties. The stress-strain curves in tension are sketched in Figure 1.3 a) and b) for tendons and ligaments, respectively. The first region of the curves is called the toe region, where the tendon is strained up to 2%. This area reflects the crimp pattern of the component fibres expanding out. The second section is the linear region, where the tendon is stretched less than 4%. All fibres have been recruited and are straightened at this location. The

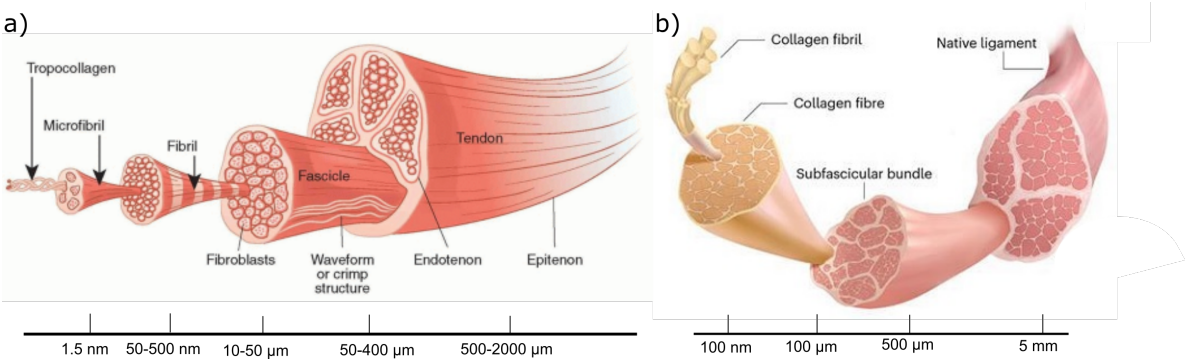


Figure 1.2: Representative illustrations of: a) tendon and b) ligament. These tissues have a hierarchical structure, with collagen molecules organized into progressively bigger bundles until the tendon/ligament is reached, adapted from (12; 13).

plastic/damage region starts when the load exceeds the linear zone and the curve's slope changes. Stretching over 4% can cause tiny tears inside the tissue, resulting in tendinopathy. Ligaments, conversely, must enable varied ranges of motion in different joints, resulting in broader strain ranges for the toe area depending on the anatomical position (anterior cruciate ligament-ACL: 4%; spine ligaments: 10-40%). They will have an ideal elastic recovery in the linear region, where the fibres of collagen are straightened, if the load is removed. Following the linear region, the fibres begin to slide with respect to one another. The linear region is followed by gradual fibre loss until the tendon or ligament fails (14; 15). Finally, the stress-strain curves of cortical/compact bone and cancellous/spongy bone are plotted in Figure 1.3 c). Cortical bone is stiffer and can withstand more considerable stresses than cancellous bone. On the other hand, critical bone fails at lower strains, while cancellous fails at much higher strains.

Table 1.1 summarizes the key mechanical properties of various connective tissues, including tendons, ligaments, and bones. These properties play a crucial role in understanding the structural integrity and functions of these tissues within the human body. Tendons are known for their remarkable tensile strength. They exhibit an elongation to fracture of approximately 8%, an elastic modulus in the range 300 to 1200 MPa, and an ultimate tensile stress of 100 MPa. Additionally, tendons display viscoelastic behavior, making them capable of withstanding dynamic loads. Ligaments, responsible for stabilizing joints, exhibit different mechanical characteristics. They have a higher elongation to fracture of 22-41%, with a wide range of elastic modulus from 5 to 441 MPa. Ligaments can withstand ultimate tensile stresses of 16-95 MPa and exhibit viscoelastic properties similar to tendons.

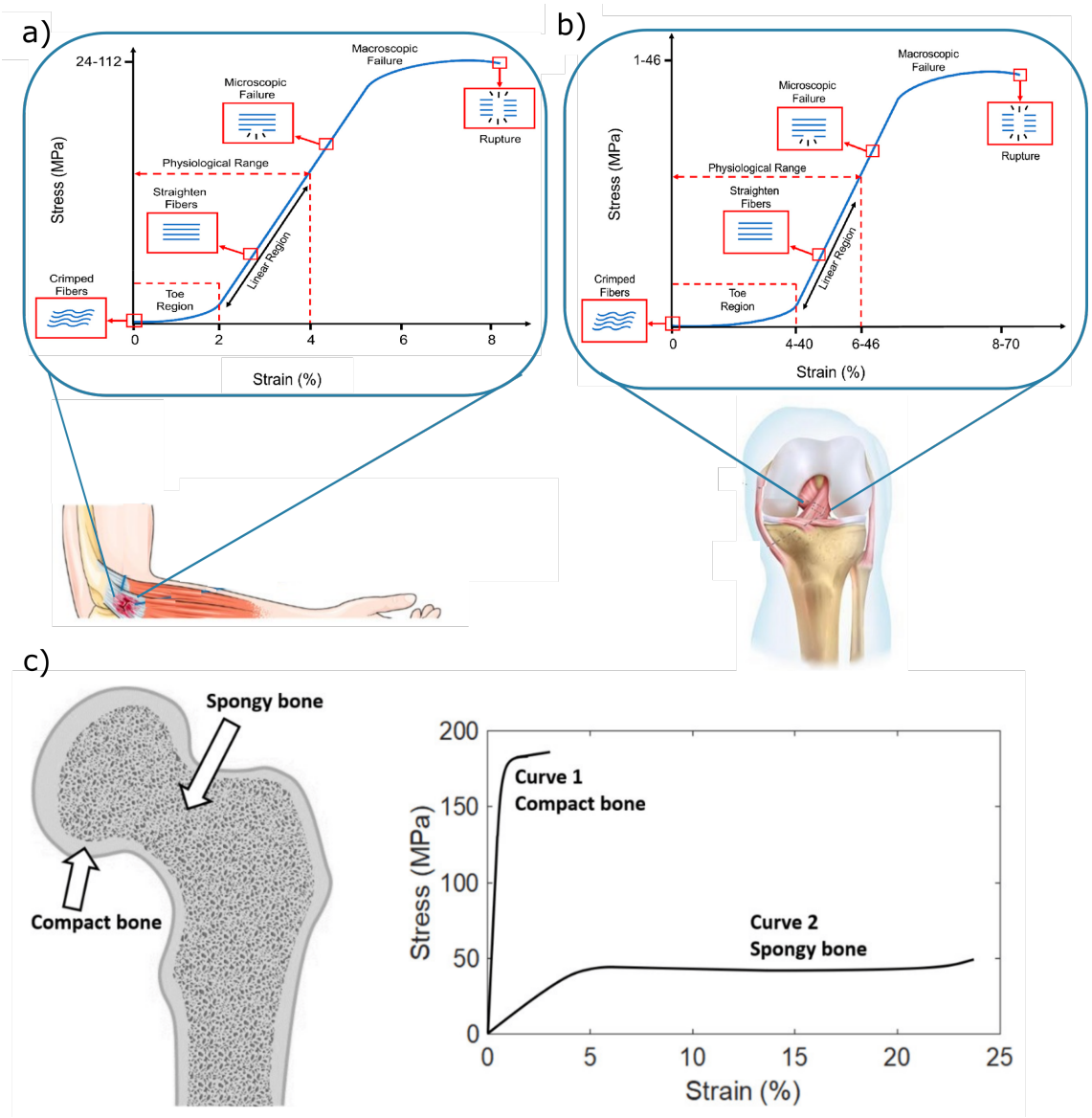


Figure 1.3: Representative a) tendon and b) ligament c) bone stress-strain curves, adapted from (16; 14; 17).

Additionally, they possess an anisotropic structure, where the orientation of the fibers within the tissue depends on the tension to which the tendon or ligament is subjected (18).

Bones exhibit a highly complex hierarchical structure, characterized by their resemblance to fiber-reinforced composite materials, and their strongly anisotropic properties further distinguish them (19). This intricate composition leads to various mechanical properties within different bone structures. For example, cortical bone, which comprises the outer layer, possesses a high elastic modulus, typically

in the range of 15 to 20 GPa. In contrast, cancellous bone in the interior features a considerably lower elastic modulus, usually between 0.2 and 0.5 GPa. The compressive strength of cortical bone is also notable, ranging from 100 to 200 MPa, while cancellous bone displays a lower compressive strength, typically between 2 and 12 MPa. Moreover, bone porosity varies, with cortical bone having 5-10% porosity and cancellous bone exhibiting significantly higher porosity levels, in the range 50-90%. Understanding these mechanical properties is essential for designing implants/scaffolds and interventions related to connective tissue injuries and bone fractures (10).

Table 1.1: Mechanical properties of some connective tissues (10).

| **Tissue** | **Properties** |
|---|---|
| Tendon | Rupture elongation (8%), elastic modulus (300-1200 Mpa), ultimate tensile stress (100 MPa) Viscoelastic behaviour. |
| Ligament | Rupture elongation (22-41%), elastic modulus (5-441 MPa), ultimate tensile stress (16-95 MPa) Viscoelastic behaviour. |
| Bone | Elastic modulus ( cortical:15-20 GPa, cancellous:0.2-0.5 GPA), compressive strength (cortical:100-200 MPa, cancellous: 2-12 MPa), porosity (cortical bone 5-10 %, cancellous: 50-90%). |

The healing process of a fractured tissue involves three phases: inflammation, proliferation, and remodeling, each with distinct cell and molecular pathways. Inflammation initiates hematoma formation and recruits cells like neutrophils, macrophages, and tissue stem/progenitor cells (TSCs). The proliferation phase includes growth factor release, forming granulation tissue, and fibroblasts producing collagen. The remodeling phase, spanning years, features the alignment of tenocytes and collagen fibers, with ongoing contributions from macrophages in tissue development and homeostasis. The duration varies based on the tendon/ligament lesion degree, lasting up to 2 years (15). In the case of bone healing, the first two phases are similar, but instead of T/L cells, bone cells are involved. The last phase, bone regeneration, which also varies according to the location and severity of the rupture, can take three to four months or more (20).

According to TE principles, a tissue-engineered device is expected to promote tissue regeneration and, at the same time, degrade, ideally at the same rate (21). Another important aspect is that to allow cells to enter and begin remolding the tissues, pores must be at least the size of the cells. Osteoblasts have a size of 10-50 $\mu$m, although they prefer bigger pores (100-200 $\mu$m) for repairing mineralized bone following implantation. T/L scaffolds require diameters ranging from approximately

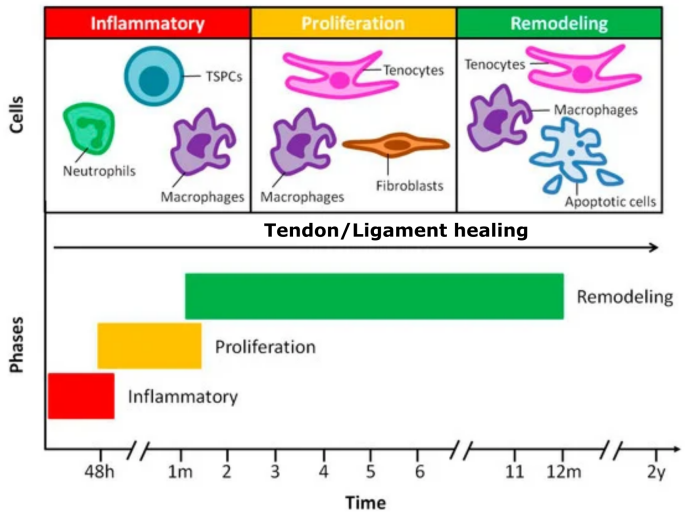


Figure 1.4: Overview of the T/L repair process in humans (15).

250 to 500 $\mu$m to enable cell ingrowth and the flow of nutrients and waste products. This porous structure should also be interconnected (22; 23).

### 1.1.2 Connective tissues disorders: Prevalence and incidences

Genetic factors, aging, and trauma contribute to connective tissue failure, which causes pain, disability, and expensive medical costs, emphasizing the need for repair and regeneration treatments (4; 5; 24).

Tendon and ligament injuries, for example, are among the most prevalent forms of injuries in the body, particularly among young and physically active populations. The Achilles tendon, rotator cuff, and anterior cruciate ligament (ACL) are the most often injured tendon-bone junctions. Around 100,000 ACL reconstruction procedures, 75,000 rotator cuff repairs, and 230,000 Achilles tendon repairs are performed annually in the United States. Furthermore, tendon tears are difficult to repair. They are linked with postoperative problems such as re-rupture, elongation, muscle atrophy, reduced function, and poor reconstitution of the tendon-bone interface, as well as individual morbidity (25; 26). There is no suitable technique for obtaining a successful tendon repair, and standard surgical repairs, in which the allograft/autograft of a tendon is linked to the bone using non-degradable sutures and anchors, have been documented to fail in 20-90 % of instances (27). Radiography and animation, respectively, of ACL implant are displayed in Figures 1.5, a) and b) where it can be seen the metal devices anchoring the graft and part of a ligament from the patient itself or from another person that was sutured.

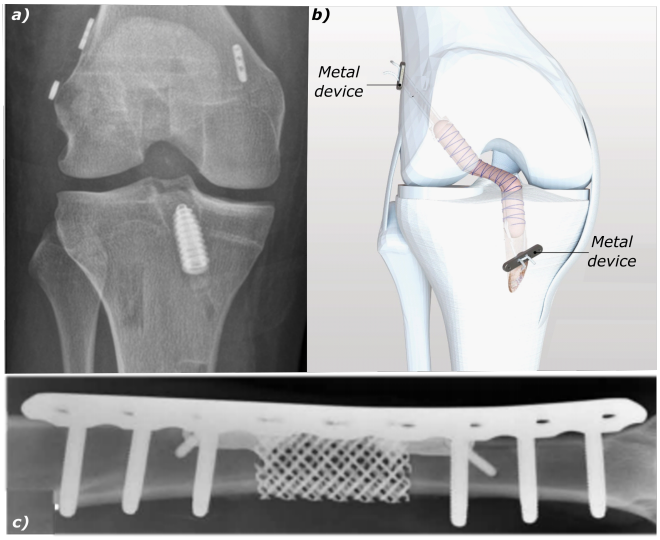


Figure 1.5: a) Radiographs obtained in a patient who underwent revision anterior cruciate ligament reconstruction (28), b) scheme/animation of the ACL reconstruction device, c) Radiography of bone with a bone plate and scaffold, adapted from (29).

Also, the regeneration and repair of bone tissue has become an urgent need (20). As in the tendon and ligament case, metal implants are the most effective way to treat bone defects for bone grafts. Figure 1.5 c) displays a metallic bone place with screws and a metallic scaffold. Most implant devices are made of metals and alloys like pure Ti (cp-Ti), 316L stainless steel (SS), and Co–Cr–Mo alloys. Ti–6Al–4V is the preferred implant material due to its high strength and corrosion resistance. In addition, annealed austenitic stainless steel, due to its exceptional ductility (40 % - 50 % elongation to failure), is convenient to reshape steel implants during surgery so that they conform to the surface contours of the bones, because each patient's anatomy and bone structure are unique. This property is essential for complex cases. Additionally, it enables minimal invasive procedures, providing the surgeon with greater control and precision (30).

This latter fact encourages the development of novel biomaterials to restore tissue function and give instructional cues for better healing. Many solutions have evolved, but no material that perfectly replicates the human tendon/ligament or bone has been developed (4).

### 1.1.3 Current solutions for repair/substitution of T/L tissues

Despite substantial advances in tendons and ligaments, there is no gold standard, and currently available treatments include autografts, allografts, and prosthetic grafts(26).

Available commercial tendon and ligament grafts are shown in Table 1.2, which can be divided into biological and synthetic depending on the origin. The biological grafts include products like GraftJacket™, Restore™, and TissueMend™, derived from human or animal tissues. They are used for various tendon and ligament repair applications. The synthetic grafts encompass products such as LARS ligament and Poly-Tape, made from synthetic materials like PET and PLLA and used primarily for ACL and tendon repair.

Table 1.2: Available commercial tendon and ligament grafts.

| Tissue graft | Name | Origin/material | Repair Target | Ref. |
|---|---|---|---|---|
| Biological | GraftJacket™ | Human dermal matrix | Rotator cuff,Achilles/patellar/quadriceps tendon | (31) |
| | Restore ™ | Porcine small intestine | | (31) |
| | TissueMend ® | Mucosa | Rotator cuff,Achilles/patellar/quadriceps tendon | (31) |
| | CuffPatch™ | Bovine dermal matrix | | (31) |
| | Permacol™ | Porcine small intestine mucosa | Rotator cuff | (31) |
| | CelGro ™ | Porcine/bovine tissue | Rotator cuff and its BTJ | (32) |
| | BEAR® ™ | Bovine tissue | ACL and its BTJ | (33) |
| Synthetic | LARS ligament | PET | ACL | (34) |
| | Poly-Tape | PET | ACL, patellar/quadriceps tendon | (35) |
| | X-Repair | PLLA | Rotator cuff,achilles/patellar/quadriceps tendon | (36) |
| | FLEXBAND™ | PUUR | ACL, Rotator cuff,biceps tendon | (37) |
| | Pitch-patch | PET | Rotator cuff | (38) |

Finding the best suitable combination recipes still remains challenging to mimic the anisotropic structure of tendon and ligament tissue and promote cell adhesion and differentiation of tenocytes or ligamentocytes while having the appropriate mechanical properties (39). Furthermore, current approaches have limitations and disadvantages. For example, while often effective, autografts can present complications at the donor site, have limited tissue availability, and may not always integrate well with host tissues, potentially leading to graft impingement or tension. Allografts and xenografts, mentioned in Table 1.2 as biological grafts sourced from other humans or animals, require immunosuppression, pose risks of poor tissue integration, and carry concerns of disease transmission, including zoonotic diseases in the case of xenografts. On the other hand, synthetic grafts can be prone to early rupture, experience a loss of mechanical strength over time, may not support adequate tissue ingrowth, and can produce graft debris upon degradation. These limitations emphasize the importance of carefully selecting the most suitable graft type for each patient's unique needs, considering each option's potential complications and risks to ensure a successful tendon and ligament repair procedures (39).

Many synthetic biomaterials are being studied for use as T/L substitutes, like

collagen, silk, alginate, chitosan, polycaprolactone, polyglycolic acid, and polylactic acid (40; 39; 38). They are primarily fabricated into the scaffold by electrospinning, electrochemical alignment, knitting, and freeze-drying.

Electrospinning is the most common technique for creating tissue-engineered tendon and ligament repair scaffolds. It offers the advantage of producing fibers at the nano to microscale and allows for flexibility in choosing synthetic and natural biopolymers. However, their reliance on potentially toxic organic solvents and their lower mechanical properties are the main limitations of this method (38). Furthermore, as already mentioned, the devices fabricated with these techniques showed a promising short-term improvement. However, they ultimately failed, and there is no tissue-engineered substitute that has been successfully implanted in humans to date (39; 41). For this reason, there is a need to study different techniques and post-fabrication methods, which are crucial for enhancing scaffold performance and durability.

Overall, fibrous biomaterial-based scaffolds –whose fibers are created by melting spinning without the need for solvents and then arranged into textile structures– are becoming more and more appealing because they are easy to make, have the ability to introduce regeneration elements into T/L tissues, and because the architecture of the fibrils at different nano- and microscales is crucial for controlling the mechanical properties as well as cell differentiation. Some limitations must be addressed, like microstructures preventing the best possible cell infiltration and lack of cell binding sites. Furthermore, porosity often reduces mechanical properties, and increases degradation rate (40; 42; 9).

### 1.1.4 Current solutions for repair/substitution of bone tissues

Bone substitute materials have been more studied than T/L substitutes. These substitutes are divided into five branches: natural materials, metals, synthetic polymers, ceramics, and composites.

**Metals** and their alloys, including titanium, gold, and silver, are valued for their superior mechanical properties in orthopedic devices (43; 44; 45). However, they have limitations such as stress shielding (which leads to bone loss and a weakening of the bone structure around the implant), X-ray artefacts, non-biodegradability, and the risk of implant failures (46; 47; 48; 49). Metals are primarily recommended for load-bearing applications (50).

**Bioceramic** materials, such as calcium phosphate (CaP) and bioactive glasses, play a crucial role in complex tissue repair. These materials can be bioinert, bioactive, or bioresorbable, offering diverse interactions with the body (51). CaP stands out for its advantages, like osteogenesis, reproducibility, and low cost, while bioactive glasses can stimulate tissue growth. However, crystallization can limit the effectiveness of some bioactive glasses and they lack the desired mechanical properties (strength/toughness).

**Natural** materials like proteins (e.g., silk, collagen, and fibrin), polysaccharides (e.g., starch and chitin), and decellularized extracellular matrix (dECM) have been investigated for biomedical applications. Silk and dECM are highlighted for their biocompatibility and unique properties. However, challenges exist, including resource limitations, high processing costs, and difficulties in controlling fiber size and incorporating cells (52; 53; 4).

**Biodegradable polymers**, belonging to the aliphatic polyester family, currently represent the most attractive polymers that meet the various medical and physical demands for safe clinical applications. This is mainly due to their high level of biocompatibility, acceptable degradation rates (they degrade as the new tissues are formed), non-toxic degradation products, and versatility regarding physical and chemical properties (54; 55). The synthetic biopolymers most frequently used in tissue engineering are saturated poly ($\alpha$-hydroxy esters), including poly(lactic acid) (PLA), a racemic mixture of D, L-PLA (PDLLA), and poly(glycolic acid) (PGA), poly(lactic acid-co-glycolic acid) (PLGA) as well as Polycaprolactone (PCL).

These materials degrade *in vivo* through simple hydrolysis of the hydrolytically unstable ester linkage in the polymer's backbone. Its degradation rate is around 15.2% after 180 days. Sabir *et al.* reported that PLA has 37% degradation in between 12 to 18 weeks in chloroform and methylene chloride solvent, and its complete degradation lasted between 12 to 18 months. Once degraded, the body already contains highly regulated mechanisms for completely removing monomeric components of lactic and glycolic acids (54; 51; 56).

Additionally, to enhance cellular adhesion, various extracellular matrix (ECM) protein components like gelatin, collagen, laminin, and fibronectin could be immobilised onto the plasma-treated surface of the synthetic biopolymer. Nevertheless, biopolymers tend to be too flexible and weak to meet specific applications' mechanical demands, leading to low confidence levels regarding the stability of reduced fractures (47; 57).

**Fibre reinforced composites** consist of at least two different materials, one acting as reinforcement and the other as a matrix. The reinforcement carries the applied loads and provides structural properties such as stiffness, strength, and toughness. The matrix keeps fibres in place and at a proper orientation, transfers the load to the fibres, protects them from mechanical damage, manages transverse properties of composites, and provides rigidity and shape to the structure. Thus, one of the main advantages of fibre-reinforced composites is the combination of high mechanical properties (strength and stiffness) with low density, as compared to metals such as steel or aluminum.

Self-reinforced composites (SRC) include only one polymer in forms with different physical properties (58). Alternatively, different melting points and molecular weights provide the potential to simultaneously have different isomers of those polymers in the hardener and matrix of composites (59). Because of molecular configuration in the SRC, there is a limited number of manufacturing methods to produce them, and thermomechanical procedures are the standard method to manufacture SRC. These polymers could be reinforced with hardeners like long fibres, particles, or staples (60).

Composites are inherently anisotropic. Many parameters, such as constituent materials, volume fraction, reinforcing architecture, and plate thickness, can influence their mechanical performance. An optimal composite for bone fixation can be obtained by varying all or some of them. However, due to the need for more standards and procedures, most composite bone plates have been developed based on a trial-and-error method. Limited reports have been found in the open literature addressing optimal designs for composite bone plates upon varying the parameters mentioned above, especially the fibre reinforcing architectures (61).

Table 1.3 provides a concise overview of the advantages and limitations of current solutions for bone tissue repair, as discussed previously. To summarize, metals offer strength but are non-biodegradable and vulnerable to corrosion. Bioceramics promote bone growth but lack the required mechanical properties. Natural materials are biocompatible and biodegradable but present manufacturing challenges. Biopolymers are biocompatible and biodegradable, but their mechanical capabilities are limited. Finally, fiber-reinforced composites deliver robust strength but entail complex manufacturing processes.

Table 1.3: Summary of the advantages and limitations of materials candidates for repairing bone tissues.

| Materials | Advantages | Limitations |
|---|---|---|
| Metals | - Superior mechanical properties | - Not biodegradable<br>- Corrosion products |
| Bioceramics | -Osteogenesis | -Lack of mechanical properties |
| Natural | - Biocompatibility;<br>- Biodegradable | - Manufacturing process control;<br>- Low range of mechanical properties. |
| Biopolymers | - Biocompatibility;<br>- Biodegradable;<br>- Possible integration of proteins; | - Low range of mechanical properties. |
| Fibre reinforced composites | - Good mechanical properties<br>- Low weight. | - Complex manufacturing process. |

## 1.2 Biodegradable materials

As mentioned in the previous section, several types of biodegradable materials exist. The ideal biodegradable polymer would maintain adequate mechanical strength until tissue healing (about 8-12 weeks, depending on the application) and begin to lose mass to let new tissue develop, replacing the implanted polymer (62) as shown in Figure 1.6.

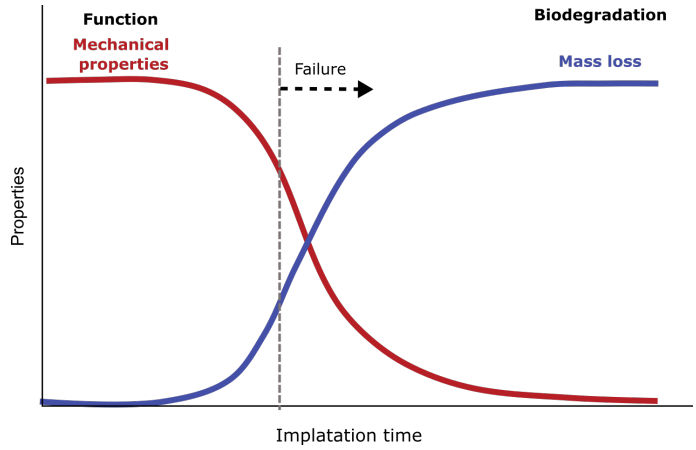


Figure 1.6: Ideal relationship between mechanical properties and mass loss of a biodegradable implant after implantation (52).

In this section, the focus will be on the biodegradable synthetic polymers, like aliphatic polyesters, since they are gaining particular interest due to their low elastic modulus, easy-to-process, tailored degradation as well as biocompatibility (63).

Additionally, aliphatic polyesters are vulnerable to hydrolytic and enzymatic chain cleavage, resulting in $\alpha$-hydroxyacids, which are generally metabolized in the human body and are commonly employed in biomedical applications (64; 20).

During the initial degradation phase, an aqueous solution penetrates the polymer, followed by hydrolytic degradation, which converts long polymer chains into shorter water-soluble fragments, a process known as reverse polycondensation. Hydrolysis is the essential degradation method for most biodegradable materials, particularly synthetic polymers. Enzymes are giant molecules that cannot penetrate the crystalline areas, and enzymatic breakdown is slow (64).

Polymer characteristics (molecule structure, ester group density) and environmental factors (like temperature, degradation medium type, and mechanical stimuli) influence hydrolysis kinetics (65). The degree of crystallinity may be an essential element since crystalline domains are less permeable to water entry, delaying the hydrolysis. Since the human body is maintained at a homeostatic level, pH should not be influenced significantly. Temperature, which usually is maintained between a range (36-37°C) in the human body, causes diffusion to increase due to greater molecular flexibility. This will also speed up the breakdown process since the molecules will be more excited, increasing the possibility of bond scissions (64). The size and shape of the samples are also relevant; for example, due to autocatalytic hydrolysis inside the polymer, larger samples (with dimensions of a few millimetres) disintegrate quicker than smaller samples (e.g., films or microparticles) (65).

Synthetic biodegradable polymers such as PLA (polylactic acid) and PCL (polycaprolactone) have relevant advantages attributed to their ease of manufacture and industrial scalability, providing biocompatible materials with controlled degradation time (66).

In the case of PLA, the degradation rate in physiological conditions can range from 10 to 48 months, depending on its poly-enantiomeric structure and the initial molecular weight. Degradation of PCL can range from 2 to 4 years under the same conditions (67; 64). Their mechanical properties are also interesting for connective tissue repair, with elastic moduli in the range of 3-4 GPa for PLA and 0.2-0.4 GPa for PCL (64). However, limitations for tissue engineering are observed by using only PLA materials, specifically those regarding the degradation rate, limited ductility, and hydrophobicity (64; 2). Conversely, PCL is very ductile but with low strength compared to PLA, resulting in a material with a ductile failure, regardless of the catastrophic failure evident in the PLA materials. Additionally, in the case of PLA,

its low strength associated with low elastic modulus usually impairs its potential use in bone tissue engineering. Their mechanical properties, lower than those of conventional metal implants, lead to low confidence levels regarding reduced fracture stability.

### 1.2.1 PLA (Polylactic acid)

PLA produced from renewable resources such as corn and sugar beets is one of the most promising thermoplastic biopolymers due to its relatively attractive mechanical properties (compared to other biopolymers), potential biodegradability, and high industrial production capacity (66). The FDA (United States Food and Drug Administration) has already approved it for use in medical devices.

PLA production procedures lead to various molecular weight grades, and lactic acid potentially creates three different stereoisomeric forms: L-lactide, D-lactide, and mesolactide, which have different properties. Consequently, a wide range of molecular weights of PLA could be produced by controlling the purity of the lactide. The ratio of D- and L-isomers and their distribution along the polymer chain influence the molecular weight and crystallinity of the produced PLA, resulting in a wide range of mechanical properties. For example, the high molecular weight PLA possesses high intermolecular forces, which can induce high mechanical characteristics; fully crystalline poly(L-lactide) (PLLA) degrades slower than amorphous Poly-d,l-lactic acid (PDLLA) (20; 65). Also, thermal properties, like different melting points, can be achieved, which provides the opportunity to produce self-reinforced composites (SRCs) of this material (59). PLLA is the preferred material for fracture fixation implants due to its higher strength than PDLLA (57).

PLA degradation can be classified as hydrolytic, enzymatic, surface, and bulk degradation, or end chain scission and random chain scission (20). There are two major stages in the degradation process. However, in a physiological environment, PLA degradation is dominated by non-enzymatic processes, mostly hydrolysis, in which the polymer absorbs water, and its chains break down into smaller pieces over time. Initially, the ester link of the PLA chain breaks, and water molecules begin to permeate the PLA matrix, resulting in a drop in molecular weight and the formation of water-soluble oligomers. Because the molecular chain in the amorphous region is loosely packed, it is more likely to come into touch with water molecules and hydrolyze. As a result, hydrolysis occurs quicker in the polymer's amorphous phases (1st mechanism) than in the crystalline parts, leading to easier recrystallization of the

amorphous regions (2nd mechanism) and the formation of regions with order structure. This process then causes polymer erosion (surface and bulk degradation) and changes their structure and characteristics, including mechanical strength reduction. Finally, when the polymer's molecular weight, Mn, falls below the solubility limit, which in the case of PLA is less than 20.000 (g/mol), the polymer mass begins to drop faster, the gaps between the chains expand, and the capacity to recrystallize declines. During the second stage of degradation, biological enzymes catalyze the breakdown of monomeric lactic acids, which are then converted into water and carbon dioxide (65; 20; 64). This entire process is represented in Figure 1.7. The amorphous phases are initially attacked, and the molecular weight of the polymer starts to decrease, followed by a decrease in the mechanical strength and, lastly, to a mass drop. As the recrystallization process stops, the degree of crystallinity may decrease in the following degradation processes (65).

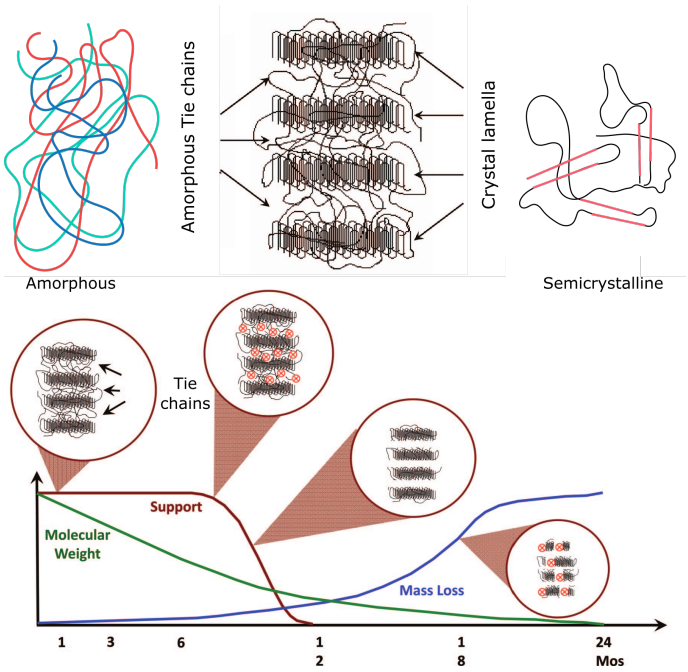


Figure 1.7: a) Schematic representations of the amorphous (left), semicrystalline (middle), and semicrystalline polymer (right). b)The change in molecular weight, mechanical characteristics, and mass loss of PLLA as degradation time increases (20).

The amount of amorphous phase present has a significant impact on the dynamics of degradation. PDLA degrades substantially faster than PLLA. Based on the molecular weight, crystallinity degree, and material form, it dissolves fully into lactic acid from 10 months to 4 years. PLLA is a less ductile and stiffer polymer that

degrades slowly (64). For this reason, having a device that combines a semicrystalline PLA with an amorphous PLA could result in a device with interesting properties for connective tissue applications.

Table 1.4 summarizes some commercially available medical devices based on PLA material. These devices serve various purposes, such as pediatric craniotomy fixation, bone fracture and fragment fixation, ligament reconstruction (ACL, PCL), finger and toe fracture fixation, ACL reconstruction, meniscus repair, and bone fracture treatment. PLA's biocompatibility and biodegradability make it a suitable choice for these applications.

Table 1.4: Current commercially available medical devices based on PLA materials (68).

| **Name** | **Composition** | **Application** |
|---|---|---|
| RapidFlap® | PLLA-PGA | Pediatric craniotomy fixation |
| Osteotrans-MX® | PLLA-$\mu$HA | Bone fracture and fragments fixation |
| Osteotrans-OT® | PLLA-$\mu$HA | Ligament reconstruction (ACL, PCL) |
| Grand Fix™ | PLLA | Finger and toe fracture fixation |
| Pinn-ACL® Cross pin | PLLA | ACL reconstruction |
| Genesys™ Matrix | PLDA/$\beta$-TCP | ACL/PCL graft fixation |
| BioStinger® Meniscal | PLLA | Meniscus repair |
| SmartNail® | PLLA | Bone fracture |
| Orthomesh® | PLLA | Bone grapfts or fragments fixation |

PLA degrades faster than PCL in general, and by blending different amounts of these polymers, it would be possible to tailor the degradation time. Furthermore, PLA degradation products are known to reduce local pH, accelerate degradation, and induce inflammatory reactions. However, adding PCL minimizes local acidification, reducing the inflammatory response (65; 69). Furthermore, because PLLA is glassy at body temperature (glass-transition temperature 60 °C), whereas PCL is rubbery (glass-transition temperature 60 °C), the blend might improve the mechanical qualities of pure PLA. Compared to pure PLLA, the compound's elongation at break and strength are enhanced.

### 1.2.2 PCL (Polycaprolactone)

Carothers and Hill were the first to synthesise polycaprolactone (PCL) in the 1930s (70). It is a biodegradable, aliphatic, semicrystalline polyester that can be manufactured using a variety of processes and has a range of molecular weights (14,000-100,000) and different characteristics. This polymer is also FDA-approved for use in various products. It has been widely used in tissue engineering due to its biocompatibility, tunable biodegradability, good strength, ease of synthesis, availability, cost efficacy, facile modification into different shapes due to low melting point, less acidic by-products when compared to other polyesters, and extremely high drug permeability (2; 21). This highly ductile and stiff polymer has an elastic modulus of roughly 0.21-0.44 GPa.The slow degradation rate of this material, lasting from 2 to 4 years at body temperature, can be attributed to the recurring presence of five hydrophobic -CH2 moieties (2; 21; 71).

When utilised as a biomedical implant, PCL typically experiences the two-stage degradation process, also found in PLA: first, hydrolytic degradation, in which ester bonds are broken by water, followed by intracellular destruction by enzymes (63; 71). Hydrolysis, as in the case of PLA, occurs in three stages, with the first being characterised by losses in molecular weight (0-20 weeks), followed by a loss in mechanical characteristics (20-46 weeks), and finally by a loss in mass (46-80 weeks). These stages are not independent, with the duration of each and the degree of overlap between them determined by the influencing factors like the local environment, the molecular weight of the polymer, and the morphology of the test specimen. Because of the slow degradation rate, autocatalysis is not generally mentioned as a PCL degradation process (71).

Non-enzymatic hydrolysis appears prominent in the orthopaedic context where PCL is most typically employed. However, because of its slow breakdown rate, limited cell adherence, and non-osteogenic qualities, several composites based on the combination of PCL with other biomaterials have been developed (71). In recent years, new biomaterials have been studied to improve PCL properties and some studies are presented in Table 1.5. These combinations, processed using methods such as electrospinning, 3D printing, and freeze extraction, lead to improved scaffold properties. Notable outcomes include enhanced mechanical properties, decreased degradation rates, improved cell adhesion and proliferation, and increased bioactivity. One of the most recent papers demonstrated that PLA/PCL/HA/silica obtained through freeze extraction resulted in scaffolds with good hydrophilicity, optimal cell

Table 1.5: List biomaterials blended with PCL.

| Materials | Processing | Results | Reference |
|---|---|---|---|
| PCL/PGA/$\beta$-TCP scaffold | Solvent casting; Compression molding; Sintering . | Improved mechanical properties; Decrease of degradation time | (77) |
| Nanofibrillated chitosan with PCL scaffolds | Electrospinning | Good wettability; Enhanced tensile strength; Improved cell adhesion and proliferation. | (78) |
| PCL/gelatin /nanohydroxyapatite scaffolds | Electrospinning | Enhanced human osteoblast proliferation; Improved cellular attachment | (73) |
| Nanofbrous PCL scafolds with silver-doped hydroxyapatite | Electrospinning | Antibacterial efficiency; Enhance human fibroblast proliferation | (74) |
| PCL/PLA nanofibrous scaffolds | Eletrospinning | Increased the mechanical properties Increase in bioactivity | (79) |
| Nanoparticles hybrid hydroxyapatite/PCL scaffolds | Direct emulsifcation-solvent Evaporation method | Enhanced osteogenicity; Biocompatibility | (75) |
| Microcrystalline cellulose / PCL scaffolds | 3D printing | Improved the mechanical strength | (80) |
| PLA/PCL/HA scaffolds | FFF printing | Improved the mechanical properties | (76) |
| PLA/PCL/HNT scaffolds | FFF printing | Improved elongation Adequate citocompatibility Reduce degradation rate | (81) |
| PLA/PCL/HA/silica scaffolds | Freeze extraction | Good hydrophilicity Optimal cell attachment Improved mechanical properties | (72) |

attachment, and improved mechanical properties (72). Other investigations combine PCL with HA (hydroxyapatite), an osteoconductive ceramic material, which promotes bone regeneration and integration with surrounding tissues (73; 74; 75; 76; 72).

## 1.3 Current challenges on biodegradable polymers for biomedical applications

The field of tissue engineering holds great promise for revolutionizing how injuries and degenerative conditions in the human body are addressed. Key to its success is the development of scaffold materials that can support tissue regeneration. Among the materials under investigation, biodegradable polymers, such as Polylactic Acid (PLA) and Polycaprolactone (PCL), have gained considerable attention. However, the path to creating effective scaffold materials is laden with a number of scientific, biological, and market-related challenges:

- **Mechanical/degradation:** biodegradable polymers have low elastic moduli. One significant challenge is enhancing their mechanical properties to closely approximate those of natural bone, ligament, or tendon tissues. Achieving

this balance is a complex task. Another challenging aspect is aligning the degradation time of these polymers with the regeneration time of the surrounding tissues. This requires a thorough understanding of how these materials degrade over time and how this degradation process impacts their mechanical properties. Furthermore, individual variations in factors like age, gender, and physical activity can lead to significantly different tissue repair rates. Designing scaffolds that can accommodate these variations and support effective tissue regeneration is another challenge in tissue engineering.

- **Biological challenges**: These polyester materials have a hydrophobic behaviour, which can hinder bioactivity. Additionally, ensuring that scaffolds have enough porosity and the proper pore size for nutrient exchange without compromising mechanical properties is a delicate balance that needs to be achieved.
- **Market Challenges:** Considering the limitations and availability of materials currently on the market adds complexity to the research. Finding cost-effective and readily available materials that meet the desired criteria can be challenging.

Addressing these challenges will be crucial for advancing tissue engineering applications using PLA and PCL materials.

## 1.4 Textiles

As previously discussed, fibrous biomaterial-based scaffolds have garnered increasing attention in TE due to their potential to tailor their performance through textile engineering. This section will address the commingling processing method and textile structures employed for tissue regeneration.

### 1.4.1 Commingling

Commingling is a manufacturing method that produces a single yarn by blending or intermingling two or more different natural or synthetic fibres (82). The difference between commingling and other yarn manufacturing methods –like co-wrapped yarn and core-spun yarn– is depicted in Figure 1.8. The combination of different fibers allows synergistic effects by increasing the mechanical properties, durability, and degradation of the yarns compared to those obtained with one type of fibres. Furthermore, a homogeneous distribution of reinforcement and matrix reduces the

matrix's mass transfer distance during processing, resulting in a fast and complete impregnation of the reinforcement filaments and a good impregnation of the matrix into the fibres once the yarn is hot pressed (61; 83). The appropriate fibre-to-matrix ratio can also be reached by adjusting the quantity of component yarn used during hybrid yarn manufacture. A second benefit is the commingled hybrid yarns' processability by practically all known textile-manufacturing processes (83).

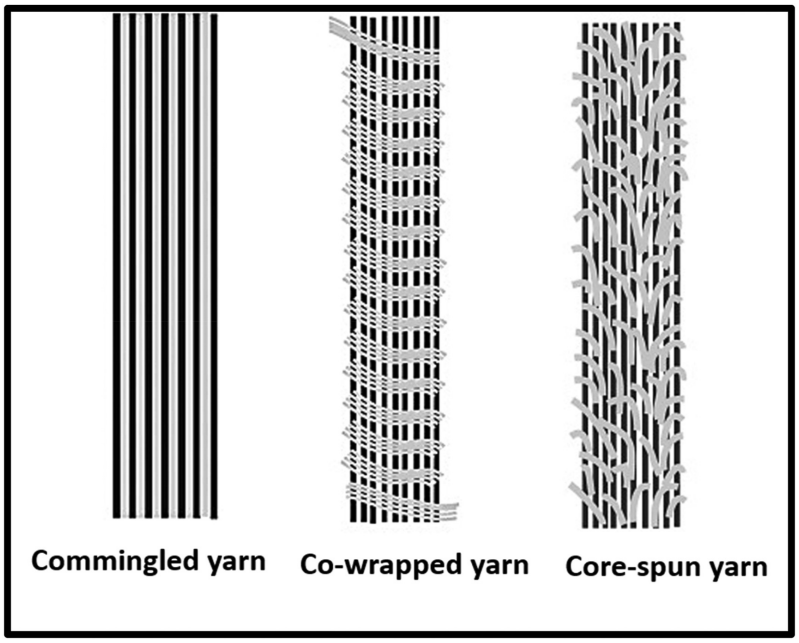


Figure 1.8: Types of hybrid yarns (84).

Commingled yarns can be further processed into textiles such as woven, knitted, and braided architectures using standard textile processing techniques. By selecting biodegradable fibres and the appropriate fabric architecture, textiles manufactured with commingled yarns can meet the different requirements of biomedical applications, becoming excellent candidates for sutures and TE scaffolds for bone, cartilage, ligament, and tendon because of their suitable mechanical properties (85; 43). Moreover, mass-produced materials for medical devices with various shapes and mechanical properties can be delivered using traditional textile engineering strategies (53; 86; 87).

### 1.4.2 Weaving

Fibre-based techniques such as weaving, knitting, braiding, and electrospinning have emerged as promising platforms to form porous constructs for biomedical applications (53; 88; 10). Additionally, fibre alignment, fibre diameter, roughness yarn type, and

structure can influence the cell adhesion and arrangement and allow a tremendous structural and mechanical variety for their application (10; 89), Figure 4.3.

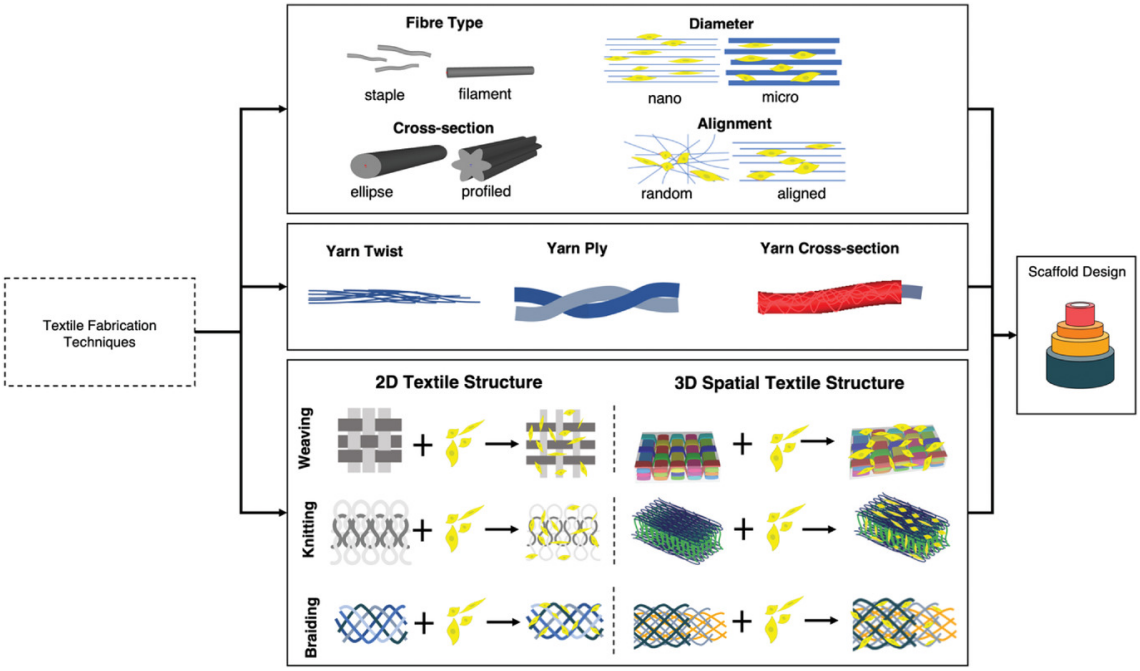


Figure 1.9: Textile manufacturing structures (fiber, yarn, and fabric) parameters that can determine the mechanical properties, regulate cell-material interaction, and cell behaviour (89).

These textiles structures have been investigated for different applications (90; 55) like surgical meshes for hernia repair (91) and pelvic organ prolapse (POP) (92), scaffolds for regeneration of different tissues such as cartilage (93), ligaments (26) and tendons (94), bone reconstruction, small joint reconstruction (95), bladder (96), skin (97) and blood vessels (98).

Woven structures are lightweight, strong, and flexible. In comparison, woven scaffolds are significantly stronger (42% higher) and stiffer (85% higher) than knitted scaffolds (26). Laranjeira *et al.* (99) reported that woven scaffolds were 85% tougher and had an 8.8 times higher tensile load than the braided scaffolds (Figure 4.4). Additionally, changing the weaving density of warps and weft yarns allows fabric strength, stability, and porosity to be easily controlled. The textile architecture provides the surface necessary for cell adhesion and growth, while its internal porosity is required for cell migration and communication and to promote nutrient transport. The anisotropic behaviour of tissues such as skin, skeletal muscles, connective tissues, and bone regeneration can also be mimicked using yarns from different materials and densities for warp and weft orientations (100). For instance, Moutos *et al.* (101)

created 3D PGA (polyglycolic acid) woven scaffolds with mechanical properties similar to native articular cartilage. Abrahamsson *et al.* (102) fabricated 3D woven PCL (polycaprolactone) scaffolds and seeded them with human mesenchymal stem cells suspended in collagen gel for osteochondral tissue regeneration (53). Another study investigated PLA-PCL woven bio-textile fabricated electrospun nanofiber yarns. PCL nanofibers were processed to plain weave fabrics and then interlaced with PLA multifilament fibres. However, the fabricated materials had small pore structures (103).

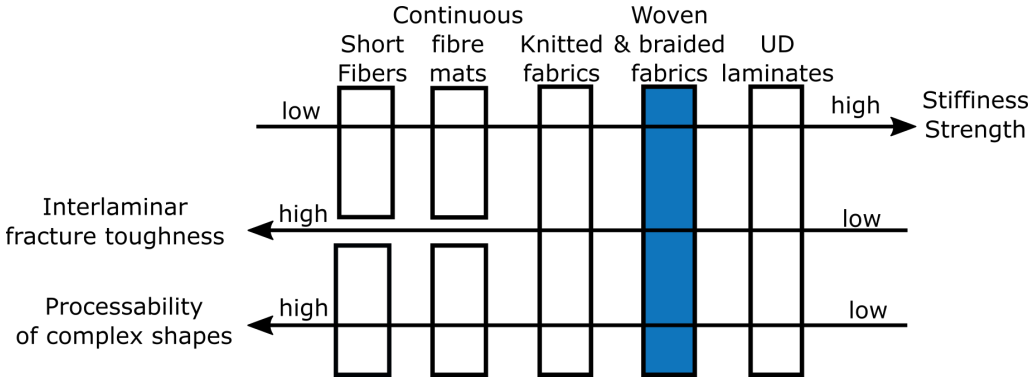


Figure 1.10: Overview of main existing reinforcement structures in composites and their properties, (104).

Table 1.6 provides an overview of various woven fabrics employed in connective tissue applications, highlighting their unique properties and the specific tissue to which they are applied. These woven materials play a crucial role in tissue engineering, contributing to developing practical solutions for tendon, tendon-to-bone junction, ACL (Anterior Cruciate Ligament), and tendon/ligament replacement. The properties of these materials, such as symmetry, anisotropy, osteoblastic differentiation, and porosity, make them valuable in addressing specific tissue engineering challenges.

Table 1.6: Woven fabrics used for connective tissue applications.

| Material | Properties | Tissue | Ref |
|---|---|---|---|
| Woven PET | high symmetry<br>defined deformation behaviour | Tendon | (105) |
| 3D woven HA | structurally anisotropic | Tendon to bone junction | (106) |
| Woven PSN@EG | improved osteoblastic differentiation | ACL | (107) |
| Multilayer silk woven | porosity allowed cell colonization | T/L replacement | (108) |
| PCL ES weave | suitable strengths | ACL | (109) |

## 1.5 Self-Reinforced Polymers

Physical blending is a method of modifying the mechanical characteristics and degradation kinetics of PCL/PLA that involves physically integrating of components such as other polymers, drugs, ceramics, or other desirable molecules inside the polymer matrix (71). In this context, composite materials are made up of a stiff and strong material, the reinforcement (usually in the form of fibres), and a softer continuous component, the matrix. The role of the reinforcement, as the name implies, is to carry the applied load and offer structural qualities such as stiffness, strength, and thermal stability. On the other hand, the matrix maintains the fibres in place and adequately oriented; it carries the load to the fibres; it shields the fibres from mechanical damage; and gives the structure stiffness and form (104).

The mechanical performance of these materials may be altered by the materials employed as reinforcement and matrix, the reinforcement volume fraction, and the reinforcement orientation or arrangement. Another crucial component is having adequate interfacial bonding between the matrix and reinforcement. However, due to chemical differences between these materials, solid and stable interfacial bonding is typically challenging in classic fibre-reinforced materials (110).

To address the aforementioned issue, single polymer composites (SPCs) or self-reinforced composites (SRCs) were introduced (Figure 1.11). SRC are materials in which the reinforcements (fibres) and continuous (matrix) phases are made of the same polymer or polymers with the same chemical content but distinct chemical structures, resulting in strong and continuous interfaces and, consequently, improved mechanical properties. Additionally, another advantage is the end-life recyclability since it can be achieved by using the same polymer for both the fibres and matrix phases (111; 112; 110; 104).

SRCs formed by non-biodegradable oriented polyethylene (PE) filaments and PE powder with different melting points were first developed in 1975 by Capriati and Porter (58). SRCs of polyglycolide acid (PGA) was the first biodegradable composite used in biomedical devices in 1988, and afterwards, because of its high fast degradation rate, SRCs of PLA were employed for bone fixation in 1992 (113), and also as sutures, rods screws, and plates (114). Since then, several investigations have been carried out on the application of SRC of PLA for bone fixation (115), mandibular bone fixations (116; 117; 118), and beyond the non-biomedicine studies (56; 119). Törmälä (120) investigated the mechanical properties of single polymer

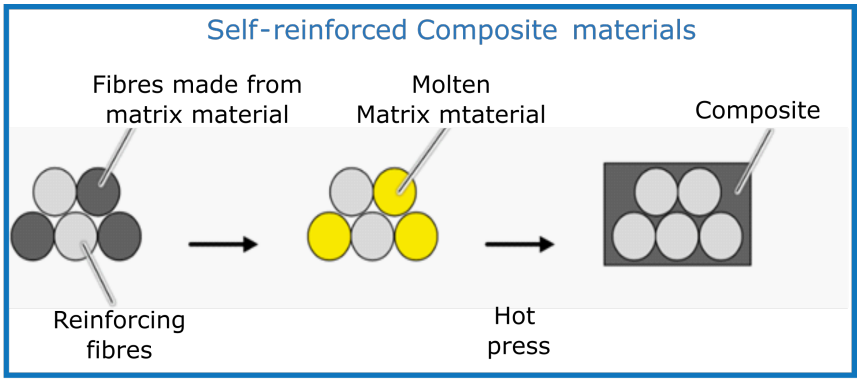


Figure 1.11: SRCs manufacturing process: from commingling yarns to consolidated plates.

composites reinforced by PLA fibres. These authors showed that embedding fibres in the PLLA matrix increased the bending modulus and strength of the composite to 10 GPa and 300 MPa, respectively, while PLLA only reached 5 GPa and 70 MPa, respectively. Hot-compression moulding was utilized by Li and Yao (121) to make PLA-SPCs consisting of two amorphous PLA sheets as the matrix and a layer of high-crystallinity PLA fibres, yarns, or plain textiles as reinforcement. Tensile tests showed that the strength of PLA-SPCs improved by around 30% with respect to PLA. On the other hand, most composite plates developed so far have used UD (unidirectional) laminates (61) and discontinuous short fibers (1) as reinforcement. This limits the application of these materials because they result in poor mechanical properties perpendicular to the fiber direction (61).

Table 1.7 shows some self-reinforced materials used for biomedical applications. Materials like UHMWPE (Spectra®), PMMA, and PLA (Polylactic Acid) are processed using hot compaction woven textiles to enhance their mechanical properties. These self-reinforced composites find applications in areas like hip fixation and tissue engineering.

In the case of PLA materials, self-reinforced materials were created and improved by adjusting copolymer ratios (L/D). Various fixation devices are also on the market, particularly for low load-bearing applications or for children (124).

There have been very few investigations on PLA-PCL fibre-reinforced composites. Fan *et al.* (125) investigated PLA-reinforced PCL composite membranes made by multi-spinneret blended electrospinning. They were able to increase the tensile mechanical properties, leading to an elastic modulus of 6.1 GPa and a strength of 33 MPa. Guarino *et al.* (126) manufactured a PCL three-dimensional porous composite

Table 1.7: Self-reinforced composites used for biomedical applications.

| Material | Process | Properties | Ref |
|---|---|---|---|
| UHMWPE | UHMWPE (Spectra®) fibers hot compaction. | 10× higher tensile strength and modulus difficult and costly processing high melt viscosity. | (122) |
| PMMA | Woven PMMA fibers | Hip fixation not biodegradable | (123) |
| PLA | highly oriented PLLA fibers hot-compression | 2.1× higher mechanical properties | (120) |
| PLA | high-crystallinity PLA fibers hot-compression | 30% higher strength | (121) |

scaffold that incorporated two separate reinforcing geometries: particles and long fibers. The porogen agent was sodium chloride crystals, while the reinforcing ones were poly(lactic acid) (PLA) fibers and calcium phosphate. They obtained a scaffold with a much better mechanical response by up to an order of magnitude. Ju *et al.* (127) studied the effect of the diameter of the PLA fibers on the physical properties of the PCL and concluded that the addition of the PLA fibers, particularly of smaller fibers, improved the dynamic storage modulus, tensile yield strength, and elastic modulus of the PCL, indicating that this was the best reinforcement. One of the main disadvantages is that exact temperature control is required since these materials have a narrow processing temperature window. Poor performance will be found if temperature is insufficient or overheating takes place during composite manufacturing (110).

Furthermore, a hybrid yarn can be used to further improve the interfacial property between the matrix and the reinforcement. This method mixes the thermoplastic polymers into fibres with the reinforcing fibre, resulting in a uniform distribution of fibres embedded in the matrix. This hybrid yarn can be attained by many spinning processes such as wrap spinning, air-jet spinning, and commingling spinning (104).

## 1.6 Requirements for designing scaffolds for T/L or bone repair and regeneration

A designed scaffold for T/L and bone repair and regeneration should ideally meet the following characteristics simultaneously:

## 1.6. Requirements for designing scaffolds for T/L or bone repair and regeneration

- Mechanical support: to mimic the mechanical and functional properties of the tissues. Thus, it should be able to withstand the mechanical forces and stresses that the tissue would typically experience, such as tension and load bearing. The elastic modulus should be in the range 5 MPa to 20 GPa and the ultimate strength from 16 MPa to 200 MPa, depending on whether tendon, ligament, or bone materials are addressed.

- Structural:

  - Geometry and Surface Area: The scaffold's geometry is crucial. It should provide the necessary mechanical properties and surface area for cell attachment, growth, and proliferation. The three-dimensional structure of the scaffold can influence the cell behaviour.
  - Porosity: Effective diffusion of nutrients and removal of waste products should be facilitated within the scaffold to support cell viability and tissue growth. The pore sizes should be between 100-400 $\mu$m.

- Biological :

  - Biocompatibility: To elicit a suitable biological response in the body, including the absence of immunogenic reactions.
  - Bioactivity: To have the ability to interact with surrounding living tissues. Bioactive scaffolds are designed to stimulate cellular migration, cellular differentiation, tissue formation, and integration into the host tissue. The goal is to promote natural tissue growth and regeneration while avoiding undesirable processes such as scarring.
  - Biodegradability: the ability of the polymer chains to be broken down by the body over time. This property is crucial because tissue formation should coincide with scaffold degradation. The products of scaffold degradation must also be non-toxic and easily disposed of by the body without causing side effects.

- Other properties:

  - Reduced Abrasion: To minimize abrasion and enable smooth tissue motion, the scaffold should provide an appropriate surface texture or structure;
  - Noninvasive Imaging: The scaffold should be visible in noninvasive imaging methods like X-rays for tracking and monitoring and transparent for radiation treatments.

Additionally, requirements for bone regeneration:

- Osteoinductivity: In the context of bone tissue engineering, there is a specific focus on osteoinductive scaffolds. These are scaffolds that have a high ability to induce the formation of bone tissue. Osteoinductive materials can encourage the differentiation of stem cells into osteoblasts (bone-forming cells) and promote bone regeneration.

In summary, the design and use of scaffolds in TE aims to create materials that provide structural support and actively facilitate tissue regeneration and integration into the host environment. This requires careful consideration of biocompatibility, biodegradability, immune response, bioactivity, and specific properties relevant to the type of tissue being engineered, such as osteoinductivity for bone tissue (128; 129; 15).

## 1.7 Motivation and objectives

This thesis is motivated by the overarching goal of advancing the development of biodegradable textile polymer composite materials for applications in connective tissue engineering. The primary objectives of this research endeavour include:

- Material development: To develop novel manufacturing routes to create a broad spectrum of materials with diverse mechanical properties. The aim is to provide the flexibility to tailor these materials and manufacturing techniques according to specific application requirements. A primary focus of this objective is to gain a deep understanding of how various processing parameters influence the properties of these materials. This comprehensive understanding will empower the development of versatile, customizable materials for a range of connective tissue applications.

- Mechanical behavior and service life evaluation: To study the mechanical behaviour of these materials throughout their entire lifecycle. This involves subjecting these materials to conditions that mimic their service life, spanning from initial implantation within the body to degradation over time. Conducting these tests and assessments under representative conditions aims to understand how these materials perform over time, ensuring that their mechanical properties align with the intended application and durability requirements. This objective

will provide valuable insights into the long-term performance of these materials in connective tissue applications.

- Biological assessment and biocompatibility testing: to conduct a series of biological tests specifically focusing on biocompatibility. Essential tests to understand the intricate mechanisms of interaction between cells and the materials developed. Additionally, these assessments aim to verify the absence of any toxic chemical species within the materials, ensuring the safety and suitability of the materials for biomedical applications.

## 1.8 Structure of the thesis

This thesis is structured into six chapters to assist the reader in understanding how PLA-PCL textile and composite materials are manufactured and characterised. The second chapter, **Chapter 2**, covers the entire manufacturing process, from individual yarns through hybrid yarns, woven textiles, and composite materials. The characterisation strategies (mechanical, thermal, structural, degradation, and biological) are presented in **Chapter 3**. Furthermore, the section Results is separated into two chapters. The first chapter, **Chapter 4**, is dedicated to the characterisation of woven textile materials, while the results of composite materials are presented and discussed in **Chapter 5**. Finally, **Chapter 6** summarises the conclusions and future work.

# Manufacturing Processes

# 2

Several manufacturing processes have been implemented for the production of the fibre-reinforced composites in this thesis. The starting point is the production of the commingled yarns serving as raw material for weaving textile dry fabrics and consolidating self-reinforced composites by compression moulding using hot-press (Figure 2.1). Four materials were produced in this thesis: two dry fabrics containing PLA/PCL and PLA/PLA commingled yarns and the corresponding consolidated composites. The PLA-PCL weaves and consolidated composites contained commingled yarns mixed in a 3:1 ratio. The PLA/PLA self-reinforced composites were made by using a commercial BIO4M® ($PLA_{HM}$/$PLA_{LM}$ yarns) containing high and low melting temperature PLA filaments in 1:1 ratio.

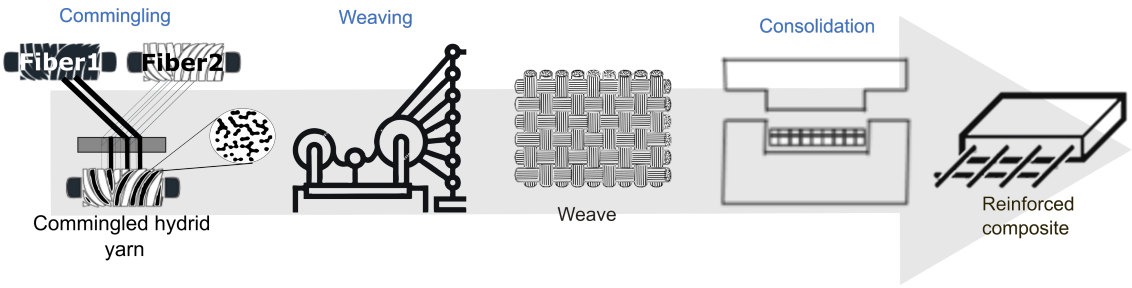


Figure 2.1: Overview of the process chain for the development of fibre-reinforced composites

## 2.1 Materials selection

Polylactic Acid (PLA) filaments of 1100 dtex (1 dtex = mass of 10 Km of yarn) were obtained from Trevira (Hatterscheim, Germany) and chosen as reinforcement. Polylactrone (PCL) fibres (330 dtex) were acquired from EMS-Grilltech (Domat/EMS,

Switzerland) and used as a matrix in the composite material. A commercial hybrid yarn, BIO4M® of 1600 dtex was obtained from Comfil (Gjern, Denmark). This hybrid yarn contains PLA filaments with high and low melting temperatures ($PLA_{HM}/PLA_{LM}$) that will play the role of reinforcement and matrix in the self-reinforced composite, respectively. Yarns were weaved into textiles at ITA (Institut für Textiltechnik of RWTH Aachen University) while consolidation by hot-press was carried out at IMDEA Materials Institute.

## 2.2 Commingling

The method chosen for producing commingled yarn was intermingling in an air jet. In this process, represented in Figure 2.2, both filament yarns are delivered separately and commingled inside a mixing box in a nozzle employing pressurised air that creates turbulences and opens and intermingles the fibres that will act as reinforcement and matrix. This route is versatile, and the induced torsion of the commingled yarns results in good cohesion, facilitating further processing (119; 82).

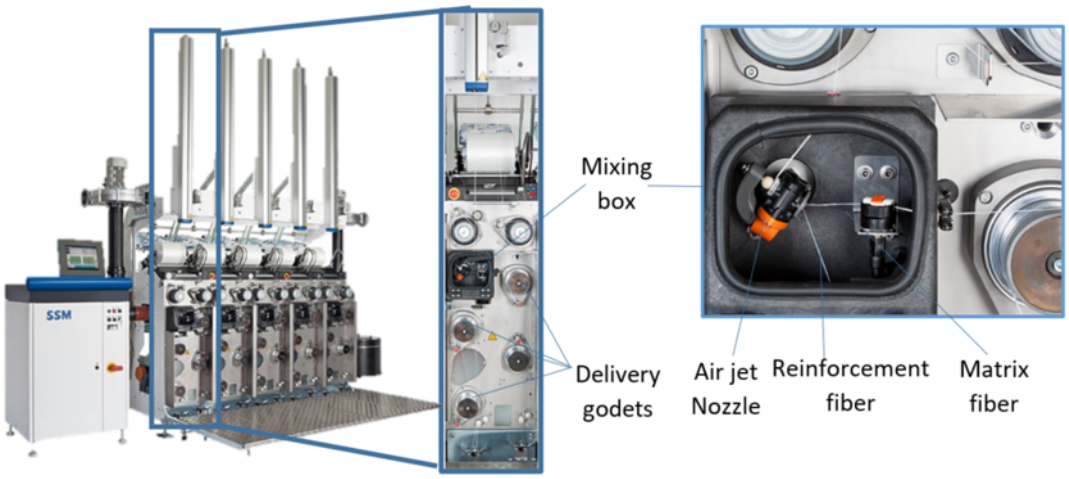


Figure 2.2: DIGICONE® fastflex™ air texturing machine, adapted from (130)

To obtain a uniform blend, the characteristics of the mingled fibres should be as similar as possible. Besides, the process parameters (speed, pressure and overfeeding rate) can be adjusted to identify a parameter set that offers the best properties for the commingled yarn. Rising air pressure increases turbulence, the number of filament breaks, and production costs. On the other hand, decreasing the air pressure reduces the turbulence. Mixing the filament yarns inside the nozzle is only possible with overfeeding. The relative speed creates this effect between the two delivery godets

and influences the quality of the yarn, namely fibre distribution and orientation. Finally, the production speed is also relevant for the hybrid yarn quality and the production costs (131; 82; 132).

A DIGICONE® Fastflex$^{TM}$ air texturing machine was used for commingling the PLA and PCL fibres (Figure 2.2). Different sets of parameters were tested, in which the production speed was maintained at 150 m/min, the air pressure was varied from 5 and 6 bar, and the overfeeding rate was varied from 1%-13%. Then, the hybrid yarn produced at 150 m/min, with 6 bar of pressure and 7% overfeeding, was woven into a modified plain weave. The longitudinal and cross-section views of PLA/PCL hybrid yarn morphology are depicted in Figures 2.3 a) and b), respectively.

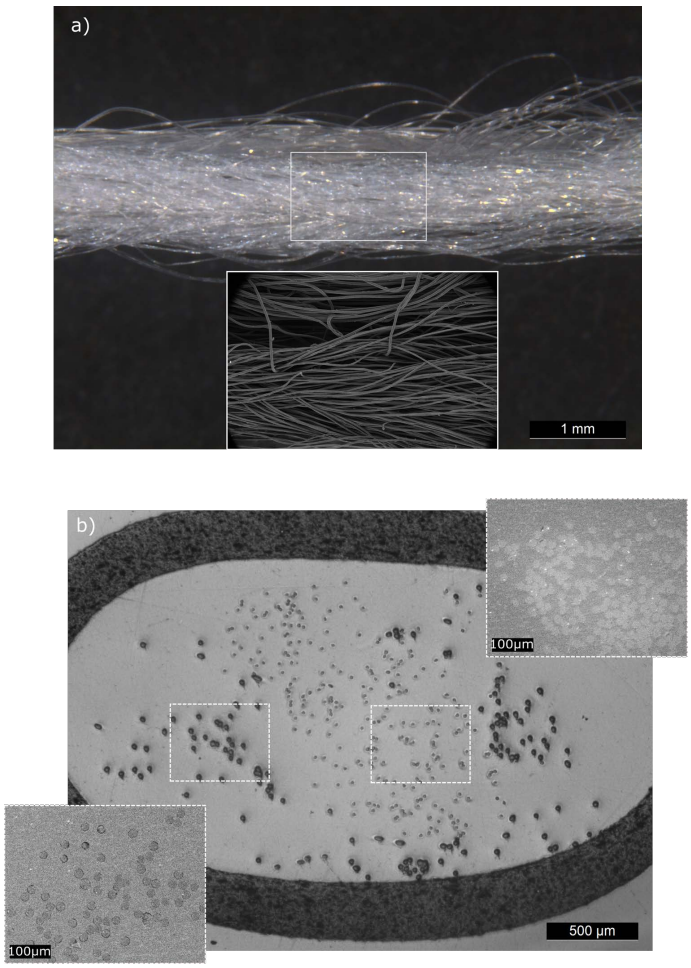


Figure 2.3: a) Longitudinal view of the PLA/PCL hybrid yarn, including a high magnification SEM image of the region marked with a square. b) Optical image of the cross section PLA/PCL hybrid yarn. High magnification SEM images of the PCL and PLA fibres in the regions marked with a square are also shown.

## 2.3 Weaving

Once the commingled yarns were obtained, a woven fabric was manufactured. The selection of the architecture was carried out based on mechanical performances and the availability of textile machines at ITA premises. Such woven fabric is characterised by two interlacing systems of threads orthogonal to each other, referred to as warp and weft threads. More specifically, the former runs in the machine direction and the latter in the perpendicular direction. Woven fabrics can be defined by the number of warp yarns per unit width ($P_{wa}$), the number of weft yarns per unit width ($P_{we}$), warp and weft crimp and surface density (133; 134; 135).

A schematic of the weaving loom used in this work and its main components is depicted in Figure 2.4 a). Under regulated tension, warp yarns are wound on the warp beam, rolling off it parallel to each other. Each warp yarn is connected to a harness or shaft, a frame positioned across the loom with a set of heddles mounted. The heddle is a wire or thin plate with an eye hole through which the warp threads are pulled. A shed, a gap between the warp yarn, is formed when a harness goes up or down because the warp yarns inserted on it go up (harness 2) or down (harness 1). While the shed is formed, the reed is positioned at the back dead centre, and weft yarn may be inserted using a weft insertion device such as a shuttle, projectile, air/water jet or rapier. Once a weft yarn is in position, the harnesses move in opposite directions, closing the shed, moving the reed front and locking the weft in the fabric. Lastly, the cloth beam moves the fabric forward, and the process is repeated (133; 134).

A weave texture is repeated in both directions (machine and cross), and this repeating pattern defines the minimum unit multiplication, which builds up the woven textile. There are three basic weave patterns: plain, twill and satin weave. Plain weave, depicted in Figure 2.4, is the most basic, the tightest and the most resistant pattern to in-plane shear movement with low drapability (135; 136). For these reasons, the plain weave was chosen.

The weaving machine used to produce the woven fabrics was a Narrow weaving Jakob Müller NH2 53 (Figure 2.5). The spools were placed in the creels and inserted into the machine. The same procedure was done with the BIO4M® yarn. The weft density was set to be 30 yarns/cm, and a modified plain weave pattern, as shown in Figure 2.6, was produced to achieve a single thick layer that would provide good mechanical properties. For this purpose, a kind of 4-layer plain weave was

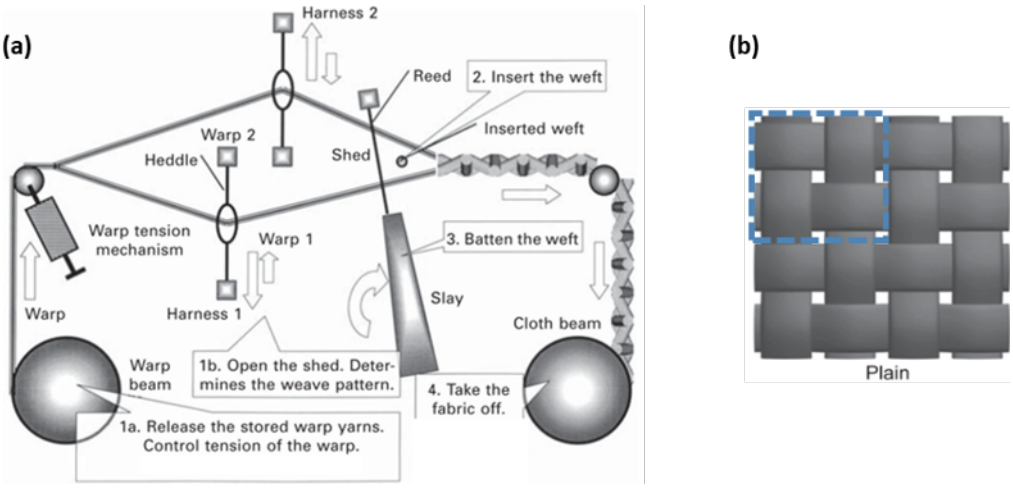


Figure 2.4: (a) Schematic diagram of a weaving loom adapted from (133) (b) Plain weave, dashed blue represents the unit cell adapted from (135).

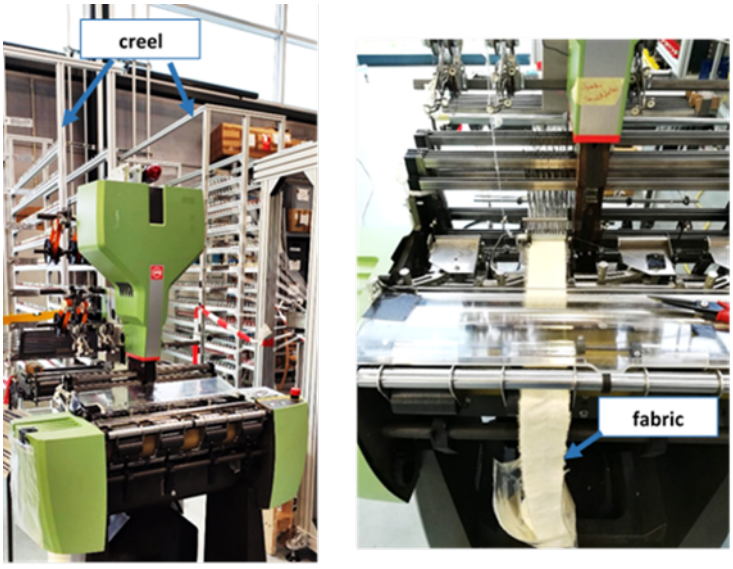


Figure 2.5: Narrow weaving Jacob Muller NH2 53.

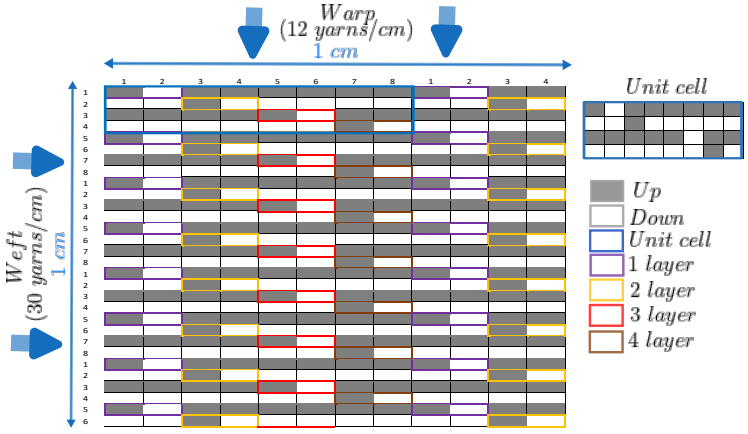


Figure 2.6: 2D sketch of the fabric architecture (10 mm × 10 mm).

conceptualised through the thickness of the weave. The first two warp yarns would belong to the first layer, one up and one down, and all of the other yarns in this layer would be up. The $3^{rd}$ and $4^{th}$ warp yarns belonging to the second layer (also $3^{rd}$ up and $4^{th}$ down ), and all the other yarns in this layer would be down (instead of being up as in the $1^{st}$ layer ), meaning that when the weft yarn is placed. The reed is pulled in; this second layer would go below the $1^{st}$ layer, giving thickness to the fabric. The same happens with the $3^{rd}$ layer and the $4^{th}$ layer. The final weave appears like an eight-harness satin weave (3 counts/mm) in the warp direction, while a standard plain weave (1 yarn/mm) was used for the weft direction. Tapes of 57 mm in width and 2 ± 0.10 mm in thickness containing two layers of the hybrid PLA/PCL tapes were produced and, in the case of the PLA-PLA tapes, presented the same thickness and 50 mm in width. After manufacturing, all the tapes were stored in a vacuum bag under refrigerated conditions to avoid any water uptake from the environment.

## 2.4 Compression moulding

This last step to manufacture the composite is compression moulding or consolidation by hot pressing, one of the standard manufacturing processes for thermoplastic composites. It consists of heating, consolidation and cooling, and the primary process variables are hold time, temperature and pressure. Compression moulding is a process with reduced cycle time, reasonably cheap and allows the production of composites with different shapes. However, the required equipment, hot press and mould are still expensive for some applications (104; 136).

The hot pressing process occurs in two stages. Initially, the material conforms

to the lower part of the mould while the upper part compresses the fabric and the temperature increases. In the second stage, the fibres with low melting temperatures in the commingled yarns melt, and a microscopic flow wets out the fibres with high melting temperatures. In thermoplastic polymers, its high melt viscosity can lead to difficulties in matrix penetration into the fibre preform, resulting in poor fibre wetting and adhesion. Hence, a significant decrease in viscosity is necessary, and the matrix polymer is heated above its melting temperature, T$m$. Nevertheless, precise processing temperature control is critical during composite consolidation. Overheating may lead to a sharp reduction of fibre properties while insufficient heating may result in low adhesion strength between fibre and matrix (82; 131; 137).

Proper processing pressure and holding time can also help to improve the matrix penetration and matrix-to-fibre adhesion or achieve the desired level of crystallinity or transcrystallinity in semicrystalline polymer matrices. However, the reinforcement fibres will become misaligned if the pressure significantly increases during consolidation. Moreover, the manufacturing process becomes efficient if the consolidation time is shorter (138).

The rate of impregnation is also affected by the fabric structure, the yarn dimensions and shape, the number of fibres per yarn, the fibre diameter and the quality of commingling. After the hold time, applying pressure during the cooling ( below the glass transition temperature) is also essential to prevent residual stress generation, degrading the composite's mechanical properties (82).

A hot-press from Fontijne Grotnes (model TP400, the Netherlands) was used for the consolidation of the PLA-PCL and PLA$_{HM}$-PLA$_{LM}$ woven fabrics. Three layers of the woven textiles, Figure 2.7 a), were sandwiched between the male (top) and female (bottom) steel mould as shown in Figure 2.7 b). The number of layers was chosen to achieve a laminate at least 2 mm in thickness. The temperature, pressure and holding time were varied to determine the processing parameters required to produce fibre-reinforced composites with optimum mechanical properties.

As mentioned previously, the lower limit of the processing temperature window for the PLA-PCL woven composite is the minimum temperature required for melting or softening the matrix to provide sufficient wetting and interfacial bonding. The upper limit refers to the onset of the melting peak of the reinforcement fibre. Differential Scanning Calorimeter (DSC) results showed that the melting temperature of the PCL fibre was 64 °C (lower limit) and that the onset temperature for the PLA was 160 °C. With this material, one set of parameters was tested, as can be seen in Table

2.1.

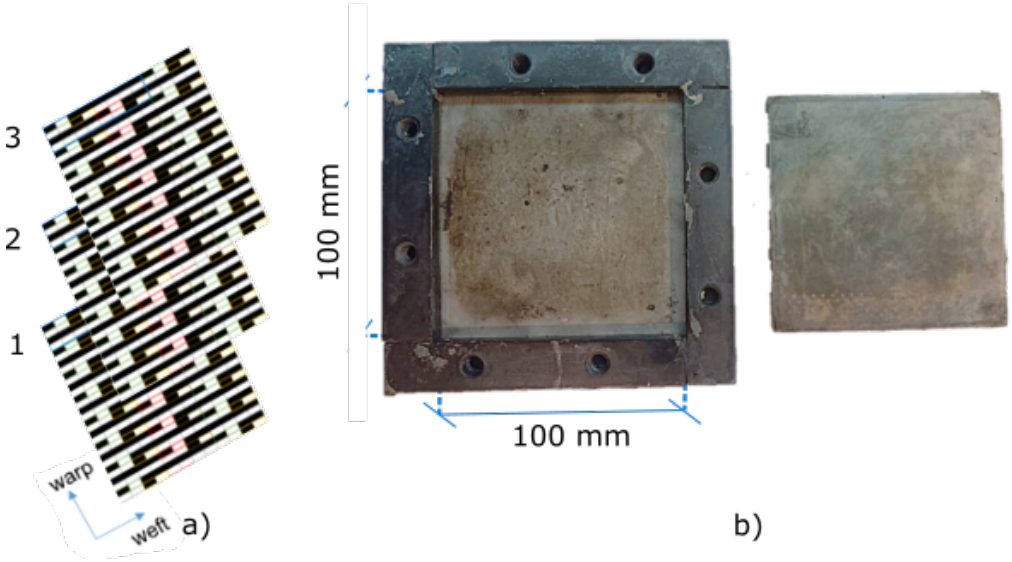


Figure 2.7: a) Schematic how the three layers of weave are introduced in mould b) Steel mould used in the production.

Table 2.1: Experimental parameters to manufacture PLA-PCL composite laminates

| **Heating rate** (°C/min) | **Cooling rate** (°C/min) | **Temperature** (°C) | **Holding time** (min) | **Pressure** (MPa) | **Layers** |
|---|---|---|---|---|---|
| 10 | 1 | 110 | 10 | 2 | 3 |

Previously, a heat treatment was performed on the PLA (reinforcement yarns), and it was discovered that greater temperatures would result in a drop in mechanical performance, which is why 110 °C was chosen.

Regarding $PLA_{HM}$-$PLA_{LM}$ woven composite, the heating and cooling rates were set to be 10 °C/min and 1 °C/min, respectively. The heating rate was chosen according to values found in the literature (66; 104; 137; 114). Due to equipment constraints, the cooling rate was set at 1 °C/min. It was evident from the DSC results that the onset of melting of the PLA filament with low melting temperature was 140 °C. The onset temperature of the PLA with high melting temperature was around 165 °C. Thus, the lower limit and upper limits of the processing temperature window were set at 145 °C and 165 °C. Table 2.2 summarises the different sets of processing parameters used with this material.

The compaction pressure was set to 2 MPa according to the results in the literature (66; 104; 137; 114). The holding time was set between 10 and 20 minutes. Such

Table 2.2: Experimental parameters to manufacture PLA-PLA composite laminates

| **Heating rate** (°C/min) | **Cooling rate** (°C/min) | **Temperature** (°C) | **Holding time** (min) | **Pressure** (MPa) | **Layers** |
|---|---|---|---|---|---|
| 10 | 1 | 145 | 10 | 8.66 | 4 |
| 10 | 1 | 145 | 10 | 2 | 3 |
| 10 | 1 | 160 | 10 | 2 | 3 |
| 10 | 1 | 155 | 10 | 2 | 3 |
| 10 | 1 | 155 | 10 | 2 | 3 |
| 10 | 1 | 150 | 10 | 2 | 3 |
| 10 | 1 | 150 | 20 | 2 | 3 |
| 10 | 1 | 155 | 20 | 2 | 3 |
| 10 | 1 | 160 | 20 | 2 | 3 |
| 10 | 1 | 165 | 20 | 2 | 3 |

variation was intended to understand if increasing the holding time would induce higher crystallisation and better mechanical properties. Three layers of the woven textiles, $[0°]_3$, were sandwiched between the male (top) and female (bottom) steel mould. For producing PLA-PCL composites, heating and cooling rates were set to be 10 °C/min and 1°C/min, respectively. Consolidation was done at 110 °C for 10 minutes and with 2 MPa. Regarding the PLA-PLA composite, a temperature of 165°C for 20 minutes at 2 MPa was used during the consolidation process.

In order to check if the quality of the composite was good and to check the best combination of manufacturing parameters a first screening was carried out using ultrasonic scans, tensile tests and observation of the cross-sections in the optical and scanning electron microscope.

The ultrasonic inspection was performed by an automated C-Scan ultrasonic scanning (TRITON 1500, Tecnitest). This equipment was used to detect internal defects in the composites (resin-rich regions, voids or cracks). The specimens were immersed in a water bath, and a probe of 5 MHz was used.

The cross-sections of the composites were prepared by mounting the laminates into epoxy resin and then through grinding and polishing processes. P600, P800 and P1000 sandpaper were used for grinding for 1 minute and 30 seconds each to remove the epoxy above the sample and possible bubbles. 9, 3 and 1 $\mu$m cloths were used for polishing with diamond past and lubricant for 2 minutes. This process was

repeated till obtaining a clear image of the cross-section. The polished cross-sections were examined in an OLYMPUS BX51 optical microscope.

The tensile properties of the composite woven materials (PLA-PLA and PCL-PLA) were obtained according to ISO/DIS 527-4 "Test conditions for isotropic an orthotropic fibre-reinforced plastic composites" (139) standard although with reduced coupon dimensions according to the plate dimensions. Tests were carried out without using end tabs and gripped only with sandpaper. The static tensile tests were performed at a 2 mm/min cross-head rate using a desktop Instron 5966 testing rig equipped with a 2 kN load cell at room temperature and pre-tension of 10 N. Each composite had 4/5 specimens being tested to characterise the experimental variation of the mechanical properties. Each specimen had 10 mm of width, with approximately 30 mm of initial distance between grips and about 2 mm thickness. The strain values were read from an Instron 12.5 mm gauge length resistive extensometer.

The tensile fracture areas of the composites were examined using an Apreo 2 S LoVac (ThermoFisher, Scientific). They were coated with a gold layer to make the samples conductive and reduce the charge effect. Also, a reduced voltage of 5kV was used for the same reason.

Finally, the consolidation process of the PLA-PCL composite was carried out done at 110 °C for 10 minutes subjected to a pressure of 2 MPa. The combination of parameters that resulted in the best properties the PLA-PLA composite were 165°C for 20 minutes subjected to a pressure of 2 MPa.

# Experimental techniques

# 3

Both the PLA-PCL weave and composite and the $PLA_{HM}$-$PLA_{LM}$ weave and self-reinforced composite were evaluated and examined in terms of degradation properties (structural, mechanical, thermal properties), void content and microstructure. The following sections describe experimental techniques to characterise the materials produced.

## 3.1 Thermal, mechanical and degradation characterisation

### 3.1.1 Yarns Characterization

The tensile properties of the PLA and PCL separately and of commingled PLA/PCL yarn and BIO4M® yarn were determined according to DIN EN ISO 2062 by using a STATIMAT 4U (Textechno, Herbert Stein GmbH  Co. KG Textile Mess- und Prüftechnik, Mönchengladbach, Germany) equipped with a 100 N load cell. Tensile tests were carried out on 30 yarns of 250 mm length in a climate testing chamber as per DIN EN ISO 13 (23 °C). A strain rate of 250 mm/min was used in the tensile tests with an initial pre-load of 2,0 cN/tex for the texturised (BIO4M® ) and commingled yarns and 0,5 cN/tex for the multifilament yarn (PLA and PCL). The solid cross section of the yarn is given by $S = \lambda/\rho$, in which the measured linear density of the PLA/PCL yarns was d=188 tex (g/1000 m) and $\rho_{yarn}$ the bulk density of the yarns, $\rho_{PLA} = 1250 Kg/m^3$ ,was calculated from the density of both polymers ($\rho_{PLA} = 1250 Kg/m^3$ and $\rho_{PCL} = 1140 Kg/m^3$) taking into account that the PLA/PCL ratio was 3/1.

### 3.1.2 Woven fabrics and composites characterization

#### 3.1.2.1 X-ray computed microtomography

The textile's woven architecture was analysed by X-ray computed micro-tomography in a Phoenix Nanotom using a Mo target and 0-mode nano focus. The voltage of the X-ray tube was set to 60 kV, and the current was 200 $\mu$A, rendering a resolution of 11 $\mu$m per voxel.

#### 3.1.2.2 *In vitro* degradation tests

Coupons of $10\times10$ mm$^2$ were cut from the tapes and coupons, and *in vitro* degradation tests were carried out by fabric and composite immersion in PBS fluid with an initial of pH 7.2 at 37°C and 50°C following ISO 13781. 37°C is the actual physiological temperature, while 50°C was selected to accelerate the degradation rate of the materials, as employing an accelerated testing methodology provided insight into the anticipated outcomes at 37°C following an extended period.

**Mass and pH evolution**

For each testing condition (temperature and immersion time), three $10 \times 10$ mm$^2$ specimens were placed in a flask containing 30 mL of PBS per gram of material. The degradation process was studied at 2, 8, 16, 22, 30, 40, 50, 80 and 160 days. The PBS solutions were not changed during the degradation experiment, considering that this would reflect the worst scenario possible. The pH of each solution was recorded at each point in time. The dry mass of the specimens was determined after placing them in a desiccator for 48 hours and was compared with the initial mass.

**Molecular weight evolution**

Gel Permeation Chromatography (GPC) (2414 system from Waters), including a Waters 2424 refractive index detector, measured the molecular weight evolution during degradation. The eluting solvent was tetrahydrofuran (THF), and the instrument was calibrated with a set of narrow polystyrene standards before testing.

**Thermal behaviour**

The thermal behaviour of both the PLA and PCL fibres before commingling and the BIO4M® material before and after degradation was assessed using differential scanning calorimetry (DSC) on a Q200 instrument from TA Instruments. The samples were heated from room temperature to 200°C at a heating/cooling rate of 10°C/min in a $N_2$ atmosphere. The first heating (cycle 1) provides information

about the effect of the PBS solution (degradation fluid) on the physical properties of the materials that may lead to changes in the glass transition temperature ($T_g$), the cold crystallisation temperature ($T_{cc}$) and the melting temperature ($T_m$). This first heating removes the thermal history of the material, and the behaviour of the subsequent cooling cycle is only affected by the chemical changes in the polymers that occurred during the degradation process and the exothermic peaks due to crystallisation $T_c$ were determined in the cooling cycle. Finally, the re-heating (third cycle) was used to confirm any chemical degradation as a modification of $T_g$, $T_{cc}$ or $T_m$. These points were analysed, as well as enthalpy of fusion ($\Delta H_{\text{melt}} J/g$) were analysed using the Universal Analysis software (TA Instruments). The degree of crystallinity of the fibres was estimated as the ratio of the actual melting enthalpy $\Delta H_m$ to the theoretical one for 100% crystallinity (93 J/g for PLA (140) and 139 J/g for PCL (141)).

$$\%Crystallinity = \frac{\Delta H_{melt}}{\Delta H_{f100\%}} \times 100 \tag{3.1}$$

**Mechanical behaviour**

The mechanical behaviour of the woven samples in the air at room temperature was determined using uniaxial tensile tests in the warp direction following the guidelines in ISO 13934 (142). However, the fabric width was increased to 57 mm and 50 mm ( for PLA-PCL weave and PLA-PLA weave, respectively ) to grip the samples for the mechanical tests. At least six specimens were tested to consider the variability of the mechanical performance of the fabrics.In the case of the composites, the mechanical tests, which were performed by ISO/DIS 527-4, using a dog bone specimen with a width of 10 mm, an initial distance between grips of approximately 30 mm, and a thickness of approximately 2 mm.

The tensile tests were performed at a 10 mm/min crosshead rate using a desktop Instron 5966 testing rig equipped with a 2 kN load and a pre-load of 10 N. The strain values were measured using digital image correlation (DIC) (Correlated Solutions VIC-2D) from the optical images acquired with a digital camera at a rate of 2 images per second. However, because of the lack of correlation for high strains, DIC was only used to determine the elastic deformation of the material prior to the peak load. The deformations after the peak load were estimated from the crosshead displacement of the machine and the initial distance between the grips.

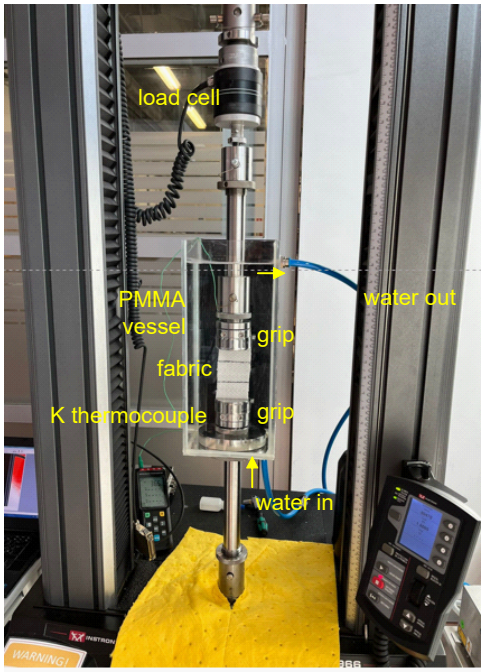


Figure 3.1: Experimental set-up used for the tensile tests in water at 37°C. Water re-circulation is carried out with an external pump. Specimens and grips are totally immersed in water. A transparent recipient is used to acquire images with a camera to measure deformations by digital image correlation.

The woven textiles were graded by introducing samples of 160× 57 or 50 $mm^2$, and the composites by introducing samples 75× 10 $mm^2$ in flasks with the PBS solution with the same concentration of 30 mL per gram of material. Degradation tests were conducted at different temperatures (37°C and 50°C) and at different times (40, 80, and 160 days of immersion). Six samples were used for each immersion time and temperature, and they were tested in uniaxial tension with the samples immersed in water at 37°C. Irrespective of the temperature used for material degradation, tests were carried out at 37°C. The experimental set-up is formed by a vessel containing plain water re-circulated at 37°C, as shown in Figure 3.1. The re-circulation flow was low to ensure reduced turbulence that could result in interferences with the digital image correlation system to measure the strain. In addition, tensile tests of as-manufactured textile and composite samples were carried out after 24 hours of immersion in water at 37°C using the same experimental set-up for comparison with the degraded samples (143). The PLA-PLA weave degradation at 50 °C was not conducted due to the change in sample shape. The experiments were conducted in an immersed state at 37°C because this closely mimics in-vivo conditions. Numerous

studies have shown considerable reductions in mechanical properties when testing in an aqueous environment at 37°C compared to dry conditions (144).

## 3.2 Biocompatibility tests

Additionally, according to the guidelines for producing absorbable polymeric implants, biocompatibility tests are the most critical ones to provide information about the viability of cells in contact with the materials (145). Appropriate biocompatibility provides cell attachment, allowing cells to function normally with effective cell migration to the implant site and enabling cell proliferation (85).

Cytotoxicity assays include a direct test, which provides a qualitative analysis to access the cell morphology and cell attachment, and an indirect test, which provides a quantitative analysis of the cytotoxicity of a material. For the abovementioned purpose, the tests were performed using the guidelines outlined in the International Standard ISO 10993-5 and ISO 10993-12.

Four different types of samples were tested: a woven fabric produced with a hybrid yarn of PLA and PCL, and a hot pressed laminate produced from the PLA/PCL, a woven fabric a dry woven fabric produced with a hybrid yarn ($PLA_{HM}$/$PLA_{LM}$), a hot pressed laminate produced from the $PLA_{HM}$/$PLA_{LM}$ woven fabric.

### 3.2.1 Indirect test

Pre-osteoblasts cell line from mouse calvarial MC3T3-E1 sub-clone 4 (ATCC CRL-2593) were cultured in a complete medium consisting of alpha-MEM (Invitrogen, USA), 10% of fetal bovine serum (FBS) (Invitrogen, USA), and 100 U/ml of penicillin and 100 $\mu$g/ml streptomycin (Pen/Strep, Invitrogen, USA). Cells between passages 11 and 13 were used for the experiments and kept at 37 °C in a humidified incubator (5% $CO_2$ and 95% atmosphere). The medium was renewed every two days, and cells were used after reaching 90% of confluence.

The cytocompatibility of the samples was evaluated by measuring the mitochondrial activity by the MTT (3-(4,5-dimethylthiazol-2-yl)-2,5-diphenyl tetrazolium bromide) assay. Initially, the sample was immersed in 70% ethanol for 10 min and then washed with PBS. Afterwards, the sample extracts were prepared by immersion in a complete culture medium at a 0.1 g/mL ratio and 37°C for 72h. The samples were then removed, and the extract was transferred to a reaction tube and stored at 4°C. In parallel, cells were seeded at a concentration of 5.000 cells/$cm^2$ for 24

h. Afterwards, the culture medium was removed and replaced with two-fold serial dilutions of the extract (100%, 50%, 25%, 12.5%, 6,25%, and 3.125%). Then, cells were incubated at 37°C, and after 24h, the extract was replaced with fresh culture medium containing MTT (Sigma-Aldrich, Germany) at 5mg/mL in a proportion of 10 $\mu$l per each 100 $\mu$l of medium and incubated at 37°C for three h. The medium was then removed, and Dimethyl Sulfoxide (DMSO, Sigma-Aldrich, Germany) was added to dissolve the formazan crystals. The absorbance value was measured using a spectrophotometer (Tecan Infinite Mplex) at 570 nm and normalised to the control readings. The negative control for cytotoxicity was for cells without exposition to any extract. The experiments were performed in triplicate.

A simplified schematic of the indirect test is represented in Figure 3.2.

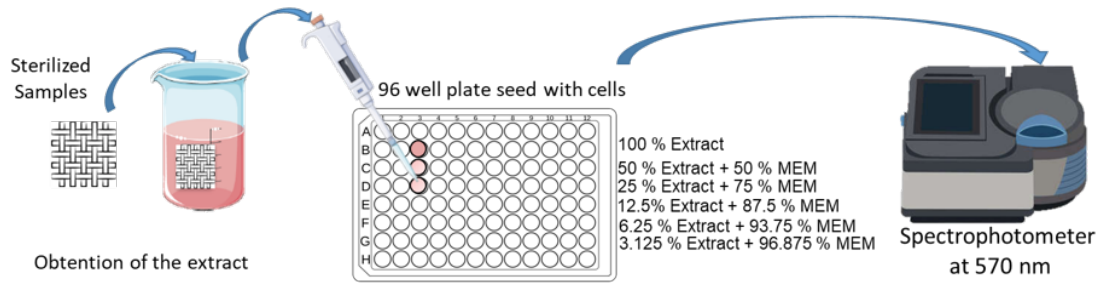


Figure 3.2: Simplified schematic of the indirect test

### 3.2.2 Direct test

Cell-material interaction was studied on the four samples with dimensions $10 \times 1 \times 1\text{mm}^3$. They were cleaned in ethanol, as described above, and MC-3T3 cells were directly seeded on the surface at a concentration of 10.000 cells/cm$^2$. They were incubated at 37°C for 24h and fixed with 4% paraformaldehyde (Sigma-Aldrich, Germany) solution for 30 min. Two different experiments were performed: an immunofluorescence staining to observe cell morphology and their cytoskeleton organisation and an observation by Scanning Electron Microscopy (SEM) to analyse the direct interaction between cells and the material. For the cytoskeleton staining, the fixed cells were treated with 0.5% of Triton X-100 (Sigma) for 10 min. Afterwards, cells were washed three times with PBS and incubated at room temperature for one hour in a dilution of 1:300 for Alexa Fluor-488 Phalloidin (A12379, Invitrogen, USA) and 1:1000 for DAPI (D9542, Sigma, Germany). Finally, cells were washed and observed under a fluorescence microscope (Olympus FV3000, Japan) at 20X magnification.

The sample preparation for SEM observation consisted of a dehydration process using serial solutions of 30%, 50%, 70%, 80%, 90%, and 100% of ethanol for 15 min each. Finally, the samples were air-dried, sputter-coated with gold, and observed by SEM (Zeiss EVO MA15, Germany).

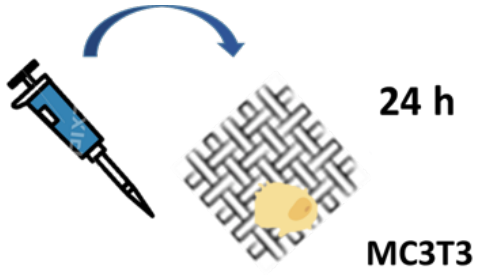


Figure 3.3: Simplified schematic of the direct test

### 3.2.3 Contact angle measurement

Contact Angle (CA) measurements were performed in a Drop Shape Analyzer (DSA25E, Krüss, Germany) with Type II water and a complete culture medium (the same medium used for the cell tests). A 3$\mu$L sessile drop of each liquid was deposited on the materials. The free surface energy was calculated from Neumann's equation,

$$\cos\Theta_L = 2(\gamma_S/\gamma_L)^{0.5}\exp\left[-\beta(\gamma_L-\gamma_S)^2)\right] - 1 \tag{3.2}$$

where $\Theta_L$ is the CA measured in the surface of the fabric, $\gamma_S$ the surface free energy of the solid, $\gamma_L$ the liquid surface tension and $\beta$ an empirically set coefficient related to a specific solid surface ($\beta \approx 1.247 \times 10^{-4}$)(146).

# Woven textiles properties 4

## 4.1 PLA-PCL woven textiles

The PLA-PCL fabric is composed by commigled yarns of PLA:PCL in a ratio 3:1. The woven architecture of the textile was analyzed by means of X-ray computed micro-tomography. The microstructure of the textile in different planes and with different magnifications is shown in Figure 4.1. It depicts clearly the fiber yarns (white regions) and the porosity (black regions) between yarns. The porosity of the woven PLA-PCL was 35% and can be categorized into interconnect porosity, establishing a connection with the surface, porosity existing between fibres, and within bundles of fibres. The interconnect and in-between bundle of fibre porosities are of particular significance, as they facilitate the ingress of cells and nutrients into the material. The pores and canals created exhibit dimensions in the 200-300$\mu$m, aligning with the recommended pore diameter range (50 to 710 $\mu$m) for bone regeneration. It is crucial to underscore that the optimal pore size for tissue regeneration depends on the specific tissue type. Kramschuster *et al.* (2013) suggests that macropores ranging between 150 and 350 µm are optimal for bone regeneration. For fibrocartilaginous tissue production, recommended pore widths fall within the 200 to 300 µm range, while neovascularization necessitates smaller pores in the order of 5 µm (147).

The top view and the cross-section of the PLA-PCL textile are depicted in Figure 4.2. The white agglomerated sections are the result of a laser cut performed on the materials to prevent unfolding. A two-layer weave is produced because of the type of weaving machine used and the manner the weft yarn is utilized to bind the edge (Figure 4.2b).

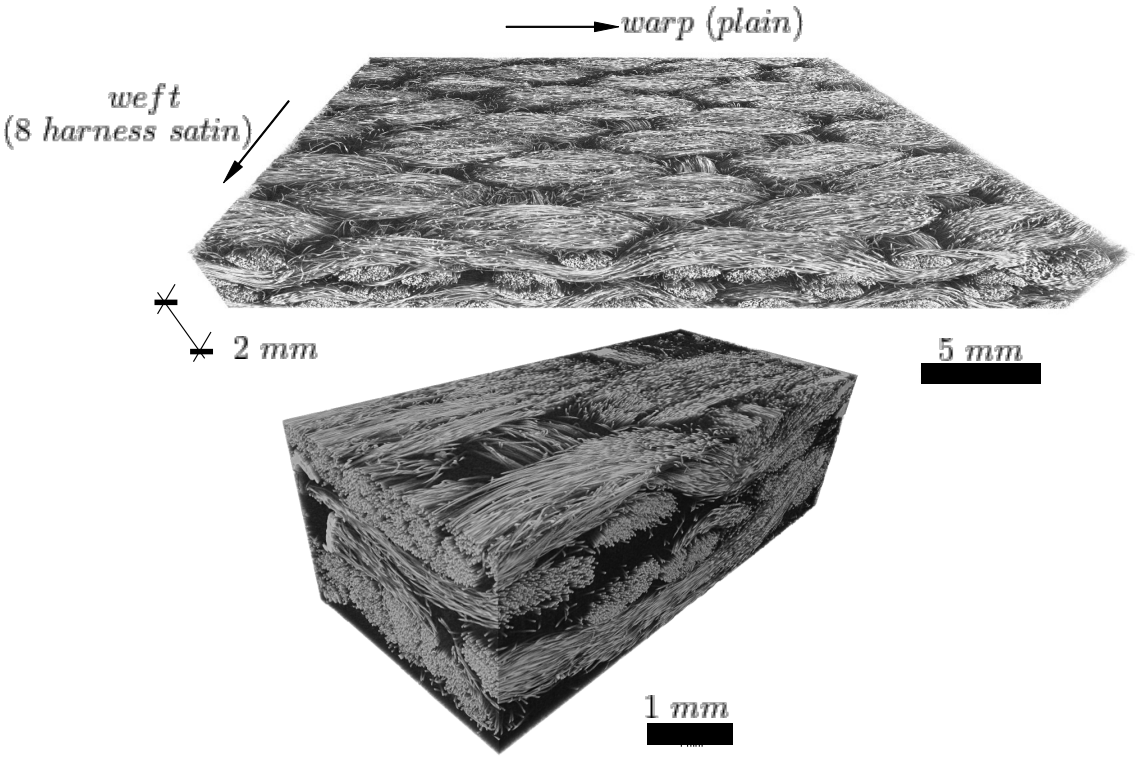


Figure 4.1: X-ray tomograms of the PLA-PCL fabric at different magnifications and planes.

### 4.1.1 *In vitro* degradation tests

The evolution of the dry mass of the fabric and the average and the standard deviation of the pH of the solution in three samples are plotted in Figures 4.3 a and b, respectively, as a function of the immersion time at 37°C and 50°C. The dry mass was kept constant during 160 days in the samples immersed in PBS at 37°C. The pH also remained constant (around 7) for 80 days, and the initial oscillations in the pH were due to PBS evaporation during the experiments because some of the flasks were not hermetic. Nevertheless, the pH decreased $< 4$ after 160 days. This reduction indicates polymer hydrolysis, releasing lactic acid, but the mass of the polymer degraded was not large enough to induce noticeable changes in the dry mass. The samples immersed at 50°C showed a dry mass loss of 20% after 160 days, which was also associated with a pH reduction due to polymer hydrolysis.

The dry mass and pH changes were consistent with the optical appearance of the textile samples after immersion. The as-produced textile weaves were white and flexible (Figure 4.4a). The samples immersed in PBS at 37 °C (Figure 4.4b) did not show any relevant change in the colour, shape or size compared to the as-

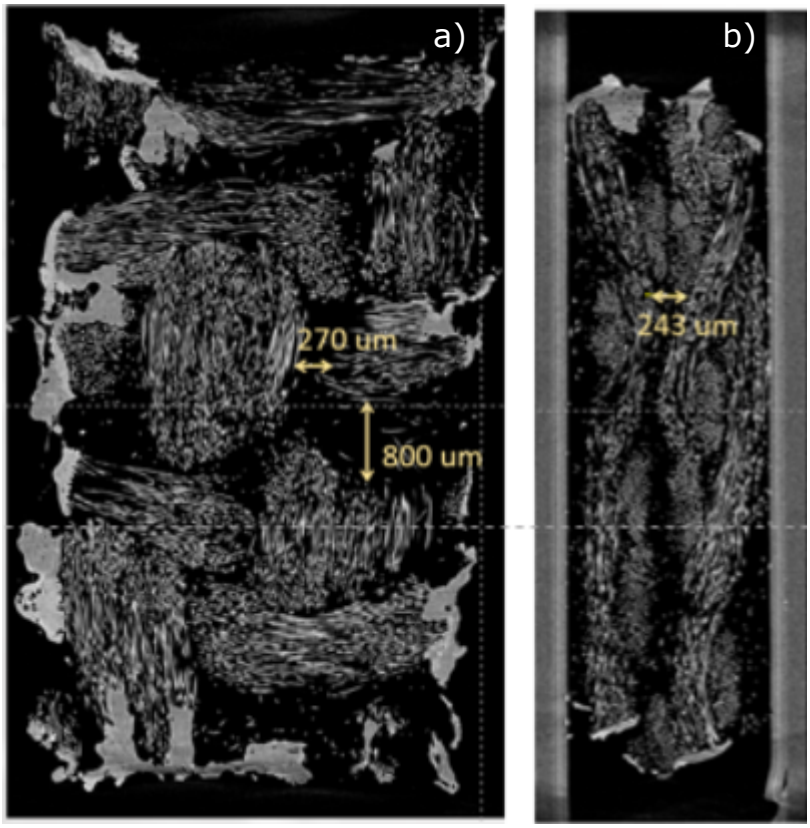


Figure 4.2: a) top view and b) and cross section images obtained by XCT of the PLA-PCL weave. The fabric thickness is 2 mm .

manufactured ones. However, the naked eye could appreciate the degradation of the samples immersed in PBS at 50°C during 160 days (Figure 4.4c). The samples were surrounded by debris (marked with red arrows), and the fabric flexibility decreased, probably indicating degradation products restricting the relative mobility of the filaments in the textile yarns.

The thermal properties of the yarns and fabrics were evaluated by DSC and GPC. The glass transition temperature, the melting temperature and the enthalpy of melting of PLA fibres measured by DSC were $T_g = 64°C$, $T_m = 174°C$ and $\Delta H_m = 55J/g$, respectively. In the case of the isolated PCL yarns, the glass transition temperature was not observed in the DSC tests while $T_m = 64°C$ and $\Delta H_m = 79J/g$. The degree of crystallinity of both fibres was estimated as the ratio of the actual melting enthalpy $\Delta H_m$ to the theoretical one for 100% crystallinity (93 J/g for PLA (140) and 139 J/g for PCL (141)) resulting in similar values of 60 and 56% for PLA and PCL, respectively.

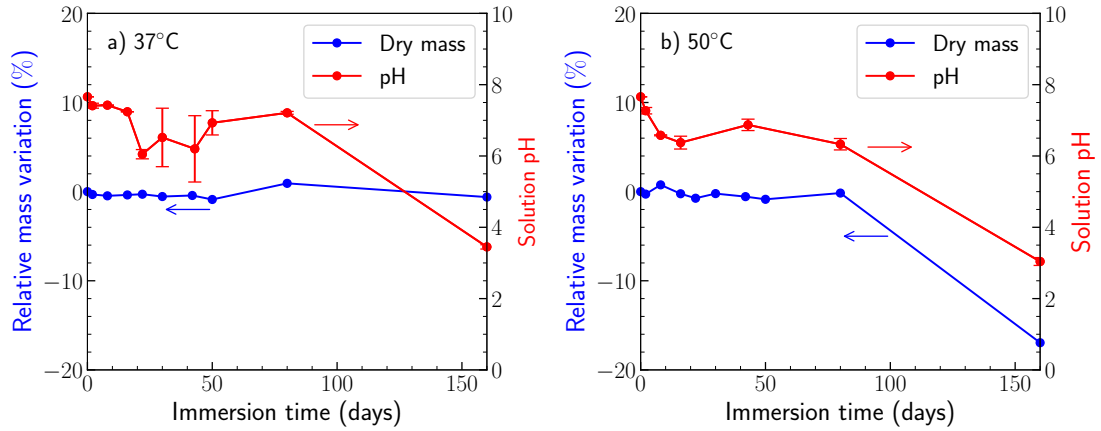


Figure 4.3: Evolution of the dry mass of the PLA/PCL woven samples and the pH of the PBS solution as a function of the immersion time at: a) 37°C, b) 50°C.

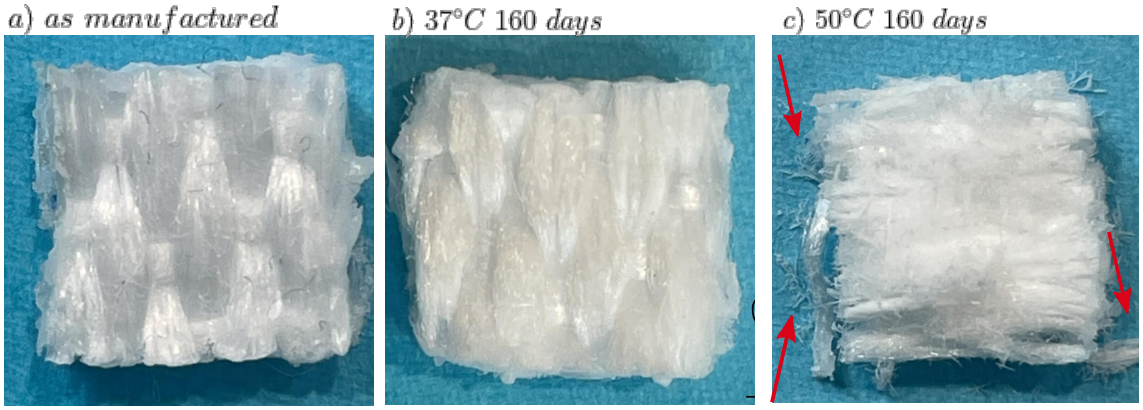


Figure 4.4: Optical appearance of PLA-PCL woven textile. (a) As manufactured, mass loss =0%, pH=7. (b) After 160 days of immersion in PBS at 37°C, mass loss =1%, pH = 3.5. c) After 160 days of immersion in PBS at 50°C, mass loss =17%, pH = 3.0. The red arrows show the debris around the textile.

The heating-cooling-reheating curves of the woven fabrics are depicted in Figure 4.5a and b after immersion in PBS at 37° and 50°C, respectively, up to 160 days. The glass transition temperature of the PLA fibres was $T_g^{PLA} = 64$°C which overlapped with the melting point of the PCL yarns. No significant differences in the heat flow curves of the woven textiles degraded at 37°C were found as a function of the immersion time in PBS (Figure 4.5a). A very small cold PLA crystallisation peak is observed at $T_{cc}^{PLA} \approx 92$°C in the material degraded at 37°C in the first heating step, regardless of the degradation time. The final endothermal peak corresponding to the PLA melting was observed at $T_m^{PLA} = 174$°C for the as-manufactured material and

decreased slightly to 171°C when the material was immersed 160 days. During the cooling step in the DSC test, two exothermic transitions were visible corresponding to the PLA and PCL crystallisation processes ($T_c^{PLA} \approx 105$°C and $T_c^{PCL} \approx 32$°C). Nevertheless, no discernible effect of the immersion time was observed. Finally, the temperatures of the PLA and PCL melting peaks in the last heating cycle were slightly lower than those measured in the first heating cycle. However, this difference could be attributed to the PBS evaporation after the first heating cycle and to the different processing methods. The cold crystallisation peak was also not visible in the last heating cycle, indicating that all the crystals were melted. In summary, PLA and PCL were not degraded after 160 immersion days at 37°C.

These results are in agreement with the literature data. Weir *et al.* (54) reported a mass loss of 1% for Poly(L-lactide) PLLA manufactured by compression moulding after more than 1 year on immersion in PBS at 37°C in PBS. This time-lapse before a significant mass loss is consistent with the overall sequence of aliphatic polyester degradation. Water initially enters the bulk of the material, preferentially targeting chemical bonds in the amorphous phase, transforming long polymer chains into shorter ones. Consequently, the molecular weight is reduced without an extensive loss in physical properties. Water diffusion into crystalline regions is slower, delaying the hydrolytic breakdown of the ester bonds in these crystalline regions, which are essential to maintain mechanical properties. In the second step, water diffuses into crystalline regions, and the hydrolytic reaction increases considerably. A decrease follows the reduction in molecular weight in the physical and mechanical properties. Lastly, the chain fragments are attacked by enzymes, resulting in a rapid loss of polymer mass (140; 54; 148). Regarding the PCL degradation, Pitt *et al.* (149) showed that the mechanism of *in vivo* degradation is qualitatively the same as the one reported for PLA and its copolymers. Lastly, Vieira *et al.* (150), investigated various combinations of biodegradable fibres, including PLA-PCL. They noted that even after 16 weeks (approximately 122 days) in PBS at 37°C, there were no significant changes in the weight of the samples composed of these fibres.

The DSC results in the woven samples immersed in PBS at 50°C did show a degradation with immersion time (Figure 4.5b). Firstly, the first endothermal peak during the first heating cycle –attributed to the PCL melting– occurred at 62°C and rose with the immersion time up to 69°C for 160 days. PCL is between its glass transition temperature and melting temperature at 50°C, leading to crystal growth during annealing at this temperature and to an increase in the melting

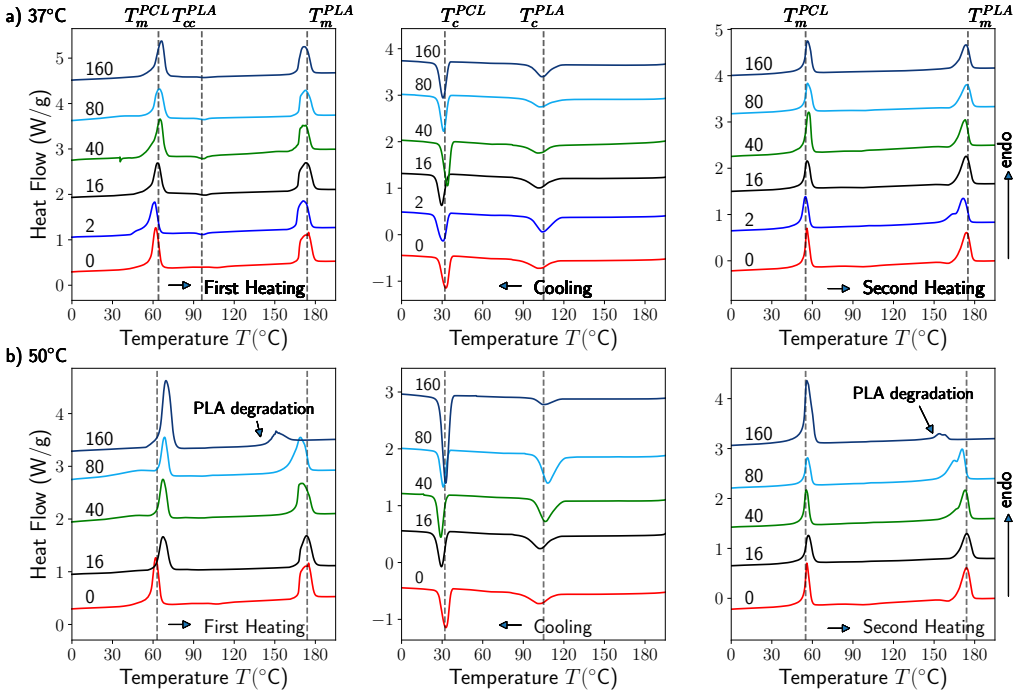


Figure 4.5: Heat flow curves during heating-cooling-reheating steps of the PLA/PCL woven fabric during DSC at a heating/cooling rate of 10°C after immersion in PBS for different number of days (indicated in each Figure). a) After immersion at 37°C, b) after immersion at 50°C. The melting ($T_m^{PLA}$), the crystallisation ($T_c^{PLA}$) and the cold crystallisation ($T_{cc}^{PLA}$) temperatures of the PLA yarns as well as the melting ($T_m^{PCL}$) temperature of PCL yarns are indicated with dashed vertical lines.

temperature. The second endothermic peak for the melting of the PLA decreased in intensity, especially after 80 days of immersion and the melting temperature $T_m^{PLA}$ also decreased from 175 to 151°C with immersion time. During the cooling cycle, two exothermic transitions were also visible, corresponding to the PLA and PCL crystallisation: ($T_c^{PLA} \approx 105$°C and $T_c^{PCL} \approx 32$°C), but no differences were found in these peaks with immersion time. Finally, the annealing time did not affect the melting peak of PCL in the second heating, indicating that the degradation of PCL was limited. On the contrary, the melting peak of PLA in the second heating cycle becomes broader with degradation time, and a double peak is visible after 40 days of immersion. These results indicate an evident degradation of PLA during immersion at 50°C, which is consistent with the mass loss and pH evolution shown in Figure 4.5. Weir *et al.* (151) reported a similar behaviour for PLA at annealing temperature over

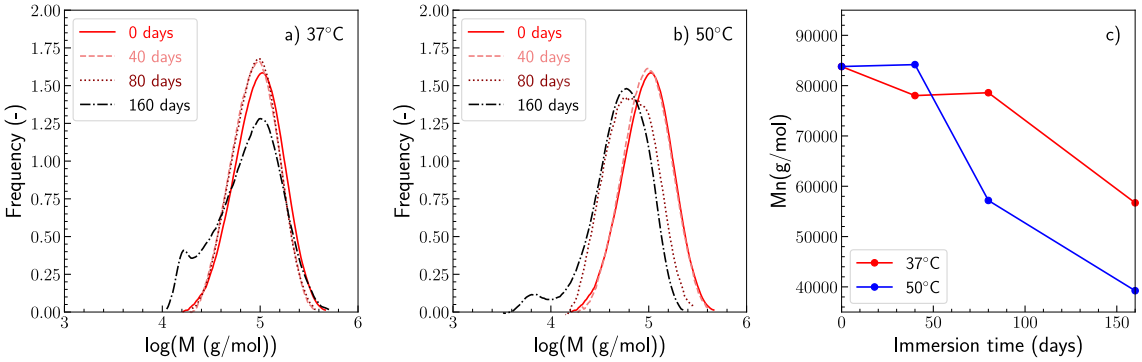


Figure 4.6: Evolution of the molecular weight ($Mw$) distribution of the PLA-PCL fabrics with immersion time at: a) 37°C, b) 50°C; c) Evolution of the number average molecular weight ($Mn$) as a function of immersion time for both temperatures.

glass transition temperature (50°C). After 50 days, they observed higher crystallinity because the hydrolysis in the amorphous region favoured the crystallisation in small crystals. These crystals melt at lower temperatures, appearing as a shoulder of the original peak, which remained unaltered because the pristine crystals were not degraded. Only one melting peak was observed at lower temperatures after 115 days, corroborating that hydrolysis also started in the crystalline regions by reducing their size and, therefore, their melting temperature (152).

The molecular weight $Mw$ distributions of the PLA-PCL fabric degraded at 37°C and 50°C obtained by GPC are plotted in Figure 4.6a and b, respectively. PLA and PCL have different molecular weights (163670 g/mol and 188921 g/mol, respectively) but one broad peak (instead of two) can be seen. No shift in the $Mw$ distribution is observed up to 80 days of immersion time at 37°C and chain scission is only observed at 160 days, leading to a bimodal molecular weight distribution, which is compatible with the degradation of the amorphous regions of PLA. These results corroborate the small drop in the melting point temperature of PLA (from $T_m^{PLA} = 174$°C to 171°C after 160 days of immersion time at 37°C). Broadening of the molecular weight distribution at 50°C is observed after 80 days of immersion (Figure 4.6b) and a bimodal distribution –with a small peak for the lower molecular weights– is found after 160 days, indicating higher degradation due to chain scission.

The number averaged molecular weight $Mn$ evolution with immersion time at 37, and 50°C is presented in Figure 4.6c, corroborating the results presented in the previous paragraph. As expected, the degradation rate was more significant at 50°C, with a 32% decrease in $Mn$ after 160 days at 37°C, in comparison to the 31%

decrease after 80 days at 50°C. These findings were in agreement with the results of the literature. For instance, Hukins *et al.* (153) demonstrated that increasing the ageing temperature by around 10°C approximately duplicates the degradation rate in most polymers. Furthermore, the degradation rate shown in Figure 4.6c demonstrate an initial time in which $Mn$ is maintained, followed by a rapid loss.

*In vitro* and *in vivo* studies on semicrystalline PLLA (54) at physiological temperature revealed that $Mn$ decreased with immersion time, and a substantial reduction of about 80% was reported after 308 days. Other accelerated studies at 50°C on PLLA materials indicated a reduction of 50% in molecular weight after 49 days (154) and a knockdown of 54% was found after 160 days at 50°C. The presence of the PCL, whose degradation is slower, reduces the drop in $Mn$ in comparison with PLLA homopolymer(149).

### 4.1.2 Mechanical behavior

#### Yarns and fabric behaviour

Tensile stress-strain curves of the PLA, PCL and PLA-PCL hybrid yarns were obtained from the load-displacement $P - \delta$ curves recorded during the tests. The nominal stress $\sigma = P/S$ was calculated from the load $P$ and the solid equivalent cross-section of the yarn $S = \lambda/\rho$ obtained from the yarn linear density $\lambda = dtex/10000$ and the bulk polymer density $\rho$. The strain, $\epsilon$, was calculated from the yarn elongation obtained from the cross-head displacement of the machine, $\delta$, and the yarn gauge length $L_0$ as $\epsilon = \delta/L_0$. Representative $\sigma - \epsilon$ curves obtained from three individual tests of PLA, PCL and PLA-PCL hybrid yarns are shown in Figure 4.7a. The averaged tensile properties obtained from 30 yarn tests per condition are presented in Table 4.1. They correspond to the elastic modulus $E$ (initial slope of the stress-strain curve), the yarn strength $\sigma_{max}$, the strain-to-failure $\epsilon_{max}$ and the tenacity $g$ (volumetric energy) defined as the area below the stress-strain curve ($g = \int_0^{\epsilon_{max}} \sigma \, d\epsilon$).

Overall, the PCL yarns presented higher strength and strain-to-failure, but the elastic modulus was significantly lower than that of the PLA yarns. These differences were transferred to the hybrid yarns, whose behaviour was linear and elastic up to the yielding point dictated by the onset of plasticity of the PLA fibres. Then, the stress-strain curve of the hybrid yarn showed a second linear regime with a lower slope than the initial one, ending with the catastrophic failure dictated by the lowest ductility of the PLA fibres. As mentioned, the commingling ratio of PLA-PCL yarns was set to 3 to 1 in manufacturing. Therefore, after the PLA fibre failure, the

PCL fibres in the hybrid yarn could not carry the load transferred from the broken PLA fibres, resulting in a catastrophic failure. This hypothesis was corroborated by comparing the prediction of a simple iso-strain model obtained by averaging PLA and PCL yarns stress for the commingling ratio of 3 to 1, Figure 4.7a. The results of this simple model are plotted as a dashed line that accurately follows the behaviour of the hybrid yarn up to a strain of $\approx 25\%$. After this point, the model predicts the single contribution of the PCL yarns, which was not seen experimentally because of the catastrophic failure. Additionally, the hybrid yarn achieved lower stress than the PLA and PCL yarns because of the loops formed during the commingling process. Its tenacity was also lower because, as already mentioned, the beneficial effect of the PCL is not fulfilled.

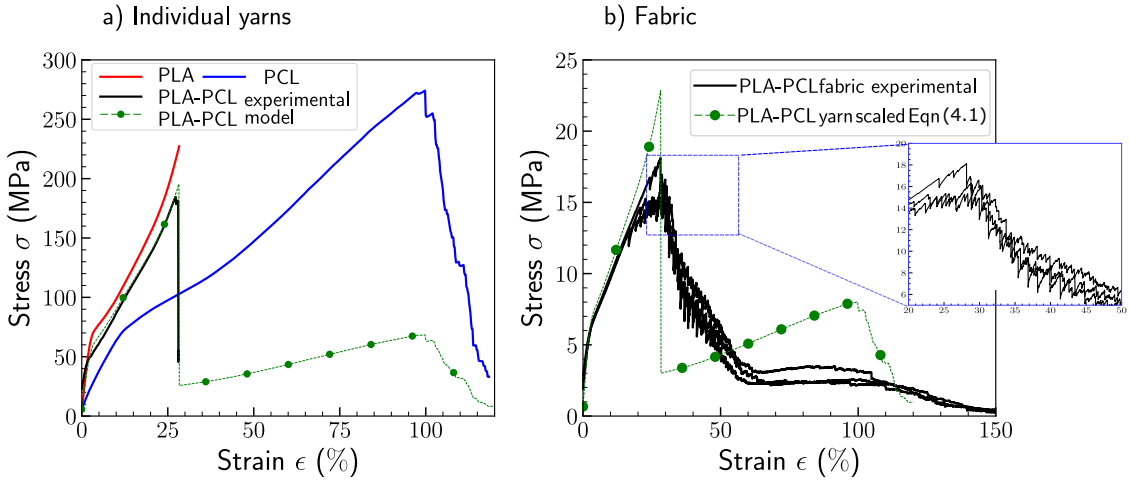


Figure 4.7: a) Tensile stress-strain curves of the PLA, PCL and PLA/PCL hybrid yarns. b) Tensile stress-strain curves of the PLA/PCL fabric. The dotted lines stand for simple iso-strain model prediction obtained by averaging PLA and PCL yarns stress for the manufacturing commingling ratio of 3 to 1.

Table 4.1: Mechanical properties of PLA, PCL and PLA-PCL hybrid yarns

| Yarn | $E$ (GPa) | $\sigma_{\max}$ (MPa) | $\epsilon_{max}$ (%) | $g$ (GPa) |
|---|---|---|---|---|
| PLA | 2.56 ± 0.02 | 220 ± 10 | 28.0 ± 0.9 | 3.5 |
| PCL | 0.54 ± 0.01 | 287 ± 9 | 98 ± 3 | 17.9 |
| PLA-PCL | 1.54 ± 0.03 | 192 ± 7 | 26.9 ± 0.8 | 3.0 |

The three tensile stress-strain curves of the as-manufactured fabrics at room temperature are reported in Figure 4.7b. The stress was calculated from the force recorded by the load cell and a nominal cross-section area of the fabric of $57 \times 1.31$ mm$^2$

while the deformation was obtained from the cross-head displacement and the gauge length of the fabric $L_0 = 90$ mm. It should be noted that the elastic modulus of the fabric was determined with the strain obtained with the digital image correlation system averaged over a region of interest of $57 \times 35$ mm$^2$ in the centre of the fabric.

The fabric behaviour resembled that of the hybrid yarns. The initial elastic region ended at the onset of plastic deformation of the PLA fibre, and the second linear slope was finished by a load drop when the strain-to-failure of the PLA fibres was attained at $\approx 25\%$ of deformation. This mechanism is also observed in the optical image of the deformed fabric (Figure 4.8). Damage (marked with arrows) was initiated at 25% deformation in the external yarns (close to the edges), which carry more deformation because of the geometrically non-linear deformation process. The load drop associated with this failure was not as abrupt as the one observed in the mechanical tests on hybrid yarns, and failure of the fabric was produced by the sequential failure of the individual yarns, which is reflected in the peaks observed at the maximum stress level. After this point, damage spreads progressively throughout the fabric with deformation (Figure 4.8), and the stress drops to reach a plateau of $\approx 3$ MPa, ending with the PCL fibres' fracture in the yarns. It should be noted that more scatter is observed in the secondary part of the deformation process, which was attributed to the damage exerted by the gripping system (e.g. uneven gripping pressure). In summary, the hybrid textiles' fracture occurred in two steps associated with the fracture of the PLA and PCL fibres within the yarns.

The fabric behaviour can also be modelled from the yarn's mechanical properties, assuming that the warp yarns carry out all the load and neglect the weft yarn's contribution. Thus, the fabric stress, $\sigma_{fabric}$ can be calculated as

$$\sigma_{fabric} = \frac{n\lambda}{\rho t}\sigma_{yarn} \tag{4.1}$$

where $n$=1 yarn/mm (warp count), $\lambda = 0.1884$ gr/m is the yarn linear density, $\rho = 1220$ Kg/m$^3$ the bulk PLA/PCL density and $t = 1.31$ mm the fabric thickness. The predictions of eq. (4.1) are plotted as a dashed line in Figure 4.7b. The agreement between this approximation and the experimental results is excellent, bearing in mind the crude simplification of the deformation hypothesis, and demonstrates the consistency between the fracture of the fibres, yarns and fabric. The secondary peak attributed to the PCL yarns in the model is not observed clearly in the experimental curves, which is replaced by a plateau region.

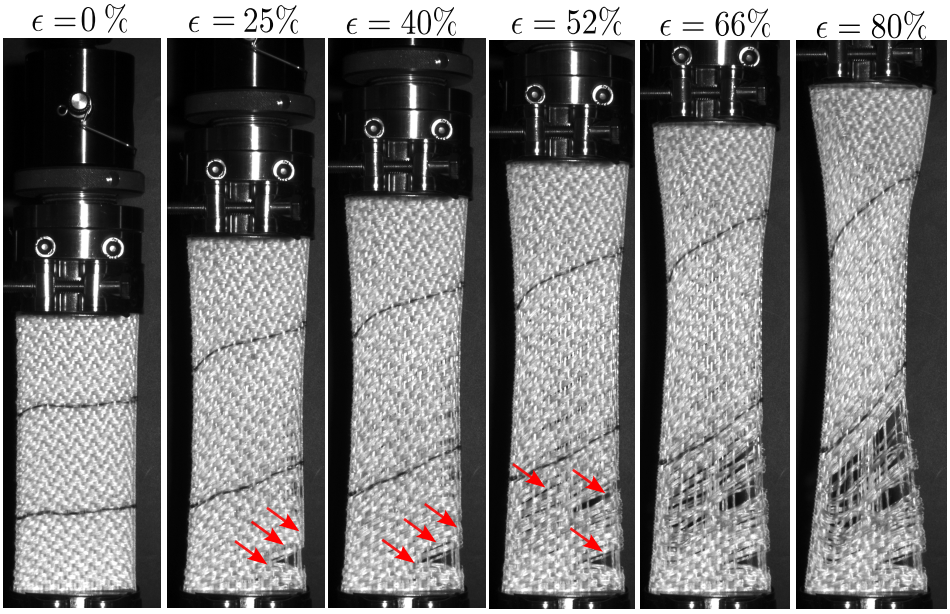


Figure 4.8: Optical images of $90 \times 57$ mm$^2$ as-manufactured fabric coupon subjected to tensile deformation (gauge length between grips $L_0 = 90$ mm) is indicated by the parallel horizontal lines that are progressively curved during deformation.

### Effect of degradation on fabric mechanical behaviour

The fabrics were immersed in PBS flasks at 37°C and 50°C, and the effect of immersion on the mechanical behaviour was assessed by performing tensile tests in immersed conditions at 37°C, irrespective of the degradation temperature during immersion in PBS. The three stress-strain curves after different immersion times are plotted in Figure 4.9a and b for specimens immersed at 37°C and 50°C, respectively. The strength of the as-manufactured fabric tested at ambient temperature in air was $16.6 \pm 1.2$ MPa and it is included in Figure 4.9 as a horizontal dashed line for comparison. Therefore, the reduction of the mechanical properties at 0 days concerning the as-manufactured fabrics should be attributed to the testing temperature (37°C) and to the water absorbed during 24 h of immersion in PBS. Addicionally, as mentioned in previous studies, the aqueous environment can influence mechanical properties by acting as a plasticizer (144). The mechanical properties of the fabric (modulus, strength, and toughness) as a function of the effect of immersion time are summarised in Figure 4.10.

The stress-strain curves of the fabrics degraded at 37°C (Figure 4.9 a), have the same shape, regardless of the immersion time. The initial elastic regime ended when the PLA fibres underwent plastic deformation, followed by a second linear region up

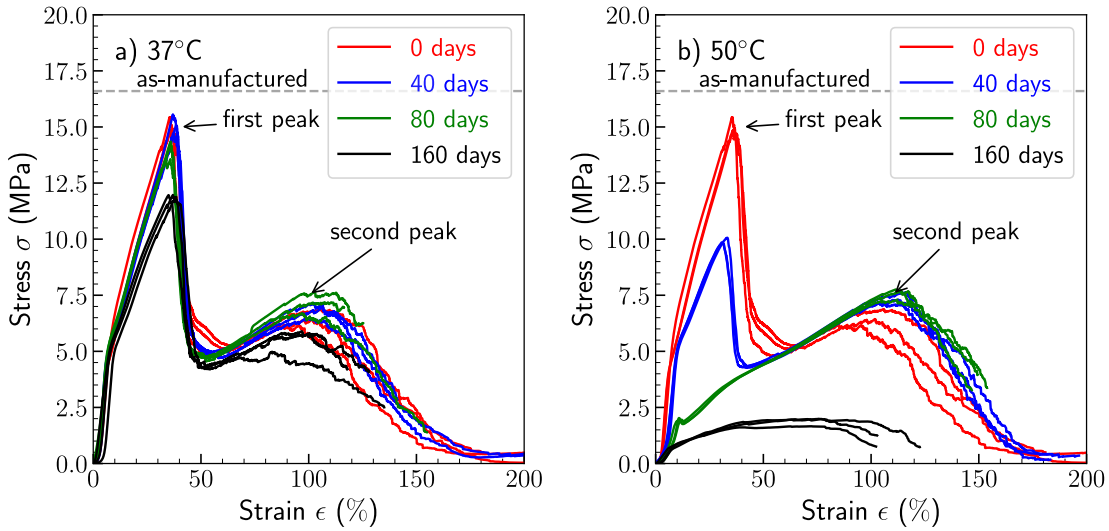


Figure 4.9: Stress-strain curves of the PLA-PCL fabrics after PBS solution immersion at: a) 37°C, b) 50°C. The tests were carried immersed in water at 37°C irrespective of the degradation conditions in PBS solution.

to the first peak. Then, the PLA fibres failed, and the remaining PCL fibres carried the load, leading to a second peak in the stress-strain curve when the strain was $\approx 100\%$. This feature is consistent with the PCL yarn failure as shown in Figure 4.7a and with the theoretical model of eq. (4.1). Moreover, the strength of the second peak did not change with immersion time. Thus, it is assumed that immersion at 37°C only modified the PLA mechanical properties, leading to slight reductions in elastic modulus, first peak strength and toughness. In contrast, the second peak strength (controlled by PCL) remained constant. No significant variation of Young modulus along degradation of PLA-PCL fibre was also observed by Vieira *et al.* (150); however, progressive reduction of the strength was noted.

Immersion at 50°C led to rapid degradation of the PLA, and the first strength peak in the stress-strain curves (Figure 4.9b) dropped rapidly with immersion time and disappeared after 80 days. The second peak –determined by the PCL behaviour– did not change significantly up to 80 days, but it did not show after 160 days of immersion at 50°C. In addition, the maximum strain supported by the fabric before complete failure was also reduced due to the degradation of the PCL fibres, and the degradation of both fibres was also shown in the dramatic reduction in toughness after 160 days of immersion at 50°C.

Overall, the mechanical properties after degradation summarised in Figure 4.10 are consistent with the results of the thermo-physical properties. Immersion in

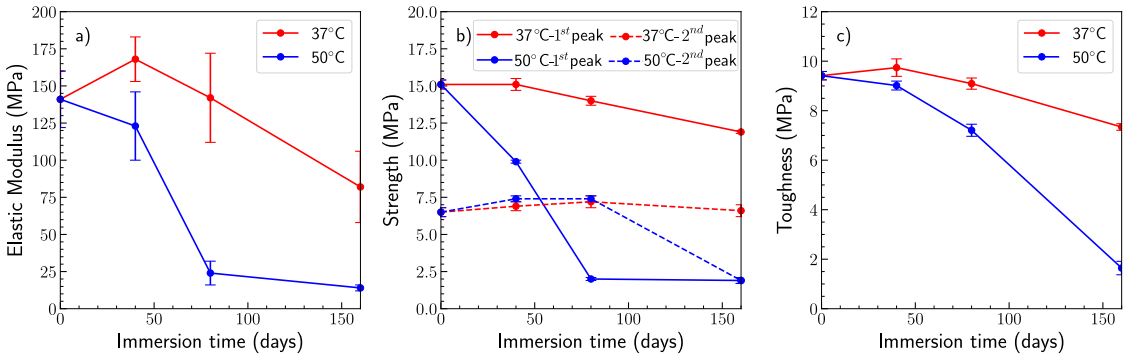


Figure 4.10: Summary of mechanical properties of PLA/PCL hybrid woven fabrics as a function of immersion time in PBS at 37°C and 50°C. a) Elastic modulus (calculated from DIC strain measurements), b) Tensile strength (primary and secondary peaks). c) Toughness (area below the stress-strain curves). It should be noted that all mechanical tests were carried out in water at 37°C, regardless of the immersion temperature during degradation.

PBS at 37°C for 80 days led to negligible degradation in the polymer structure and molecular weight (Figure 4.5a and 4.6), and the mechanical response did not change. A slight degradation of PLA after 160 days at this temperature reduced the first peak strength and the toughness. Immersion at 50°C led to an accelerated degradation, which is shown in a dramatic reduction in strength and toughness after 80 days, and that can traced to the PLA mass loss (Figure 4.3a) and the reduction in molecular weight (Figure 4.6).

Regarding potential applications, the mechanical properties of the PLA-PCL fabric within a fluid at 37°C meet the requirements of tendons, whose elastic modulus is in the range of 10 to 1070 MPa and the tensile strength between 4 to 110 MPa (155). For instance, the anterior cruciate ligament (ACL) has a tensile strength of $24 \pm 9$ MPa and a tensile modulus of $113 \pm 45$ MPa as reported in (155).In terms of strength, these findings are potentially in the lower spectrum, meaning that this parameter could be improved by, for example, increasing the PLA content or even by using stronger PLA fibre. However, a notable feature is the exceptional ductility observed, given that it spans a range of 4% to 60% in tendon ligaments. Remarkably, this investigation determined that the material initiates its failure at approximately the 50% strain. Regarding regeneration time, tendon/ligament repair is relatively slow compared to other musculoskeletal tissues, and the remodelling stage begins six weeks later (7). ACL regeneration and subsequent functionality typically take

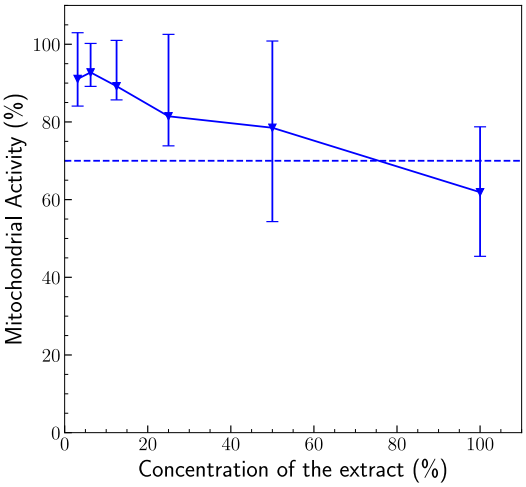


Figure 4.11: Mitochondrial activity as a function of the dilution of extracts from indirect tests in PLA-PCL fabric. The dashed line represents the limit for the non-cytotoxic material (70%) according to the standard ISO 10993-5: 2009.

at least six months (156), corresponding to the weave degradation at physiological temperature, where characteristics deterioration was observed after five months and an half. Furthermore, the post-yield ductility, related to the PCL component, is also an advantage for this type of application.

**Fabric Biocompatibility**

The mitochondrial activity of the MC3T3-E1 preosteoblasts was measured by using indirect tests with PLA-PCL extracts following the ISO 10993-5: 2009 standard. Figure 4.11 summarises the results obtained during the dilution process. According to the standard, the material tested is considered non-cytotoxic when the mitochondrial activity exceeds 70% after normalisation with the control group.

The results presented in Figure 4.11 show slight toxicity for the pure extracts with a value around $61 \pm 17\%$. The mitochondrial activity was around 80% for 50% dilution but with a large scatter band. That can be explained by the uncertainty in determining accurately the surface area of the PLA-PCL fabric (a highly porous media with a large surface/volume ratio). Therefore, slight variations in the surface area result in significant variations in the results. Moreover, the large surface area promotes the faster degradation, leading to the generation of acidic degradation products that affect cell viability. This latter problem can be controlled *in vivo* by the body's buffer system, as reported in (157).

Confocal and scanning electron microscopy directly evaluated the interaction

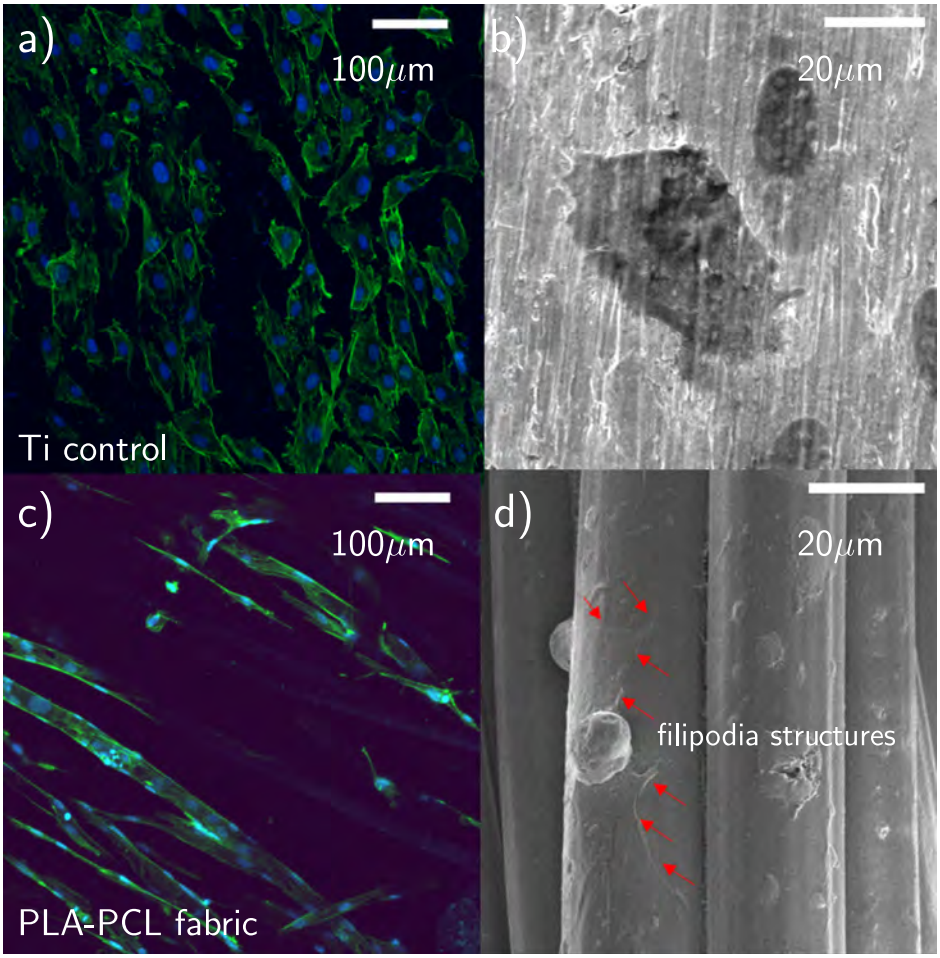


Figure 4.12: Confocal microscopy and SEM images of the interaction between MC3T3-E1 preosteoblasts and the surface of the samples,24h after seeding. a) and b) Ti control. c) and d) PLA/PCL textile. The red arrows in d) indicate filipodia structures representing the cell-material interaction.

between the cells and the textile. Figure 4.12a and c for the Ti control and the PLA/PCL fabric, respectively, presents fluorescence images. It should be noted that the fabric architecture presents a dual-scale porosity containing free spaces between adjacent yarns and between individual fibres inside the yarns. Therefore, the seeding of cells faces intrinsic difficulties associated with the interaction between the fluid in the culture medium and the polymeric fibres. The contact angle of the PLA-PCL fabric with water and culture medium was measured according to the methodology described in section 3.2.3. The results showed highly hydrophobic behaviour in deionised water with CA being $\Theta_L = 142.5 \pm 0.2°$, that diminished to $\Theta_L = 111 \pm 8°$ in the culture medium. This non-wettable behaviour, combined with the fabric's highly porous architecture, can explain the enormous differences in cell density after

seeding compared with the Ti control material.

Irrespective of the number of cells, the cells exhibited the typical triangle-like shape in both cases, with the cytoskeleton showing adaptation between neighbour cells and attachment to the material surface. The SEM images presented in Figure 4.12 b) and d) corroborated these results where the cell-material interaction can be observed more clearly. Cells bordering the fibres and aligned forming junctions or monolayers on the fibres were observed. The detection of filipodia structures on the fibre surfaces substantiates the facts of good cell material biocompatibility.

## 4.2 PLA-PLA woven textiles

The PLA-PLA fabric is composed by commingling yarns of PLA with high melting temperature with those of PLA with low melting temperature in a ratio 1:1. The pattern of this fabric (Figure 4.13) is similar to the PLA-PCL. Given this similarity, it is assumed that the porosity and pore size in PLA-PLA fabric closely resemble those of PLA-PCL. The total porosity is estimated at around 35%, with pores and canals exhibiting 200-300 $\mu$m dimensions. This assumption is rooted in the understanding that interconnect porosity, dictated by the fibre bundle spacing and fabric pattern, is dominant in both materials.

### 4.2.1 *In vitro* degradation tests

The changes in dry mass for the PLA-PLA weave and the pH of the solution were monitored at 37°C and 50°C. The average mass, standard deviation, and pH of the solution across three samples as a function of immersion time at 37°C and 50°C, respectively, are plotted Figure 4.14, a) and b). For samples immersed in PBS at 37°C, the dry mass remained constant over 160 days, and the pH of the solution was maintained around 7 during this period. Minor variations observed in the initial stages of the experiments were attributed to the non-hermetic nature of the flask. In contrast, experiments conducted at 50°C showed a 15% decrease in dry mass after 160 days, accompanied by a pH decrease from polymer hydrolysis. Maintaining dry mass and stable pH at 37°C aligns seamlessly with the visual observations, revealing unchanged textile characteristics over the 160 days (Figure 4.15a) and b)). In contrast, the observed decrease in dry mass and the associated pH reduction at 50°C (Figure 4.15 c)) correspond to noticeable alterations in the textile's appearance, characterised by a yellow colour and material separation. These visible changes


Figure 4.13: Optical image of the PLA/PLA woven fabric.

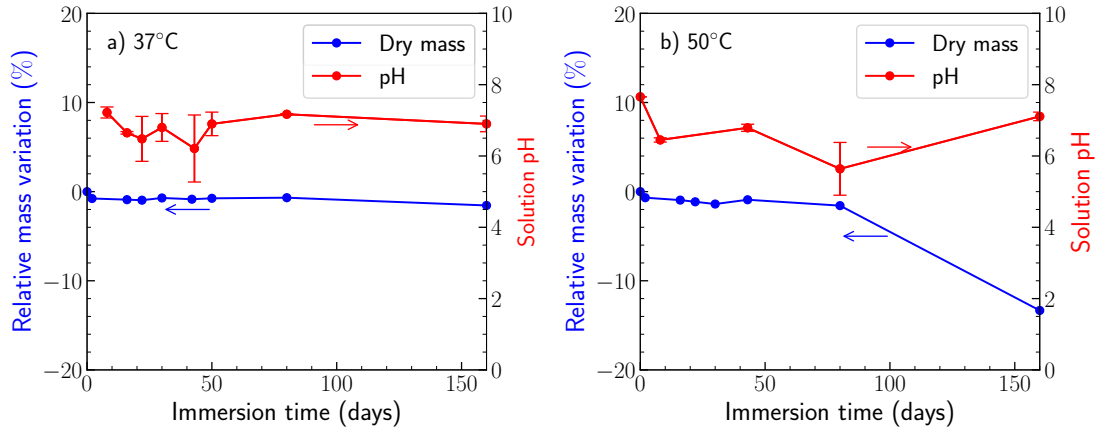


Figure 4.14: Evolution of the dry mass of the PLA/PLA woven samples and of the pH of the PBS solution as a function of the immersion time at: a) 37°C, b) 50°C.

strongly indicate the impact of polymer hydrolysis on the textile's properties. It is noteworthy that samples placed at 50°C exhibited an almost instant change in shape upon exposure to the oven. Additionally, they displayed increased rigidity, possibly attributed to relief of residual stresses, leading to shrinkage.

The thermal properties of both the yarns and fabrics were examined through DSC. The initial curve for the as-produced BIO4M® yarns and fabric (0 days) represented

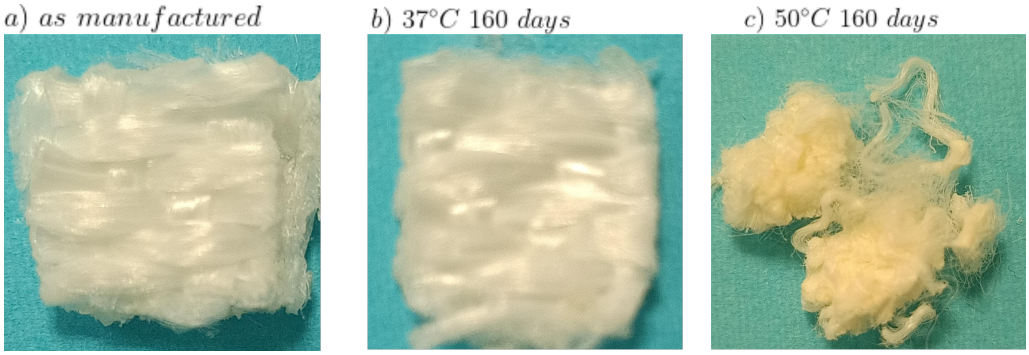


Figure 4.15: Optical appearance of PLA-PLA woven textile. (a) As manufactured, mass loss =0%, pH=7. (b) After 160 days of immersion in PBS at 37°C, mass loss =2%, pH = 7. c) After 160 days of immersion in PBS at 50°C, mass loss =13%, pH = 7.0. The shape of the weave changes completely at 50°C.

in red in Figure 4.16 reveals a peak shortly after the glass transition peak, indicative of material ageing. The glass transition temperature ($T_g$) is 63.8°C. After the $T_g$, cold crystallisation occurs, followed by two distinct melting peaks, one at a lower temperature (151.4°C) referred as $T_m^{PLAm}$, and another at higher temperature, $T_m^{PLAr}$, at 173.3°C, confirming the presence of the two PLA components in the BIO4M® yarn.

During the cooling phase, a discernible $T_g$ is observed, with no other peaks visible, suggesting that the material is entirely amorphous. In the second heating, a broader and lower temperature $T_g$ is found due to the loss of crystallinity. A more prominent cold crystallisation peak is evident, indicating the transition of the material to the amorphous phase. A minor exothermic peak, consistent with findings by Hsieh *et al.* (158), is observed just before the melting peak. This peak corresponds to a PLA metastable polymorph phase ($\alpha'$), as reported by other research groups (54).

Heating-cooling-reheating curves of PLA-PLA fabrics are depicted in Figure 4.16 a) and b) after immersion in PBS at 37°C and 50°C, respectively, during 160 days. At 37°C (4.16a), no significant differences are observed in the curves throughout the degradation period. A peak occurring just before the glass transition temperature ($T_g$) is noticeable in all curves, indicating physical ageing. The $T_g$ transition is observed at 66°$C$, and a small cold crystallisation peak at approximately 103°$C$ is present, though no discernible trend is evident over the degradation period. Both PLA melting peaks, one at a lower temperature and the other at a higher temperature, are consistently observed, independent of degradation days, with no significant changes.

During cooling, a $T_g$ transition at approximately $59°C$ remains unchanged over the 160 days. In the re-heating cycle, a sharper cold crystallisation peak at around $97°C$ is notable compared to the peak observed in the first heating. This suggests a more well-defined transition from the amorphous to the crystalline state within a narrower temperature range. However, this peak also remains unchanged during the degradation time. In summary, no clear indications of degradation are evident in the DSC curve, considering the presence of two PLA components in the yarn and the difficulty in achieving identical amounts of each PLA in all samples.

These results align with observations made in the previous section on the PLA-PCL weave fabric (Section 4.1.1) and are consistent with findings in the literature. It has been documented that the degradation of PLA at $37°C$ progresses slowly (62). For instance, Ella *et al.* (55) investigated the degradation of knitted polylactide L/D structures at 36.5°C in PBS. They noted that the weight loss of the scaffolds commenced after 28 weeks, and by 48 weeks, their weight had decreased by 10%. Weir *et al.*(54) observed a decrease of the $T_m$ and $T_g$ of PLLA materials after 44 weeks ( 308 days).

The samples degraded at 50°C (Figure 4.16 b)) exhibited noticeable signs of degradation. As previously mentioned, these samples experienced changes in shape, increased hardness, and greater fragility at this temperature. During the initial cycle, the glass transition temperature ($T_g^{PLA}$) decreased over time, and up to 43 days, the curves displayed unclear readings. Similarly, the cold crystallisation peak ($T_{cc}^{PLA}$), which was only visible in the as-manufactured (0 days) curve. These occurrences are related to the crystallization due to the immersion at a temperature near the $T_g^{PLA}$. After 160 days, a distinct alteration was evident: the two PLA melting peaks merged into a double peak, indicating less perfect crystals.

During cooling, the $T_g^{PLA}$ decreased from approximately 60°C to about 40°C after 160 days, confirming degradation. However, in the final cycle, it remained unchanged throughout the degradation period. Regarding the $T_{cc}^{PLA}$, unlike the first cycle, it appears, and after 160 days, it becomes a broad and less defined peak, extending into the melting peaks' range. Subsequently, after 160 days, the two melting peaks fused into a double peak, similar to the initial heating. Additionally, a decrease of approximately 10°C was noted in the temperature of the high melting temperature PLA.

Overall, the DSC analysis indicated a discernible difference after 160 days of degradation, characterised by shifts in $T_g^{PLA}$, changes in the cold crystallisation peak,

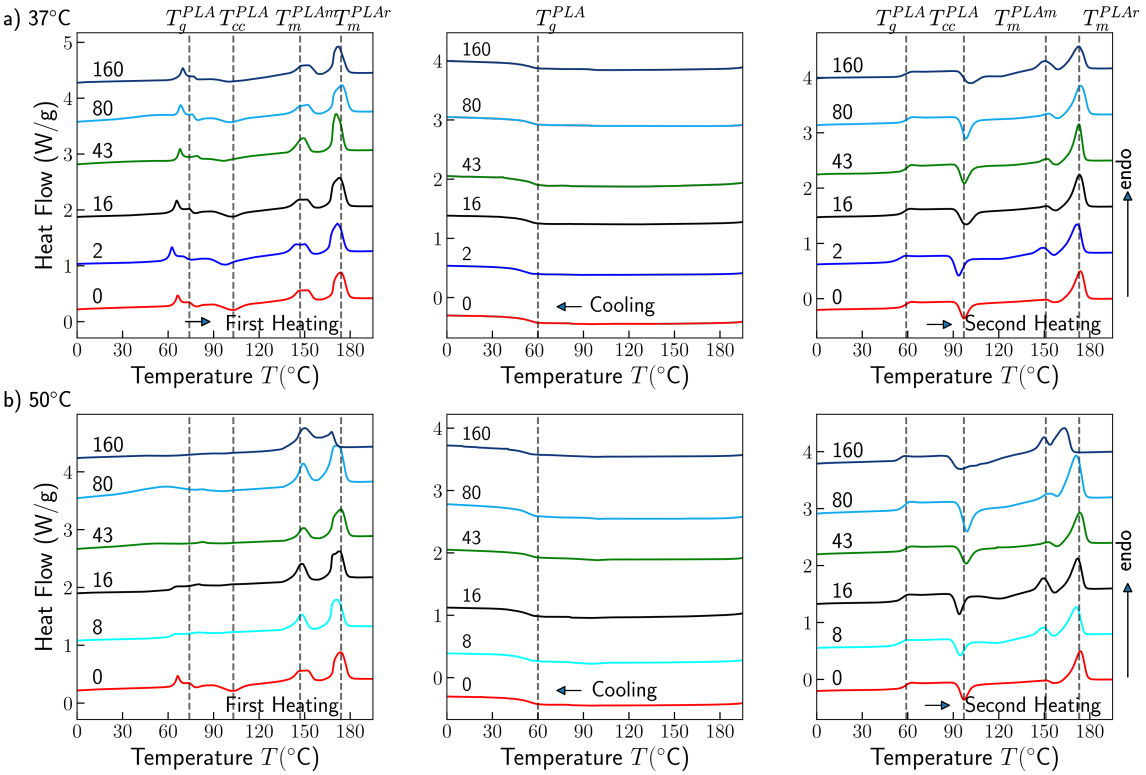


Figure 4.16: Heat flow curves during heating-cooling-reheating steps of the PLA/PLA woven fabric during DSC at a heating/cooling rate of 10°C after immersion in PBS for different number of days (indicated in each Figure). a) After immersion at 37°C, b) after immersion at 50°C. The glass transition ($T_g^{PLA}$), the crystallisation ($T_c^{PLA}$) and the cold crystallisation ($T_{cc}^{PLA}$)temperatures of the PLA yarns,$T_m^{PLAm}$ the melting temperature of PLA that will serve as matrix and $T_m^{PLAr}$ the melting temperature of the PLA that will act as reinforcement, are indicated with dashed vertical lines.

alteration in the melting peaks' configuration, and a reduction in the high melting temperature of PLA.

The findings mirror observations from the PLA-PCL weave after degradation at 50°C and align with literature regarding accelerated degradation tests. Similarly, Polak *et al.* (154) observed comparable trends during accelerated degradation (50°C). After approximately 32 and 49 days, they noted the glass transition and cold crystallisation peaks becoming indistinguishable. Additionally, there was an observed decrease in the melting peak by around 18°C after 112 days.

The molecular weight distributions of PLA-PLA fabric were analysed using GPC to observe degradation. In Figure 4.17 a) and b), are plotted the molecular weight $Mw$ distributions of the PLA-PLA fabric degraded at 37°C and 50°C, respectively. It

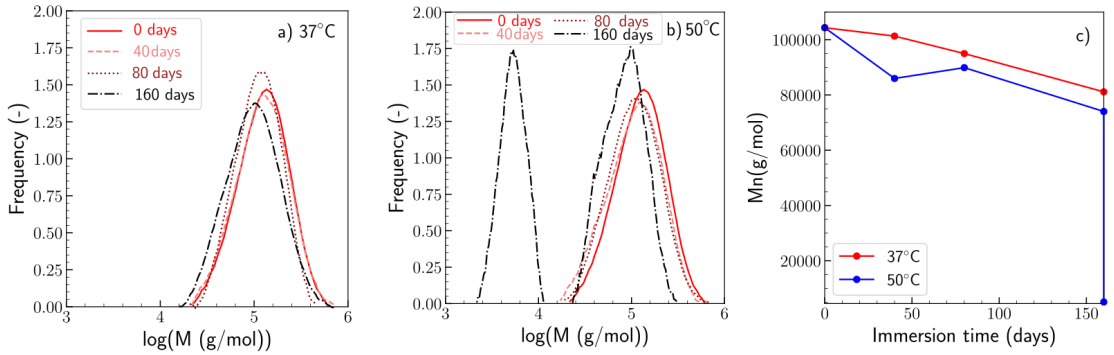


Figure 4.17: Evolution of the molecular weight ($Mw$) distribution of the PLA-PLA fabrics with immersion time at: a) 37°C, b) 50°C; c) Evolution of the number average molecular weight ($Mn$) as a function of immersion time for both temperatures.

was expected to find two distinct peaks representing two different molecular weights of PLA components with different melting temperatures but a single broad peak was observed instead. At 37°C, no significant change in molecular weight distribution was noticed up to 80 days, indicating minimal impact initially. However, a shift at 160 days suggests degradation, leading to chain scission and a shift towards lower molecular weights.

At 50°C,(Figure 4.17b), a gradual shift in molecular weight distribution was observed with the degradation days, indicating a continuous degradation process. The appearance of a lower molecular weight peak after 160 days aligns with the drop in weave mass and polymer melting temperatures, indicating substantial degradation. This pattern supports the expectation that one of the polymers degrades faster. It is plausible that the more amorphous polymer, typically characterised by a lower melting temperature, undergoes a faster degradation. Amorphous regions in polymers are often more vulnerable to degradation than their crystalline counterparts. The bimodal behaviour at 50°C, signifying the existence of both low and high molecular-weight degraded PLA fragments, was previously documented by Felfel *et al.* (159). They attributed this phenomenon to the differing degradation rates between the amorphous and crystalline phases within semicrystalline polymers.

In Figure 4.17 c), the evolution of the number-averaged molecular weight ($Mn$) with immersion time at 37°C and 50°C is depicted, supporting the observations from the previous discussion. Notably, it emphasises the gradual and slower degradation at 37°C (shown by the red line). The anticipated trend of faster degradation at 50°C is evident, with a 30% decrease in $Mn$ after 160 days compared to the 23%

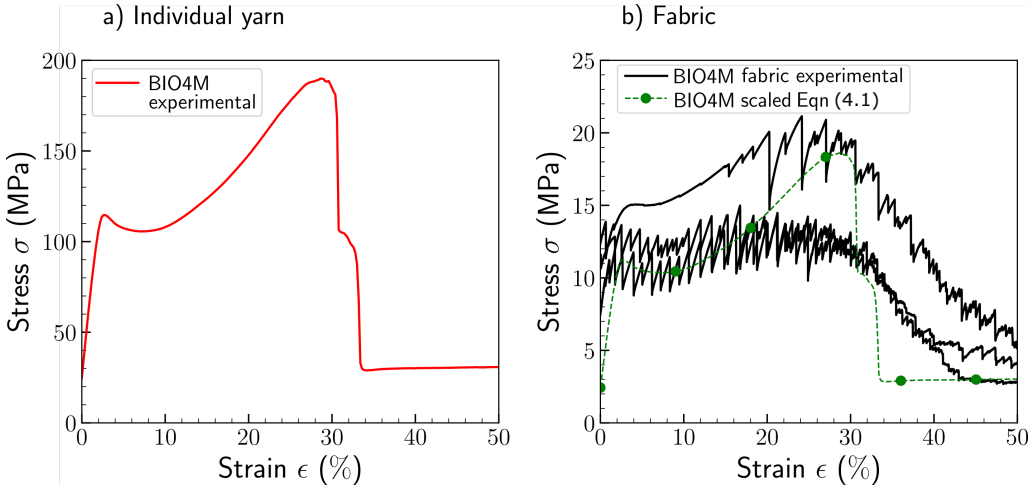


Figure 4.18: a)Tensile stress-strain curves of the BIO4M® hybrid yarn. b) Tensile stress-strain curves of the PLA/PLA fabric. The dotted lines stand for simple iso-strain model prediction based on eq. (4.1).

decrease at 37°C. This difference in degradation rates aligns with expectations based on higher temperatures accelerating degradation processes.

The degradation of the PLA-PCL weave reveals notable differences in comparison to the degradation of the PLA-PLA weave, mainly focusing on the peak with higher $Mn$. The PLA-PLA weave degrades slowly, specifically its high melting temperature component. At 37°C, the PLA-PLA weave showed a 23% decrease in $Mn$, indicating a relatively slower degradation rate compared to the observed degradation rate in the PLA-PCL weave (32%). However, considering the lower molecular peak, there is a $Mn$ drop of approximately 95% after 160 days. These findings corroborate existing literature (154), where PLLA samples (with $Mn$ = 97,650 g/mol) degraded at 50°C, decreasing by almost 95% ($Mn$ = 7,430 g/mol) after 112 days. These results strongly suggest that different weave compositions exhibit distinct degradation behaviours. Understanding these variations in degradation behaviour is crucial for tailored material design and predicting the lifespan or performance of specific structures.

### 4.2.2 Mechanical behaviour

#### Yarns and fabric behaviour

Tensile stress-strain curves of the BIO4M® hybrid yarns were derived from the load-displacement $P - \delta$ curves recorded during the tests. The nominal stress $\sigma$ was calculated from the load $P$ and the solid equivalent cross-section of the yarn

$S = \lambda/\rho$ obtained from the yarn linear density $\lambda = dtex/10000$ and the bulk polymer density $\rho$. The strain, $\epsilon$, was calculated from the yarn elongation obtained from the cross-head displacement of the machine, $\delta$, and the yarn gauge length $L_0$ as $\epsilon = \delta/L_0$. Representative $\sigma - \epsilon$ curves obtained from three individual tests of BIO4M® hybrid yarns are shown in Figure 4.18. The averaged tensile properties, including elastic modulus $E$ (initial slope of the stress-strain curve), the yarn strength $\sigma_{max}$, the strain-to-failure $\epsilon_{max}$ and the tenacity $g$ (volumetric energy) defined as the area below the stress-strain curve ($g = \int_0^{\epsilon_{max}} \sigma \, d\epsilon$), were obtained from 30 yarn tests per condition and are presented in Table 4.2. After an initial elastic region with a tensile modulus of around 4.1 GPa, BIO4M® (red line) yields at a strain of 2.8% and stress of 114.63 MPa. The filaments gradually start to break at a strain of 29% and an ultimate strength of 189 MPa.

The three tensile stress-strain curves of the as-manufactured fabrics at room temperature are reported in the same graph, Figure 4.18. In this case, the stress was calculated from the force recorded by the load cell and the nominal cross-section area of the fabric 50 $\times$1.31mm$^2$ while the deformation was recorded from the cross-head displacement and the gauge length of the fabric $L_0$ = 90 mm. As in the case of the PLA-PCL weave, it should be noted that the elastic modulus of the fabric was determined with the strain obtained with the digital image correlation system averaged over a region of interest of 50 $\times$ 35 mm$^2$ in the centre of the fabric.

Table 4.2: Mechanical properties of BIO4M ®hybrid yarn

| Yarn | $E$ (GPa) | $\sigma_{\max}$ (MPa) | $\epsilon_{max}$ (%) | $g$ (GPa) |
|---|---|---|---|---|
| BIO4M ® | 4.1 $\pm$ 0.1 | 189 $\pm$ 3 | 28.0 $\pm$ 0.8 | 8.4 |

The fabric behaviour mirrors the hybrid yarn with two distinct slopes in the stress-strain curves. Additionally, it exhibits a gradual failure pattern marked by the initiation of fibre bundle collapse, evident as peaks in the stress-strain curves similar to those observed in dry PLA-PCL materials. In its dry condition, this fabric showcases a modulus of 424.7 MPa and an ultimate tensile strength (UTS) of 15.60 MPa. As the fabric undergoes deformation (reaching 28%), damage propagates progressively, leading to a notable decline in stress levels. Figure 4.19 illustrates the fabric behaviour across various deformation stages. Although the failure of fibre bundles is not as clear as in the PLA-PCL woven textile, signs of grip failure are discernible. These inconsistencies in gripping contribute to the scatter within the curves, emphasising the uneven gripping pressure during testing.

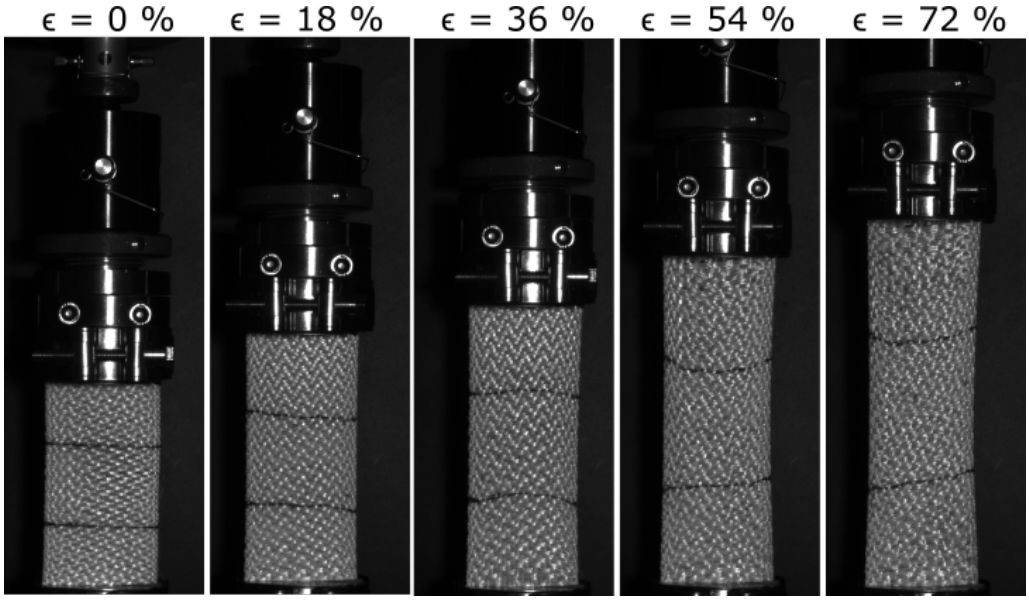


Figure 4.19: Optical images of $90 \times 50$ mm$^2$ as-manufactured fabric coupon subjected to tensile deformation. The gauge length between grips $L_0 = 90$ mm is indicated by the parallel horizontal lines that are progressively curved during deformation.

The fabric behavior was also calculated from the yarn's mechanical properties under the assumption that the warp yarns carry out all the load and neglect the weft yarns contribution. The fabric stress was calculated $\sigma_{fabric}$ from Eq.4.1, where, for this fabric, $n$=1 yarn/mm (warp count), $\lambda = 0.1600$ gr/m is the yarn linear density, $\rho = 1240$ Kg/m$^3$ the bulk PLA density and $t = 1.31$ mm the fabric thickness. The dashed line in Figure 4.18b portrays the model predictions derived from equation (4.1). Despite the inherent simplicity of the deformation hypothesis used in this equation, the striking coherence between these predictions and the experimental results is evident. This alignment not only underscores the accuracy of the approximation but also explains remarkable consistency observed between the fracture behaviour of individual yarns and the collective behaviour exhibited by the fabric.

**Effect of degradation on fabric mechanical behaviour**

The fabric mechanical behaviour was studied after immersion in PBS at 37 °C, followed by tensile tests under the same conditions. Testing at 50 °C was not feasible due to the material drastic change in shape and increased rigidity. The stress-strain curves in Figure 4.20 depict the fabric responses after different immersion times. For reference, the fabric original strength in air at ambient temperature ($15 \pm 3$ MPa) is plotted as a dashed horizontal line in Figure 4.20. Compared to the fabric in its

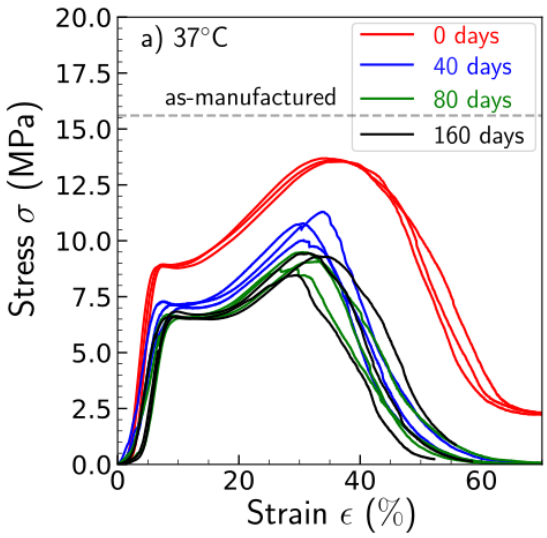


Figure 4.20: Stress-strain curves of the PLA-PLA fabrics after PBS solution immersion at 37°C. The tests were carried out immersed in water at 37°C.

original state, the observed reduction in mechanical properties at 0 days results from testing at 37°C and water absorption during the 24-hour immersion in PBS prior to testing. The evolution of the fabric elastic modulus, strength and toughness as a function of the immersion time in PBS at 37°C is depicted in Figure 4.21.

The fabrics consistently display a characteristic pattern: an initial plastic regime followed by plastic deformation until failure, typically around 40% strain. However, fibre bundle failure peaks are absent, unlike what has been observed in Figure 4.18 b), highlighting the influence of water plastification on the fabric's behaviour. The strength decreases to 13.6 MPa when immersed, and the elastic modulus is reduced to 342 MPa. The strength diminishes over 40 and 80 days by approximately 30% and 35%, respectively. During this period, the elastic modulus undergoes a significant decrease of almost 50% after 40 days, and remains with similar values even after 80 and 160 days. Similarly, the strength follows this trend. In terms of toughness, an initial increase is noted after 40 days, followed by a relatively stable level that remains slightly lower than the toughness of the non-degraded material. This trend suggests a temporary rise in toughness during the early degradation phase, followed by stabilisation at a slightly diminished level compared to the initial, non-degraded material.

The relationship between the polymer's crystalline and amorphous phases plays a

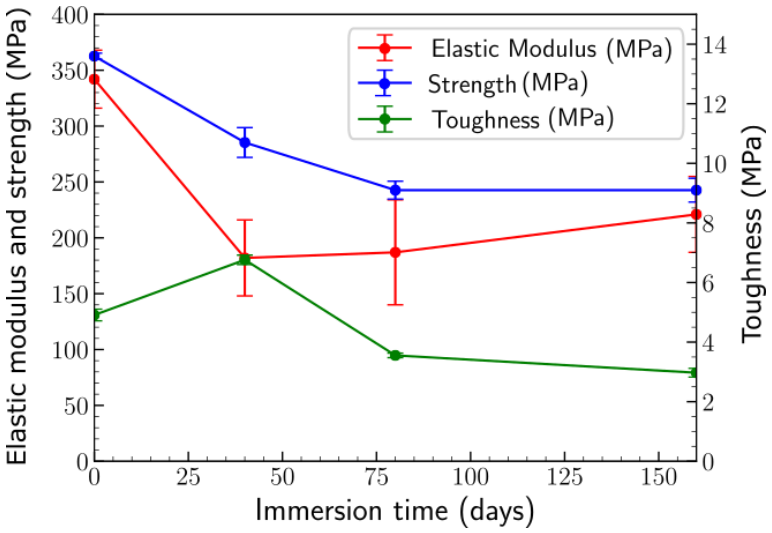


Figure 4.21: Summary of mechanical properties of PLA/PLA hybrid woven fabrics as a function of immersion time in PBS at 37°C. Elastic modulus (calculated from DIC strain measurements), Tensile strength and Toughness (area below the stress-strain curves). It should be noted that all mechanical tests were carried out in water at 37°C.

crucial role in these mechanical changes. Typically, the crystalline phase contributes to strength and stiffness, while the amorphous phase imparts ductility to the material. The interplay between these phases, where tangled polymer chains untangle under loading, provides a mechanism for gradual energy dissipation through plastic deformation (160).

The comprehensive summary depicted in Figure 4.21 showcases the fabric's mechanical performance over time. Interestingly, while the degradation at 37°C was not highly pronounced in thermo-physical aspects, it significantly impacts mechanical properties. The substantial decline in elastic modulus could potentially be linked to the degradation of PLA, known for its lower melting point. This observation aligns with the degradation pathway of polyesters, where a decrease in molecular weight precedes a decline in mechanical properties, ultimately culminating in a mass reduction.

However, a distinct behaviour was observed in Weir's study(54), where the strength declined faster than the modulus. Over 140-180 days, the modulus dropped by 7-35%, while the strength decreased by 42-63%. This discrepancy might stem from differences in the surface area. The surface area of the fabrics developed in this thesis is significantly larger than the composite materials studied by Weir et al. (54).

This disparity in surface area could contribute to slower hydrolysis processes in the latter.

A PLA-PLA weave with a tensile strength of 13.6 MPa and a higher modulus of 342 MPa for a rotator cuff tendon, particularly the supraspinatus tendon, presents an intriguing starting point. While these mechanical properties fall within or surpass the lower limits of the tendon's tensile strength (4-24 MPa) and exceed its modulus (155), further exploration to enhance the material's tensile strength could broaden its suitability.

Considering the degradation, assuming a physiological temperature without accelerated degradation tests, the material is projected to last more than six months (180 days). However, an important consideration emerges regarding the modulus. Given that it is expected to decline after 40 days, potentially falling into the range compatible with the suggested tendon properties.

**Fabric Biocompatibility**

The mitochondrial activity of MC3T3-E1 preosteoblasts was evaluated using a protocol that was identical to the one employed for the PLA-PCL weave, focusing on PLA-PLA extracts. The summarised results from the dilution process can be found in Figure 4.22. Per established standards, a material is classified as non-cytotoxic when its mitochondrial activity, after normalisation with the control group, exceeds 70%.

The results outlined in Figure 4.11 indicate slight toxicity in the pure extracts, averaging around $62 \pm 22\%$. Notably, at a 50% dilution, the mitochondrial activity peaked at approximately 80%. However, this measurement exhibited a significant spread, likely due to the challenge of precisely quantifying the surface area of the fabric. The material's highly porous nature, coupled with a substantial surface-to-volume ratio, makes accurately assessing the surface area complex. Even slight fluctuations in surface area can lead to considerable variations in the observed results. Furthermore, as also mentioned for the PLA-PCL fabric, the fabric's expansive surface area accelerates degradation, hastening the generation of acidic degradation byproducts that adversely affect cell viability. However, it is worth noting that this issue can potentially be regulated in vivo by the body's buffer system, as indicated in (157). This suggests that while the degradation products may impact cell viability in vitro, the body's buffering mechanisms could mitigate these effects in a living system.

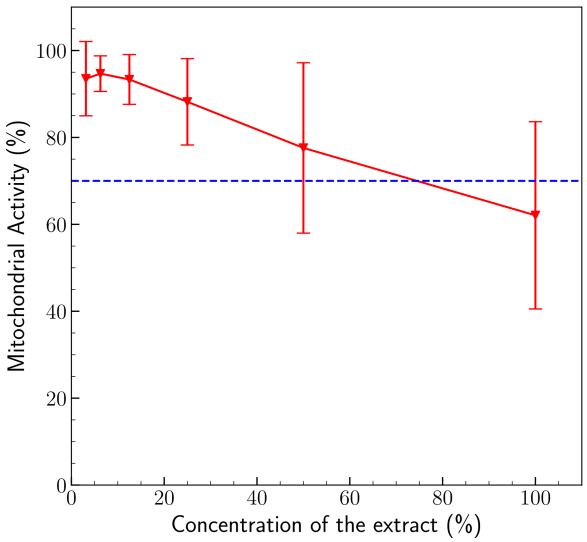


Figure 4.22: Mitochondrial activity as a function of the dilution of extracts from indirect tests in PLA-PLA fabric. The dashed line represents the limit for the non-cytotoxic material (70%) according to the standard ISO 10993-5: 2009.

Cell-textile interaction was directly assessed using confocal and scanning electron microscopy. Fluorescence images captured in Figure 4.23 a) and c) depict the Ti control and the PLA/PLA fabric, respectively. Similar challenges were encountered due to the identical fabric architecture shared by both PLA/PLA and PLA/PCL weaves. These fabrics possess a dual-scale porosity characterised by open spaces between adjacent yarns and individual fibres within the yarns, allowing cells to spread through the material's thickness.

To explore potential factors affecting cell interaction, the contact angle of the PLA-PLA fabric with water and culture medium was measured following the methodology outlined in section 3.2.3. The results unveiled a highly hydrophilic behaviour ( CA, $\Theta_L = 0°$) of the fabric towards both liquids.

There is a consistent pattern of cytoskeletal adaptation among neighbouring cells and their adherence to the material surface. This observation is supported by the SEM images in Figure 4.12 b) and d), further illustrating the interaction between cells and the material surface. These images vividly display cells aligned along the fibres, forming junctions or organising into monolayers on these fibrous structures. This emphasises cells' affinity and interaction with the material, showcasing an established cell-material interface.

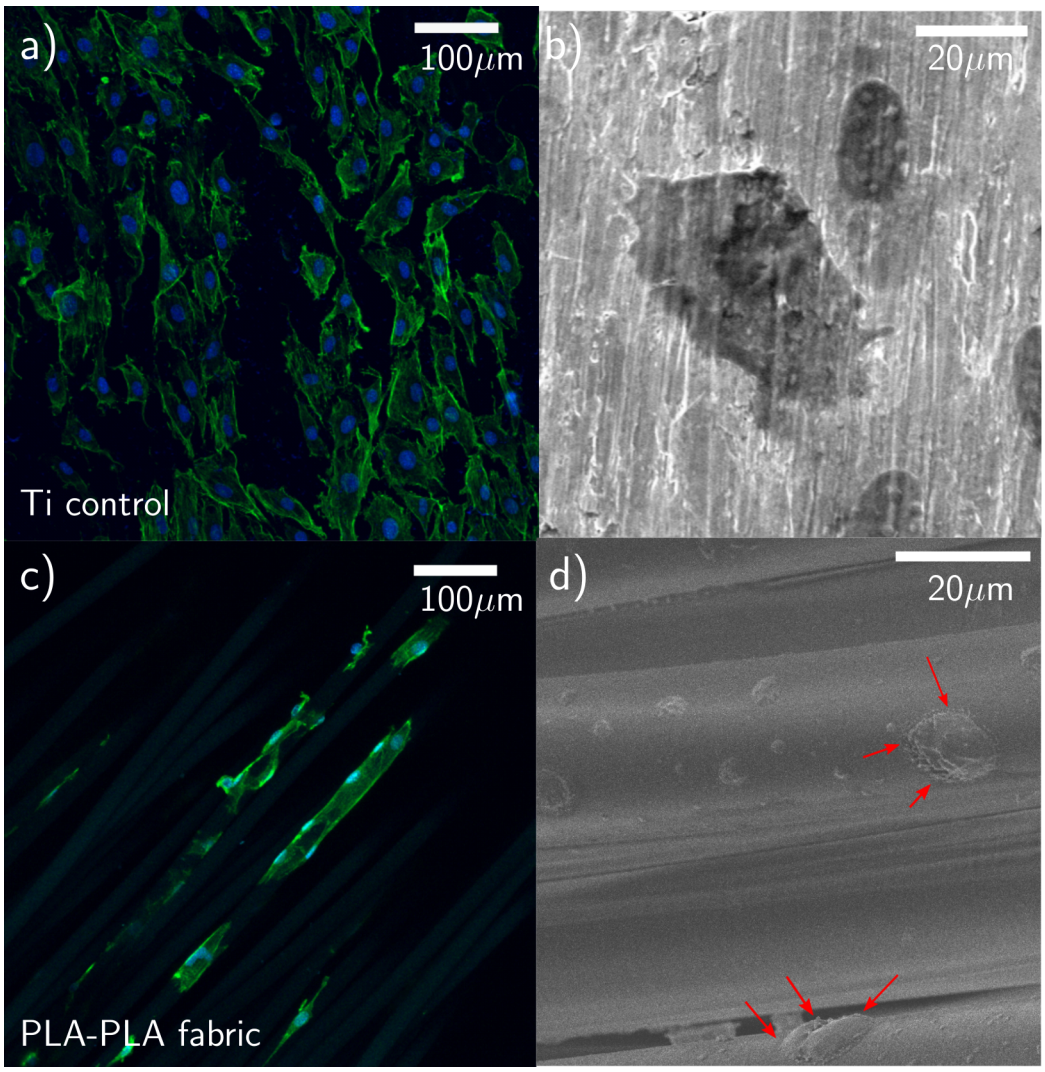


Figure 4.23: Confocal microscopy and SEM images of the interaction between MC3T3-E1 preosteoblasts and the surface of the samples,24h after seeding. a) and b) Ti control. c) and d) PLA/PLA textile. The red arrows in d) indicate filipodia structures representing the cell-material interaction.

# Composite material properties

5

The composite plates were fabricated using woven fabrics of commingled yarns, with a PLA: PCL ratio of 3:1 for the PLA/PCL composite, and woven fabrics of PLA: PLA commingled yarns in a 1:1 ratio for the PLA/PLA composite. The arrangement of fibres in the weave ensured that the reinforcement fibres were aligned in both longitudinal and transverse directions. As outlined in the manufacturing chapter (Chapter 2.1), three layers of each woven material were stacked and hot-pressed together—the hot-pressing process aimed to achieve a fully dense material without any porosity. The optical iamges of the composites panels are depicted in Figures 5.1 a) and d)). The results of the C-scan inspection of the panels (Figures 5.1 b) and f)) revealed dark colours (attenuation level less than 6 dB) that indicated regions without voids or high density in the PLA/PLA composite. In the case of the PLA-PCL laminate, the ultrasonic wave was extensively attenuated (over 30 dB - white colour), indicating inadequate consolidation with a significant amount of entrapped air due to insufficient wetting of reinforcement fibres by the matrix.

It was not easy to identify the porosity in the cross-section of the PLA-PCL laminate (Figure 5.1c) but bundles of fibres in the x-direction (weft yarns) and longitudinal direction (warp yarns) were observed. The cross-section of the PLA-PLA composite (Figure 5.1f) showed a line in the middle corresponded to the width of the fabric tapes. The fibre bundles and layers could be identified in the cross-section, indicating the reinforcements were not melted during hot compaction at 165°C and 2 MPa during 20 minutes. However, some porosity (dark spots) was still observable.

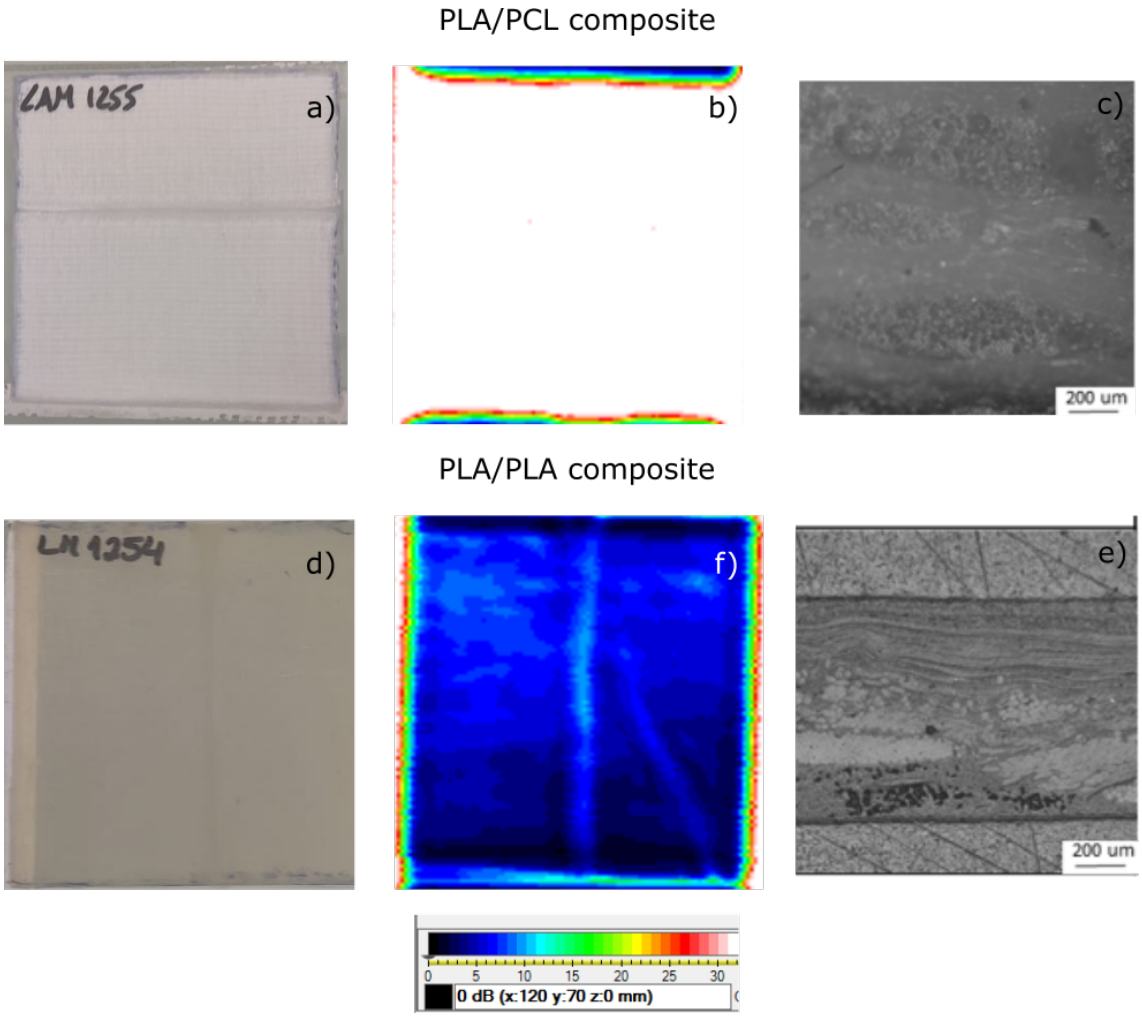


Figure 5.1: a) Optical image of the PLA/PCL composite plate. b) C-scan of the PLA/PCL composite plate. c) Cross-section of the PLA/PCL composite plate. d) Optical image of the PLA/PLA composite plate. b) C-scan of the PLA/PLA composite plate. c) Cross-section of the PLA/PLA composite plate.

## 5.1 PLA-PCL composite

### 5.1.1 *In vitro* degradation tests

Composite samples were immersed in PBS at different temperatures: 37°C and 50°C. When placed in a PBS solution at 37°C, the mass of the composite and the pH of the solution remained relatively stable over 160 days, as shown in Figure 5.2a). In contrast, samples immersed in PBS at 50°C experienced a 7% reduction in weight after 160 days, accompanied by a decrease in the pH of the solution to 3 due to polymer hydrolysis. The higher temperature notably accelerated the degradation

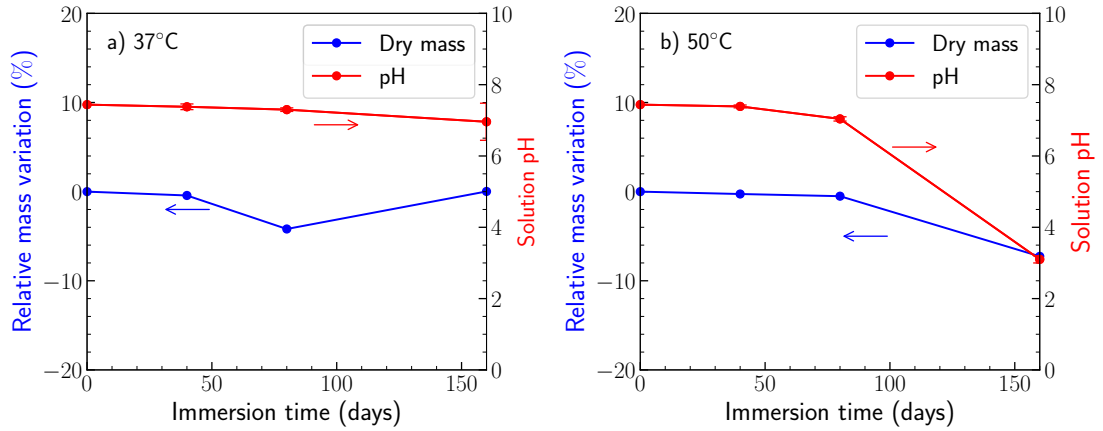


Figure 5.2: Evolution of the dry mass of the PLA/PCL composite samples and the pH of the PBS solution as a function of the immersion time at: a) 37°C, b) 50°C.

process, resulting in a more significant loss of composite mass than those immersed at 37°C.

The visual examination of the samples corroborated these findings (Figure 5.3). The initially white-coloured, as-manufactured composite gradually turned yellow after 160 days in PBS at 37°C, suggesting some degradation, but without visible material disintegration. However, the composite immersed in PBS at 50°C also changed colour to yellow and displayed increased fragility, requiring careful handling due to noticeable material deterioration. In summary, while the composite at 37°C showed signs of degradation indicated by colour change, it remained structurally intact. In contrast, immersion in PBS at 50°C significantly accelerated degradation, causing observable material fragility alongside changes in both mass and pH.

The thermal characteristics of the PLA-PCL composite material were examined by DSC to evaluate its behaviour during degradation. The heating, cooling, and reheating curves after subjecting the composite to degradation in PBS at 37°C and 50°C for a period of up to 160 days are plotted in Figures 5.4 a) and b), respectively.

In the case of the samples degraded at 37°C (Figure 5.4 a), the overall heat flow curves did not exhibit significant deviations throughout the ageing process, indicating relative stability in thermal properties. During the initial heating phase, the melting peak associated with PCL ($T_m^{PCL}$) gradually shifted towards slightly higher temperatures, from 64.2°C to 67.1°C. Conversely, no discernible changes were noted in the melting temperature peak of PLA ($T_m^{PLA}$). Over the degradation

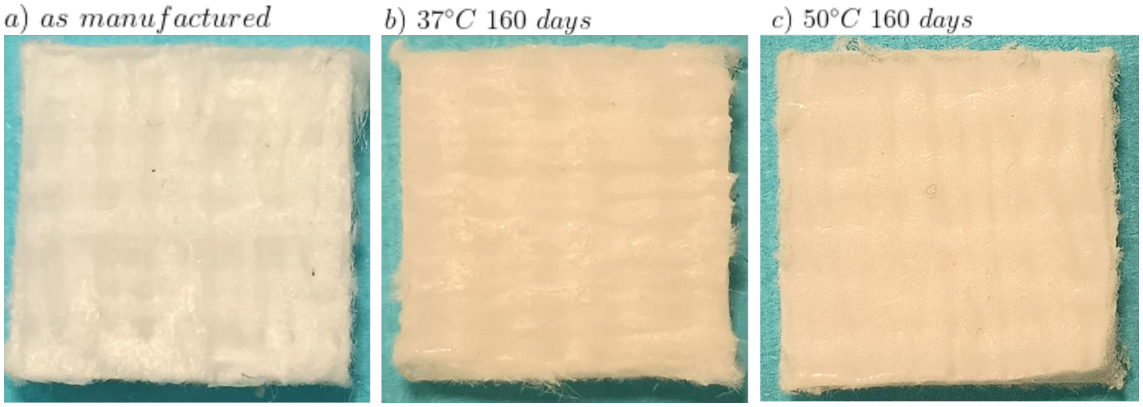


Figure 5.3: Optical appearance of PLA-PCL composite. (a) As manufactured, mass loss =0%, pH=7. (b) After 160 days of immersion in PBS at 37°C, mass loss =0%, pH = 7. c) After 160 days of immersion in PBS at 50°C, mass loss =7%, pH = 3.1.

period, the crystallisation peak of PLA ($T_c^{PLA}$) consistently moved towards higher temperatures during the cooling phase. In contrast, $T_c^{PCL}$ remained relatively constant. The first and second endothermic peaks exhibited consistency without significant variations throughout the reheating cycle. Initially, there was a slight cold crystallisation peak ($T_{cc}^{PLA}$) observed at 104°C in the as-manufactured material. However, this peak gradually diminished with prolonged degradation. Additionally, just before the PLA melting peak, the presence of the PLA metastable polymorph phase ($\alpha'$) was evident, as previously described.

To summarise, the analysis indicated a slight increase in crystallinity in the PCL component over time, while no notable changes were observed in the case of PLA. This fact confirms that, in terms of thermal properties, there is no apparent degradation of the composite material. These results are aligned with those reported for the woven materials, where the degradation of the materials was not seen at 37°C. Additionally, Guorino *et al.* (126) also observed that a composite made of poly-l-lactide acid (PLLA) fibres embedded in a porous poly(-caprolactone) matrix after 35 days of degradation in PBS at 37°C did not show significant degradation.

The PLA-PCL composites subjected to immersion in PBS at 50°C exhibited noticeable degradation over time (in Figure 5.4 b). During the initial heating cycle, a discernible shift of the first endothermic peak to higher temperatures was observed, rising from 64.2°C to 71.2°C. This behaviour was akin to what was previously visualised in the PLA-PCL weave and is attributed to the annealing process experienced by PCL due to the proximity of the degradation temperature (50°C) to the PCL

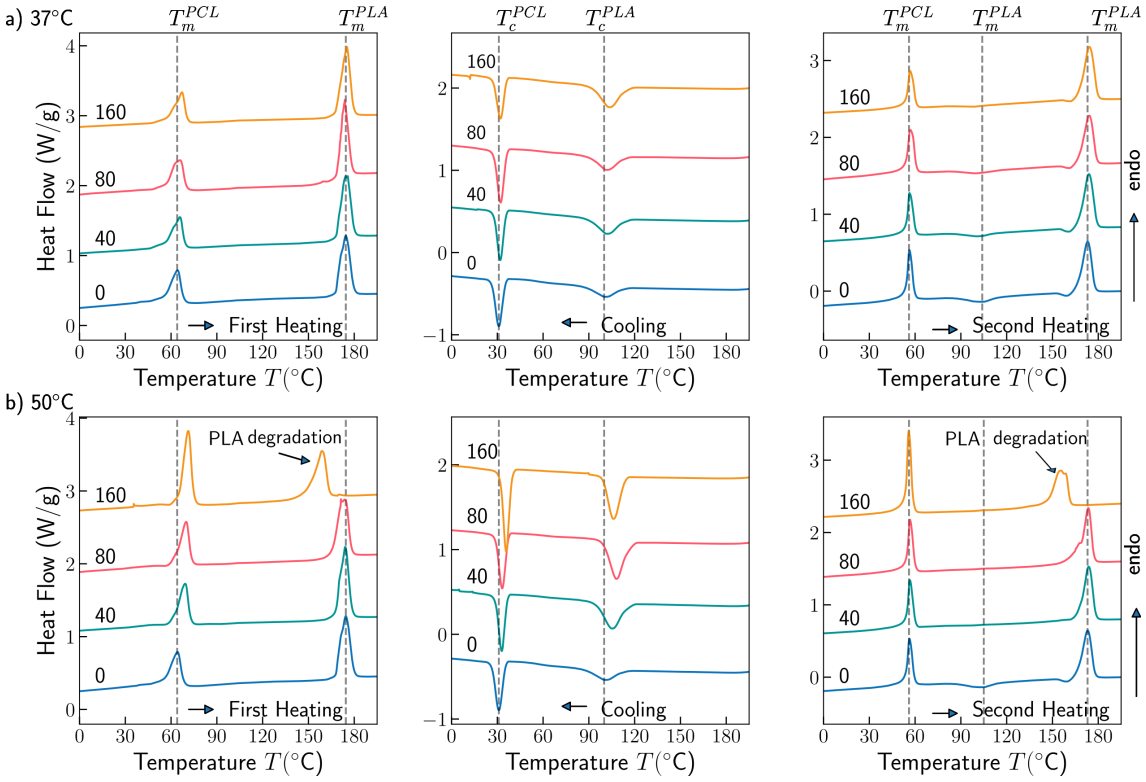


Figure 5.4: Heat flow curves during heating-cooling-reheating steps of the PLA/PCL composite during DSC at a heating/cooling rate of 10°C after immersion in PBS for different days (indicated in each figure). a) After immersion at 37°C, b) after immersion at 50°C. The melting ($T_m^{PLA}$), the crystallisation ($T_c^{PLA}$) and the cold crystallisation ($T_{cc}^{PLA}$) temperatures of the PLA, as well as, the melting ($T_m^{PCL}$) and crystalization temperature of PCL ($T_c^{PCL}$) are indicated with dashed vertical lines.

melting temperature. Conversely, the PLA melting peak temperature decreased from 174.5°C to 158.9°C, suggesting degradation and a decrease in crystalline content. During the cooling phase, similar to the samples degraded at 37°C, both the ($T_c^{PLA}$) and ($T_c^{PCL}$) peaks moved to higher temperatures, rising from 100.3°C to 106.11°C and 30.9°C to 35.8°C, respectively. Finally, reheating did not show the annealing effect in $T_m^{PCL}$ observed in the samples degraded at 37°C. Additionally, the ($T_{cc}^{PLA}$) peak was reduced over time. Notably, there was a substantial decrease in $T_m^{PLA}$, with the peak becoming smaller and appearing at much lower temperatures, and these changes confirmed the material degradation, consistent with the mass loss and pH evolution shown in Figure 5.2.

The molecular weight ($Mw$) distributions of the PLA-PCL composite, analysed through GPC, are plotted in Figure 5.5 a) and b) for the samples immersed in PBS

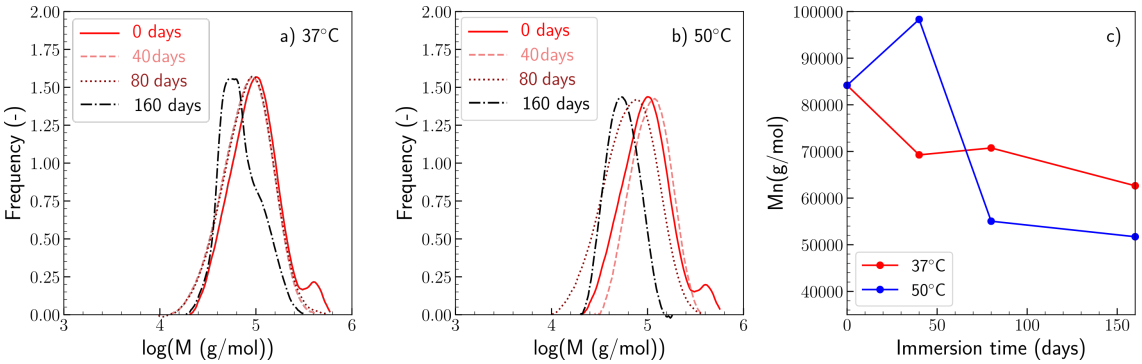


Figure 5.5: Evolution of the molecular weight ($Mw$) distribution of the PLA-PCL composites with immersion time in PBS at: a) 37°C, b) 50°C; c) Evolution of the number average molecular weight ($Mn$) as a function of immersion time for both temperatures.

at 37°C and 50°C, respectively. At 37°C, a bimodal distribution is evident in the as-manufactured sample (red line, 0 days), featuring a minor peak representing higher molecular weights alongside a broader, dominant peak encompassing other molecular weights. The smaller peak disappears as degradation progresses. A slight shift is noticeable between 0 days, 40 days, and 80 days, indicating changes in the molecular weight distribution. However, a more distinct shift towards lower molecular weights becomes evident after 160 days of degradation. Additionally, the curve exhibits a shoulder, indicating chain scission. Thus, GPC data indicate chain scission although mass loss and thermal results did not manifest these changes.

Immersion in PBS at 50°C leads to a noticeable broadening of the molecular weight distribution and the distribution widens further after 80 days of immersion (Figure 5.5 b). This substantial broadening is followed by another significant shift after 160 days, confirming the occurrence of chain scission, which becomes apparent as early as 80 days into the degradation process.

The evolution of the number-averaged molecular weight ($Mn$) over immersion time at 37°C and 50°C is depicted in Figure 5.5 c), and these results are in agreement with the previous observations. As anticipated, the degradation rate was more pronounced at 50°C. A 26% decrease in $Mn$ was observed at 37°C after 160 days, while the reduction reached 39% at 50°C. These findings align with existing literature. Díaz *et al.* (161) reported a significant decrease of approximately 30% in molecular weight for PCL composites after approximately 16 weeks. Furthermore, studies on incorporating polymer blends, as seen in the combination of PCL and PLA in this

case, have confirmed accelerated degradation compared to monolithic materials such as PCL (71).

### 5.1.2 Mechanical behaviour

#### Fabric and composite behaviour

Tensile stress-strain curves of the PLA-PCL weave and of the composite were obtained from the load-displacement $P - \delta$ curves recorded during the tests. The previous section (4.1.2) explained how the stress and strain was calculated in the case of the weaves. For the composites, stress was derived from the force data recorded by the load cell, considering the nominal cross-sectional area of the composite material measured before every test. Deformations were measured using the cross-head displacement, leveraging the gauge length of the dog bone-shaped composite samples, approximately $L_0 \approx 50$ mm. However, it should be noted that the elastic modulus was determined using strain data obtained through digital image correlation.

Representative $\sigma - \epsilon$ curves obtained from PLA-PCL weave and composite are shown in Figure 5.6 a). The averaged tensile properties obtained from three tests per condition are presented in Table 5.1. They correspond to the elastic modulus $E$ (initial slope of the stress-strain curve), the maximum strength $\sigma_{max}$, the strain-to-failure $\epsilon_{max}$ and the tenacity $g$ , already introduced in the 4 Chapter.

The behaviour of the composite material closely resembles that of the woven textile. The initial elastic region extends until the onset of plastic deformation in the PLA fibres. Subsequently, a second linear slope is observed, culminating in a load drop coinciding with the strain-to-failure of the PLA reinforcement fibres, that occurs at approximately 38% strain. This value exceeds slightly the one observed in the woven material (approximately 25%), possibly because the melting of the matrix induced some ductility in the PLA fibres. This mechanism is evident in the optical images of the deformed composites (Figure 5.7), confirming the abrupt load drop associated with the failure. In addition, the stress transfer from the gripping system is softer in the composite material than in the woven ones reducing the damage induced at this area.

Regarding mechanical properties, as detailed in Table 5.1, the elastic modulus of the composite material is roughly three times higher than that of the woven textile while its strength is approximately twice as high. Conversely, the maximum strain experiences a decrease of about fourfold. Interestingly, the composite material

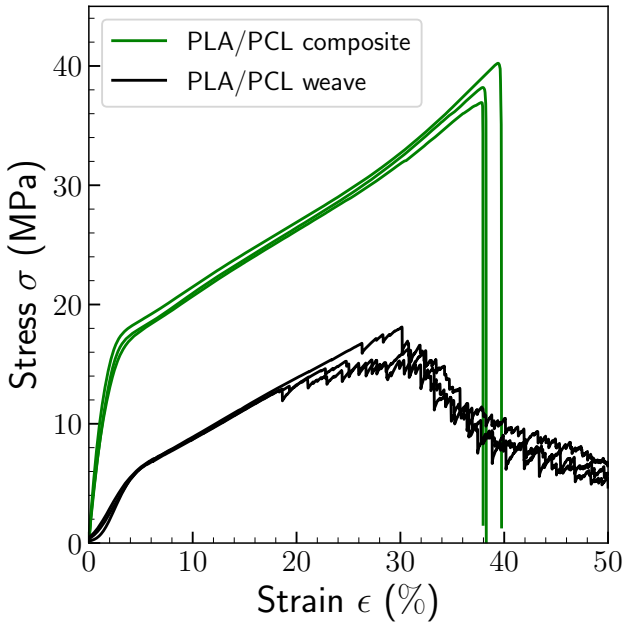


Figure 5.6: Tensile stress-strain curves of the PLA/PCL composite and weave.

exhibits about 1/3 greater toughness than the woven materials, primarily attributed to its ability to achieve higher stresses.

Table 5.1: Mechanical properties of PLA/PCL composite and weave

| Material | $E$ (MPa) | $\sigma_{\max}$ (MPa) | $\epsilon_{max}$ (%) | $g$ (GPa) |
|---|---|---|---|---|
| Weave | 142 ± 14 | 17.5 ± 0.3 | 169 ± 8 | 7.4 ± 0.5 |
| Composite | 452 ± 32 | 38 ± 2 | 38.7 ± 0.8 | 10.0 ± 0.7 |

**Effect of degradation on composite mechanical behaviour**

The tensile mechanical properties of the PLA-PCL composites in water at 37°C were measured after the PLA-PCL have been immersed in PBS at 37°C and 50°C during different times. Stress-strain curves representing three samples for each degradation period are shown in Figure 5.8 a) for degradation at 37°C and b) for degradation at 50°C. The initial strength of the as-manufactured fabric in air at ambient temperature was 38±2 MPa and is depicted in Figure 5.8 as a horizontal dashed line for reference purposes.

Compared to the as-manufactured composites, the reduction in mechanical properties at 0 days can be attributed to both the testing temperature (37°C) and

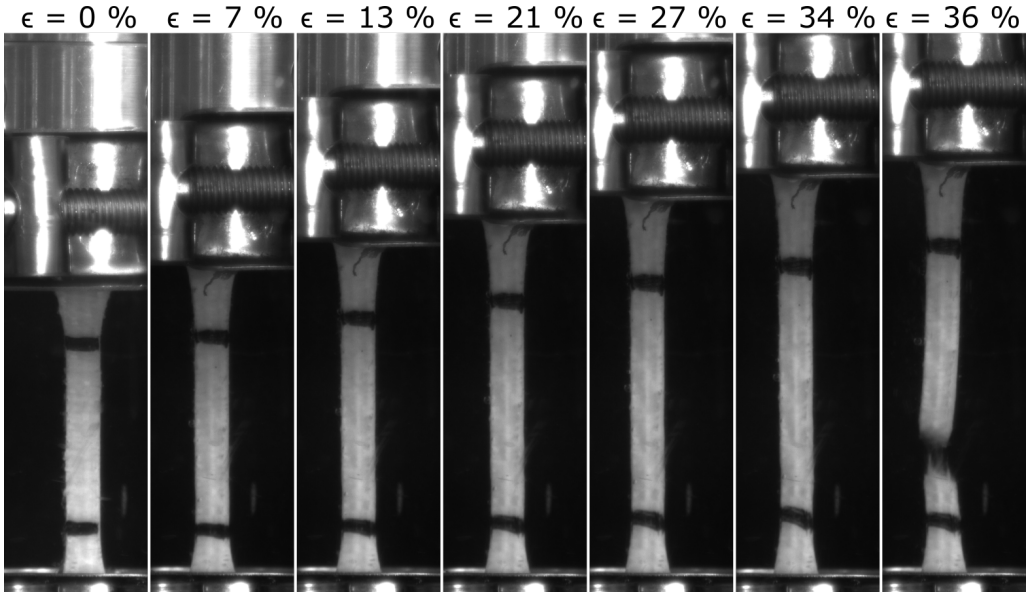


Figure 5.7: Optical images of $50 \times 10$ mm$^2$ as-manufactured composite coupon subjected to tensile deformation. The gauge length between grips $L_0 = 30$ mm is indicated by the parallel horizontal lines.

the water absorption during the immersion in pBS for 24 hours, which also influenced the strain at failure and resulted in a more ductile material. These factors significantly influenced the initial mechanical response of the materials. The mechanical properties (modulus, strength, and toughness) of the composite tested in water after different immersion times at 37°C and 50°C are plotted in Figure 5.9.

The stress-strain curves for the composites degraded at 37°C (Figure 5.8 a) exhibit consistent shapes regardless of the degradation time. The initially display an elastic region that concludes upon the plastic deformation of the PLA fibres, followed by a second linear region until failure occurs in the PLA fibres. Interestingly, there is an increase in the strain-to-failure values after 40 days of immersion, which gradually decreases until 160 days. A slight reduction in maximum strength is observed with prolonged degradation times.

Immersion at 50°C accelerated the degradation of the mechanical properties of the PLA/PCL composite (Figure 5.8 b). Similarly to the degradation at 37°C, a slight increase in strain at failure was observed after 40 days. However, the elastic modulus and maximum strength continuously decreased. After 160 days of immersion at 50°C, the samples were so compromised that they broke while being set up in the test machine.

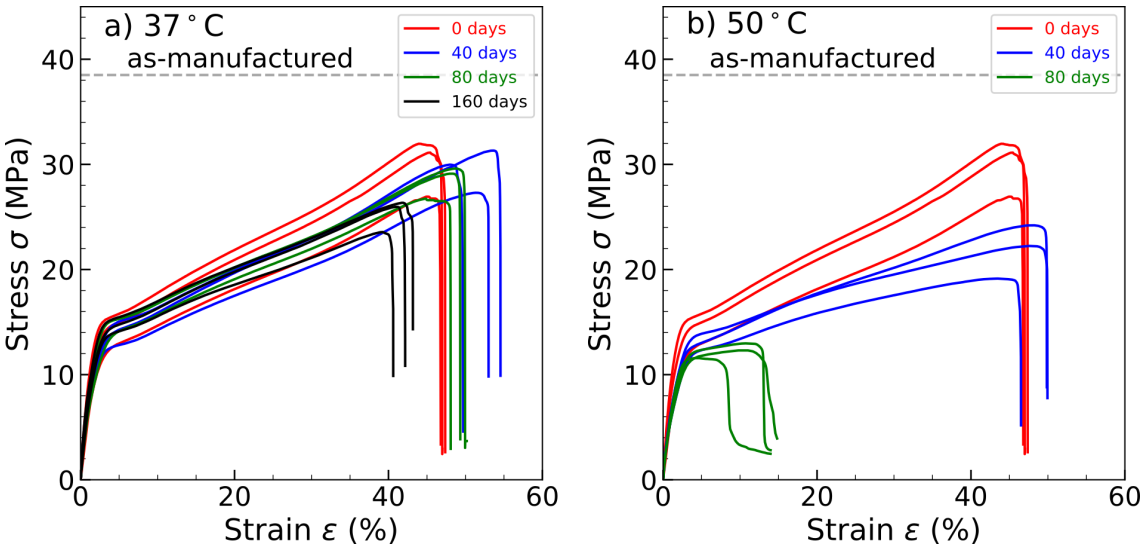


Figure 5.8: Stress-strain curves of the PLA-PLA composites after PBS solution immersion at a) 37°C and b) 50°C. The tests were carried immersed in water at 37°C.

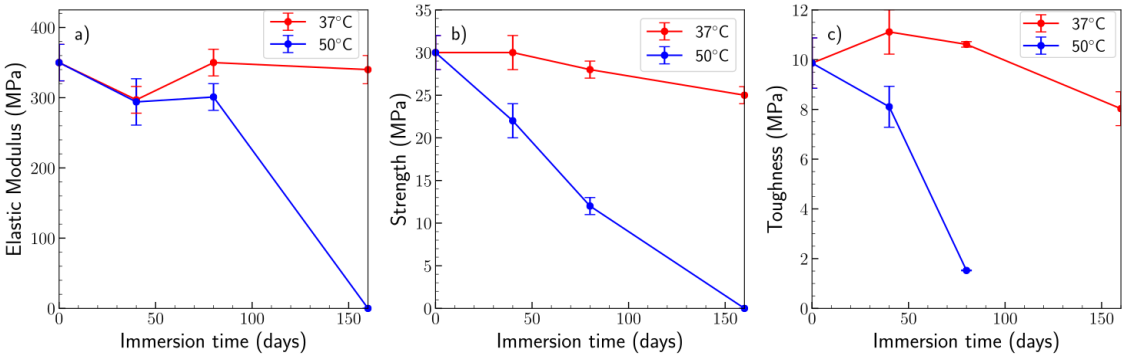


Figure 5.9: Summary of mechanical properties of PLA/PCL composites as a function of immersion time in PBS at 37°C and 50°C. a) Elastic modulus (calculated from DIC strain measurements), b) Tensile strength. c) Toughness (area below the stress-strain curves). It should be noted that all mechanical tests were carried out in the water at 37°C, regardless of the immersion temperature during degradation.

The results presented in Figure 5.9 are in good agreement with the thermo-physical properties observed, where immersion at 37°C showed a minimal mass reduction, and thermal properties did not change until 160 days of degradation. The modulus had no significant impact despite a noticeable drop in molecular weight. However, a slight decline in maximum strength was evident over time, while toughness initially increased, followed by a subsequent decrease after 160 days. In contrast, immersion

at 50°C accelerated the degradation, leading to a marked reduction in modulus, tensile strength, and toughness. These results follow the alterations observed in mass (Figure 5.2), thermal properties (Figure 5.4), and molecular weight (Figure 5.5) with immersion time at this temperature

This material exhibits mechanical properties akin to those of various tendons, such as the quadriceps tendon and the biceps tendon's long head, exhibiting an ultimate stress of approximately 30 MPa and a modulus of 200-400 MPa. These tendons fail at 10-20% strains, indicating that the composite material can withstand even higher strains. Additionally, its mechanical characteristics closely resemble the anterolateral ligament, which has an ultimate tensile strength of about 30 MPa, an elastic modulus of roughly 1 MPa at 20% strain, and a maximum strain of 35-40% (144). The estimated regeneration time for these tissues is around six months and the remodelling phase typically starts 1–2 months post-injury (162; 39). It is essential to highlight the substantial variability in this timeline, influenced by patient-specific factors like physical activity levels, gender, age, and other related aspects.

**Fracture toughness and failure mechanisms**

Based on prior findings, three specific PLA/PCL composite material samples were chosen for analysis, focusing on their tensile fracture surfaces. This examination included observing the fracture surfaces of the laminates under three conditions: at the outset (0 days) and after undergoing degradation for 160 days at 37°C, as well as for 40 days at 50°C, as depicted in Figure 5.10.

The analysis o the fractured surfaces did not reach clear conclusions. This is primarily because the matrix, which holds the composite together, is not easily distinguishable due to the high volume fraction of reinforcing fibres. In one instance, pull-out of fiber bundles is observed in the non-degraded sample (Figure 5.10 a)), and it is highlighted within a red square. Upon closer inspection (Figure 5.10b)), this feature becomes more apparent, although similar observations are not evident in the other samples. Despite these observations, deriving substantial conclusions from these visual examinations was not possible.

**Composite Biocompatibility**

The mitochondrial activity of MC3T3-E1 preosteoblasts was assessed through indirect tests utilising extracts from PLA-PCL composites, following the ISO 10993-5:2009 standard. The outcomes from the dilution process are outlined in Figure 5.11. As per the standard's criteria, when the normalised mitochondrial activity surpasses

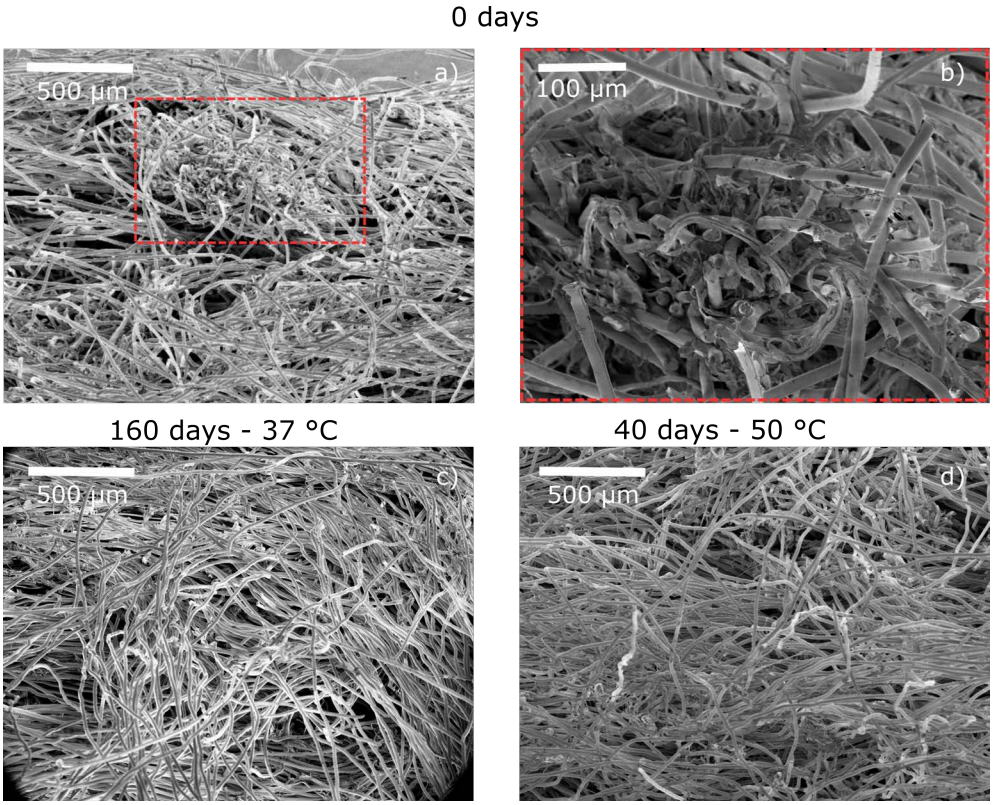


Figure 5.10: Fracture surfaces SEM images of PLA/PCL laminates with different magnifications: a) and b) at 0 days degradation, c) after 160 days degradation at 37°C, and d) after 40 days degradation at 50°C.

70% compared to the control group, the tested material is deemed non-cytotoxic.

The data in Figure 5.11 indicates slight toxicity in the pure extracts, averaging around $57 \pm 11\%$, while displaying approximately 72% mitochondrial activity at a 50% dilution. The contact angle of the PLA-PCL composite was measured in water and culture medium, following the methodology outlined in section 3.2.3. The material exhibited hydrophilic behaviour in deionised water, recording a contact angle of $\Theta_L = 88 \pm 7°$, which reduced to $\Theta_L = 83 \pm 3°$ in the culture medium. Incorporating a bioactive phase like hydroxyapatite (HA) into polymer matrices could reduce the contact angle. HA has shown the ability to significantly improve biocompatibility, increase mechanical strength, and enhance hydrophilicity. For instance, the introduction of HA nanoparticles has been observed to accelerate the differentiation and proliferation of bone cells. This, in turn, triggers the deposition of abundant mineral content rich in calcium within the scaffold, ultimately fostering the rapid formation of new bone tissues (163). Additionally, incorporating collagen could be a potential improvement. Previous studies have shown that the addition

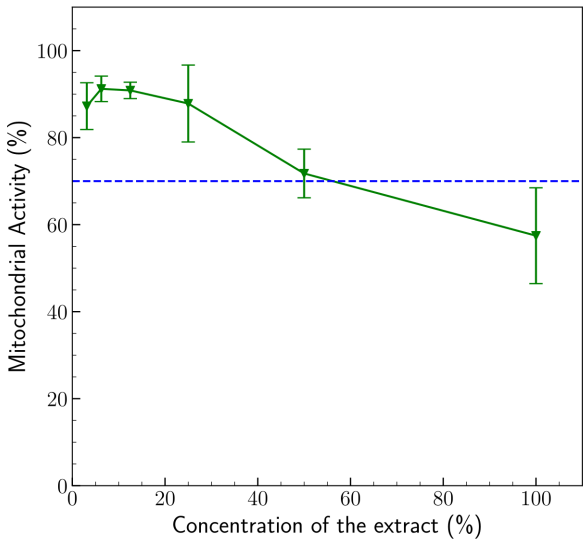


Figure 5.11: Mitochondrial activity as a function of the dilution of extracts from indirect tests in PLA-PCL composite. The dashed line represents the limit for the non-cytotoxic material (70%) according to the standard ISO 10993-5: 2009.

of collagen I, optimized for tendon integration, enhanced fibroblast viability and increased collagen secretion (144).

The cell-composite interaction was evaluated through confocal and scanning electron microscopy via direct testing. Fluorescence images in Figure 5.12 a) and c) display the Ti control and PLA-PCL composite, respectively. The fluorescence of the material made it challenging to observe the cells accurately. Consideration of an alternate dye, such as Rhodamine red, may enhance visibility in future attempts. However, the cells exhibited a round shape, as shown by the SEM images in Figure 5.12 b) and d) for the Ti control and for PLA/PCL composite, respectively, indicating they were attached to the material.

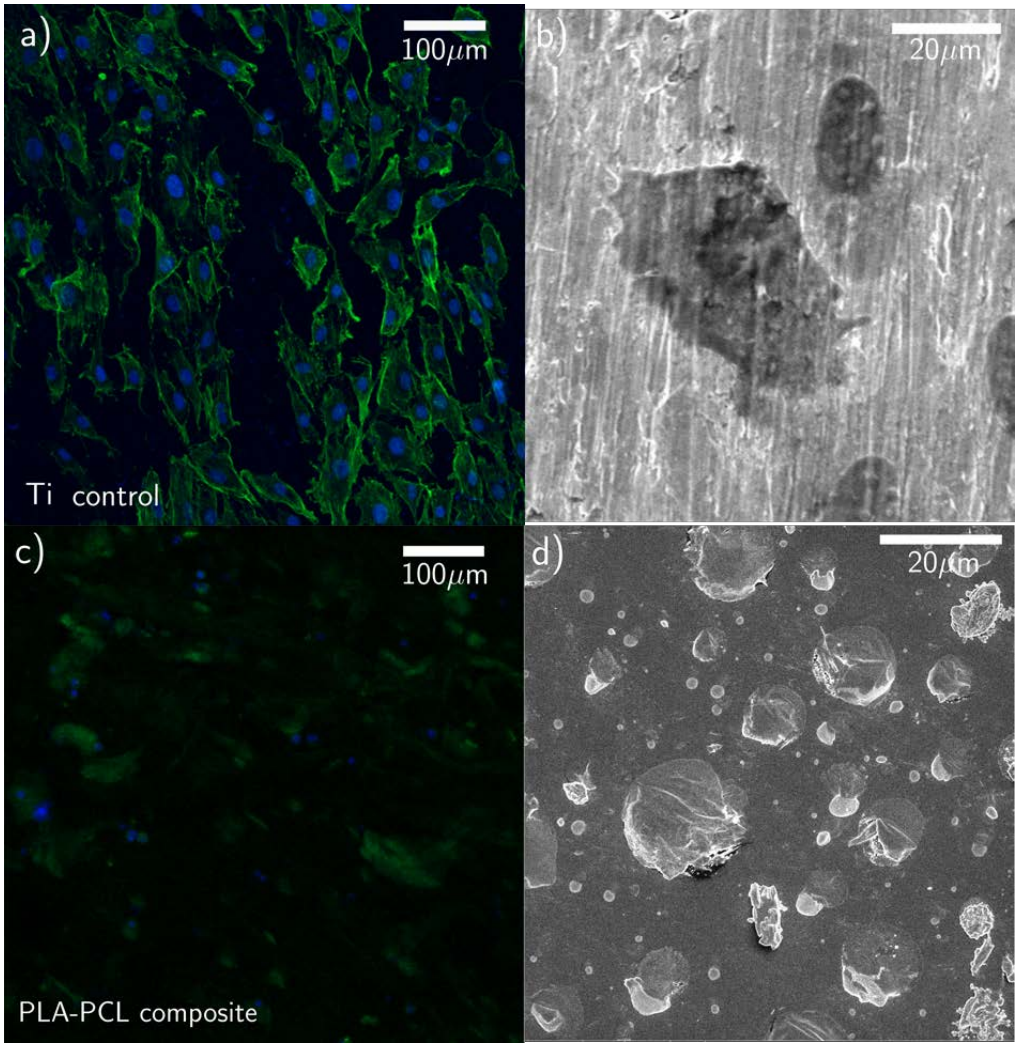


Figure 5.12: Confocal microscopy and SEM images of the interaction between MC3T3-E1 preosteoblasts and the surface of the samples, 24h after seeding. a) and b) Ti control. c) and d) PLA/PCL composite.

## 5.2 PLA-PLA composite

### 5.2.1 *In vitro* degradation tests

In line with other materials investigated in this study, changes in dry mass for the PLA-PLA composite and of the pH of the solution were continuously monitored. Figure 5.13 illustrates the trends in average mass, standard deviation, and pH of the solution of three samples after immersion at 37°C and 50°C, respectively, for different times. For samples immersed in PBS at 37°C, the dry mass remained consistent over the entire 160-day duration, and the pH was maintained around seven throughout this period. In contrast, immersion at 50°C led to a different behaviour. A 10%

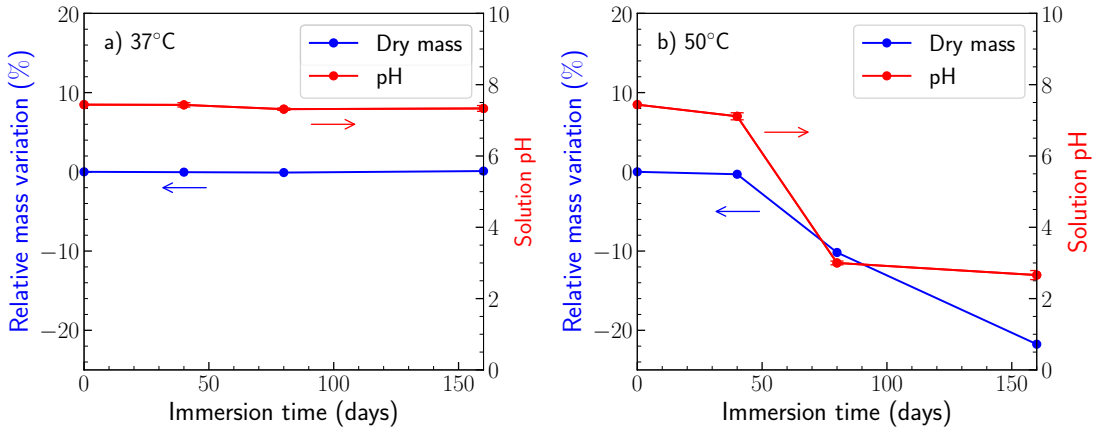


Figure 5.13: Evolution of the dry mass of the PLA/PLA composite samples and the pH of the PBS solution as a function of the immersion time at: a) 37°C, b) 50°C.

decrease in dry mass occurred after 80 days, while the pH also decreased as a result from polymer hydrolysis. A more significant reduction of 21% in dry mass was observed after 160 days, with the pH dropped to 3, indicative of an large polymer degradation process.

Visual observations of material over the 160 days at 37°C and 50°C are presented in Figure 5.14 a) and b). After 160 days at 37°C, the sample exhibited increased opacity despite of no observed decrease in mass. In contrast, the evident decrease in dry mass and the corresponding pH reduction at 50°C (Figure 5.14 c) were associated with large alterations in the composite appearance. The PLA-PLA composite displayed a complete change to a white colour, accompanied by visible disintegration, requiring cautious handling due to its fragile state. Previous findings also demonstrated that transparent PLA films become opaque and white when subjected to temperatures near their glass transition point ($T_g$), making them susceptible to mechanical breakdown (164).

The thermal properties of the composite were evaluated using DSC. The initial curve representing the as-manufactured composite (0 days), depicted in blue in Figure 5.15, illustrates a glass transition temperature ($T_g$) of 58.5°C. Following $T_g$, the curve reveals two distinct melting peaks: one occurring at a lower temperature (151.5°C), denoted as $T_m^{PLAm}$, and another at a higher temperature (180.2°C), labelled as $T_m^{PLAr}$. These peaks confirm the presence of the two distinct PLA components within the composite.

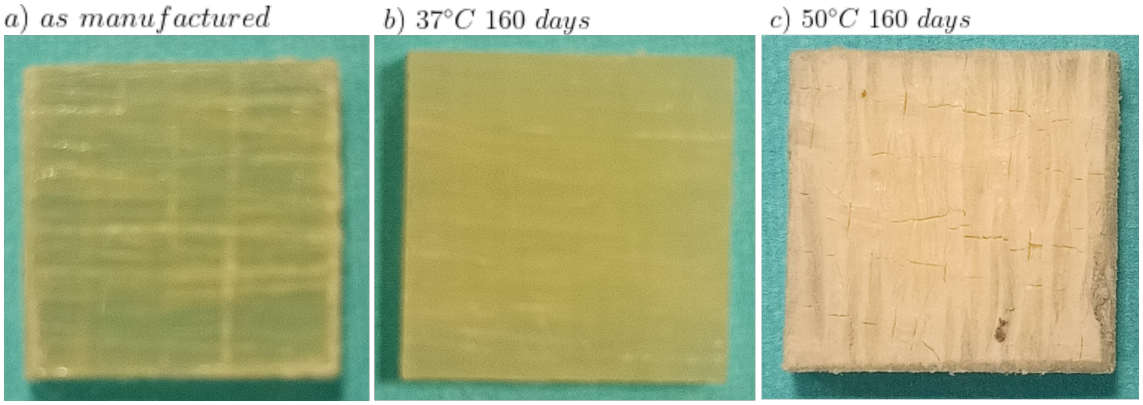


Figure 5.14: Optical appearance of PLA-PLA composite. (a) As manufactured, mass loss =0%, pH=7. (b) After 160 days of immersion in PBS at 37°C, mass loss =0%, pH = 7. c) After 160 days of immersion in PBS at 50°C, mass loss =22%, pH = 2.7.

The heating-cooling-reheating curves of PLA-PLA composites after immersion in PBS at a) 37°C and b) 50°C over 160 days are displayed in Figure 5.15. At 37°C (5.15a), minimal differences are noted in the curves along the degradation period. The glass transition temperature ($T_g$) increases over time from the initial value of 58°$C$ to 63°$C$. Both PLA melting peaks, identified at lower and higher temperatures, remain observable irrespective of the degradation time, indicating no significant alterations throughout the degradation period.

During cooling, the $T_g$ transition at approximately 56°$C$ remains unchanged over 160 days. In the reheating cycle, a more pronounced $T_g$ is observed at around 59°$C$. Additionally, a sharper cold crystallisation peak at around 96°$C$ can be compared to the peak observed in the first heating. However, this peak also remains unchanged during the degradation time. Lastly, the two melting peaks did not suffer significant changes throughout the degradation time. In summary, it is possible to say the polymer suffers some degradation due to the increment of the $T_g$ in the first heating.

These findings are aligned with the literature results. For instance, Niemelä (165) documented negligible mass loss in PLA self-reinforced composites during approximately one year of immersion in PBS at 37°C. However, after roughly two years, there was an observed mass loss of around 40%. Moreover, it has been indicated that self-reinforced PLA undergoes degradation at a slower rate compared to non-reinforced PLA. For instance, non-reinforced PLA typically exhibits a half-life of 90 weeks when comparing their half-lives (the duration required for half of the initial mass to degrade). In contrast, the self-reinforced PLA retained approximately 60%

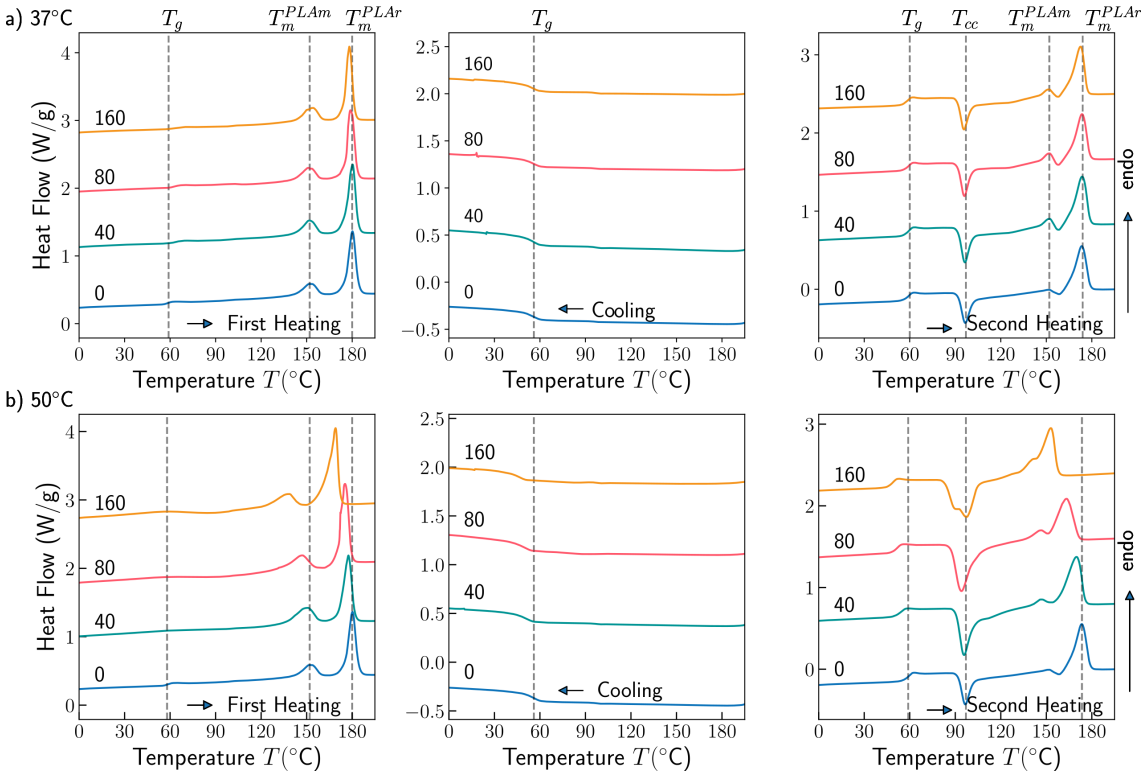


Figure 5.15: Heat flow curves during heating-cooling-reheating steps of the PLA/PLA composite during DSC at a heating/cooling rate of 10°C after immersion in PBS for different days (indicated in each figure). a) After immersion at 37°C, b) after immersion at 50°C. The glass transition ($T_g^{PLA}$), the crystallisation ($T_c^{PLA}$) and the cold crystallisation ($T_{cc}^{PLA}$)temperatures of the PLA yarns,$T_m^{PLAm}$ the melting temperature of PLA that will serve as matrix and $T_m^{PLAr}$ the melting temperature of the PLA that will act as reinforcement, are indicated with dashed vertical lines.

of its initial mass after the 104-week in vitro study period (165).

The DSC analysis of samples degraded at 50°C (Figure 5.15 b) revealed significant degradation effects. The glass transition temperature ($T_g^{PLA}$) was not observable or detectable. Over 160 days, the melting peaks ($T_m^{PLAm}$ and $T_m^{PLAr}$) decreased from 151.5°C to 137.0°C and from 180.15°C to 169.1°C, respectively. During cooling, $T_g^{PLA}$ dropped from around 56.1°C to about 46.1°C after 160 days, indicating degradation. In the final cycle, $T_g^{PLA}$ decreased by approximately 10°C. Notably, the cold crystallisation temperature ($T_{cc}^{PLA}$) after 160 days displayed a double peak. Eventually, the melting temperature decreased until both melting peaks merged. The DSC analysis highlighted substantial changes after 160 days of degradation at 50°C. These included shifts in $T_g^{PLA}$, cold crystallisation behaviour modifications, and melting peak patterns. These changes indicate a profound degradation of the

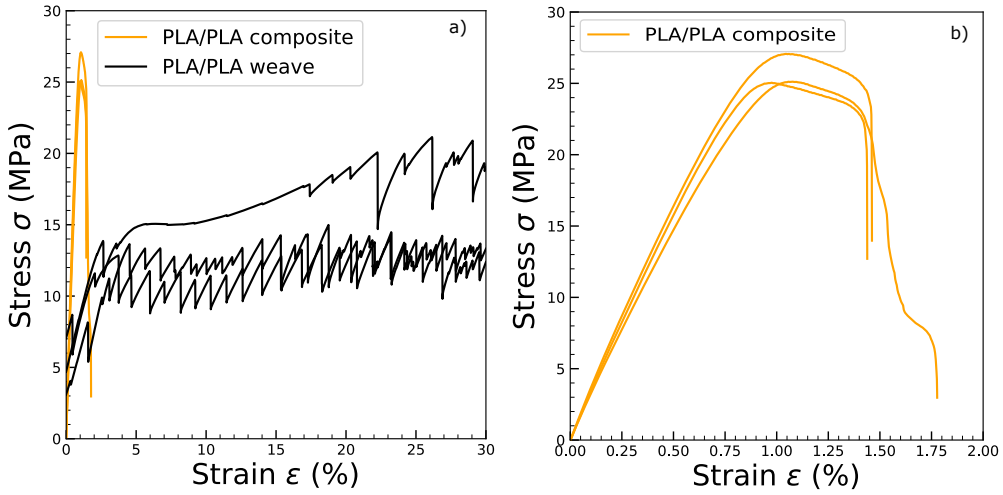


Figure 5.16: a)Tensile stress-strain curves of the PLA/PLA composite and fabric. b) Tensile stress-strain curves of the same PLA/PLA composite.

thermal properties of the composite.

Similar observations were noted in the study by Fefel *et al.* (159). They investigated the degradation characteristics of polylactic acid (PLA) composites within PBS from 21 to 85°C. Following 56 days at 50°C, the glass transition and melting temperatures had decreased by approximately 10°C. Additionally, there was a 0.2% drop in mass during this period.

### 5.2.2 Mechanical behaviour

#### Fabric and composite behaviour

The tensile stress-strain curves for the as-manufactured composites and weave are depicted in Figure 5.16. To compute the stress ($\sigma$), the applied load ($P$) divided by the nominal cross-section of the composite. Strain ($\epsilon$) was determined from the machine's cross-head displacement ($\delta$) assumming an initial gauge length ($L_0$)$approximately \approx$ 50 mm of the dog bone-shaped composite samples. In this case, the elastic modulus was determined using strain data calculated with the machine displacement obtained $\epsilon = \delta / L_0$ (and not from digital image correlation).

The averaged tensile properties obtained from three tests per condition are summarized in Table 5.2. They comprise the elastic modulus $E$ (initial slope of the stress-strain curve), the maximum strength $\sigma_{max}$, the strain-to-failure $\epsilon_{max}$ and the tenacity $g$ (volumetric energy).

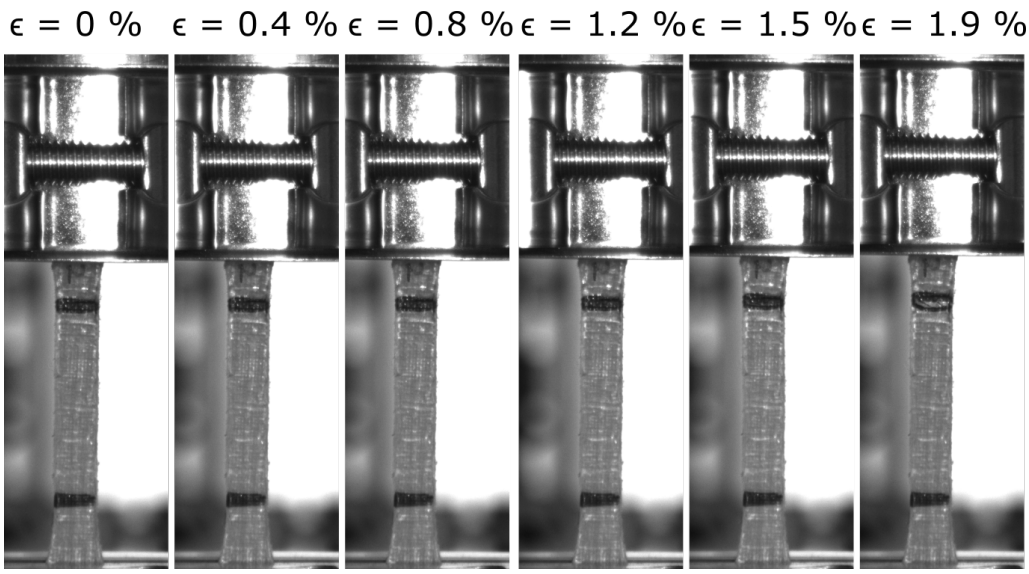


Figure 5.17: Optical images of $50 \times 10$ mm$^2$ as-manufactured composite coupon subjected to tensile deformation. The gauge length between grips ($L_0 = 30$ mm) is indicated by the parallel horizontal lines.

The composite material shows a very low ductility, as compared to all previously tested materials. Its initial elastic region stretches until a load drop, aligning with the strain-to-failure of the PLA reinforcement fibres that occur at 1.4% strain. Unlike the PLA/PCL composite, this material does not exhibit two distinct linear regions in its mechanical behaviour. This mechanism becomes apparent when observing the optical images of the deformed composites (Figure 5.17), typical of a very brittle material.

When considering the mechanical properties outlined in Table 5.2, the composite material displays a noteworthy enhancement in certain aspects. Specifically, its modulus is roughly six times greater than that of the woven material. Additionally, the composite strength is approximately double that of the weave. However, this increase in stiffness and strength comes at the cost of diminished ductility and toughness. The composite experiences a sharp decrease in the strain to failure, indicating reduced flexibility before failure and a noticeable decline in toughness compared to the woven material.

**Effect of degradation on the composite mechanical behaviour**

The PLA-PLA composites were immersed in PBS at two different temperatures, 37°C and 50°C. The mechanical properties were evaluated through tensile tests at 37°C, irrespective of the specific PBS immersion temperature. The stress-strain

Table 5.2: Mechanical properties of PLA/PLA composite and weave

| Material | $E$ (MPa) | $\sigma_{\max}$ (MPa) | $\epsilon_{max}$ (%) | $g$ (GPa) |
|---|---|---|---|---|
| Weave | 425 ± 97 | 15 ± 3 | 40 ± 8 | 6 ± 1 |
| Composite | 2854 ± 33 | 26 ± 1 | 1.4 ± 0.2 | 0.2 ± 0.02 |

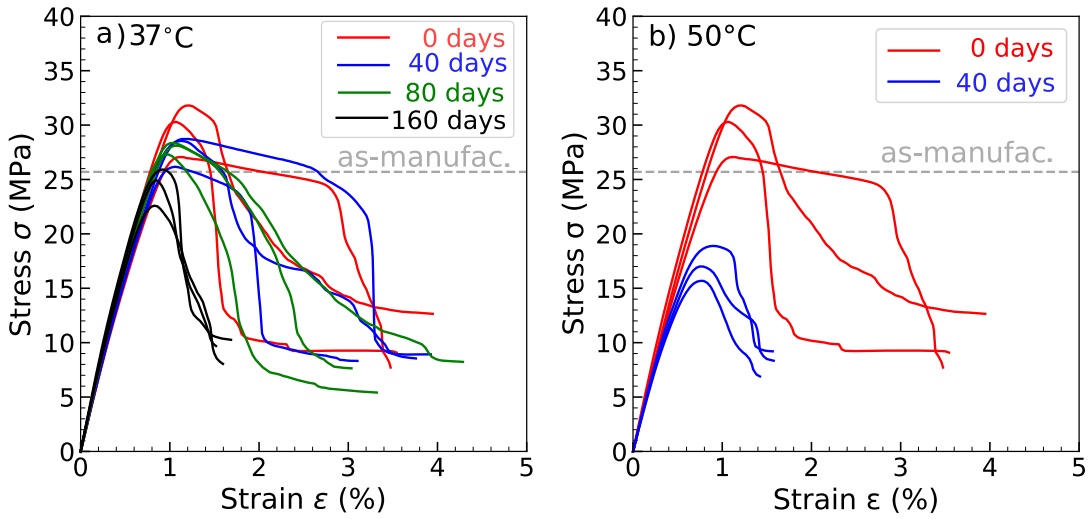


Figure 5.18: Stress-strain curves of the PLA-PLA composites after PBS solution immersion at a) 37°C and b)50 °C. The tests were carried out immersed in water at 37°C irrespective of the degradation conditions in PBS solution.

curves of three samples per degradation period at 37°C and 50°C, are plotted in Figure 5.18 a) and b), respectively. To provide a reference, the initial strength of the composite in air at ambient temperature, 26 ± 1 MPa, is represented as a horizontal dashed line in Figure 5.18. Unexpectedly, the dry material exhibited a similar modulus but lower strength than the samples immersed in water. A summary of the mechanical properties (modulus, strength, and toughness) as a function of the immersion times is depicted in Figure 5.19 .

The stress-strain curves of the degraded composites at 37°C (Figure 5.18 a) show an elastic region that continues until failure in the PLA fibres. However, the strain-to-failure values and the strength decrease after 160 days of immersion in PBS, while the modulus remains relatively stable.

Exposing the composites to immersion at 50°C, significantly hastened the degradation of the mechanical properties , as illustrated in Figure 5.18b. Within 40 days,

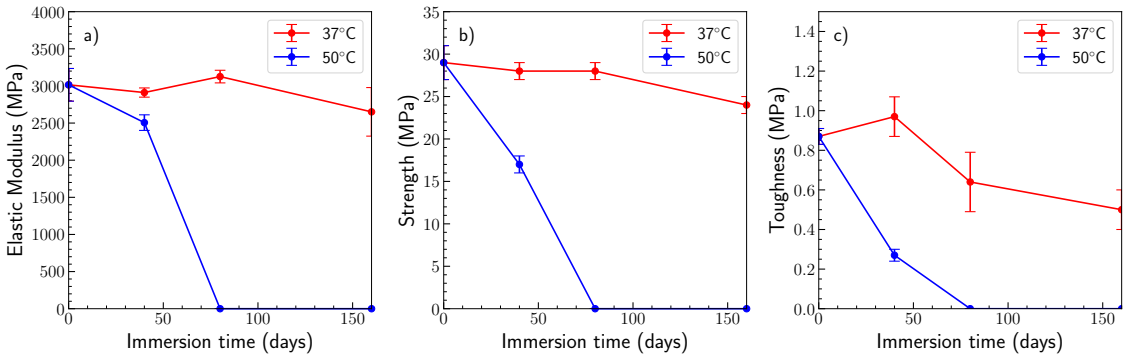


Figure 5.19: Summary of mechanical properties of PLA/PLA composites as a function of immersion time in PBS at 37°C and 50°C. a) Elastic modulus, b) Tensile strength. c) Toughness (area below the stress-strain curves). It should be noted that all mechanical tests were carried out in the water at 37°C, regardless of the immersion temperature during degradation.

the strength was reduced by half, while the modulus experienced a slight decrease. Samples degraded for 80 and 160 days became so brittle that they broke during setup in the testing machine.

The findings illustrated in Figure 5.19 are consistent with the observed thermo-physical properties. Immersion at 37°C resulted in minimal mass change and slight alterations in thermal properties, specifically a decrease in $T_g$ up to 160 days of degradation. The modulus remained relatively unaffected, but there was a gradual decline in maximum strength, while toughness initially increased before decreasing after 160 days. Again, Niemelä (165) investigated the self-reinforced composite's in vitro degradation behaviour in PBS at 37°C for approximately 104 weeks (roughly two years). It was observed that the material's mechanical properties became immeasurable after about 75 weeks (1.5 years) in this environment. After around one year of degradation, these composites retained only about 15% of their initial shear strength, showcasing a significant loss compared to the observed degradation of approximately 17% in tensile properties after 160 days (about five months) at 37 °C, as observed in this study.

Conversely, immersion at 50°C significantly hastened degradation, causing fast reductions in modulus, tensile strength, and toughness. These results closely parallel the changes observed in mass (Figure 5.13) and thermal properties (Figure 5.15). Comparing both degradation scenarios, it is evident that degradation after 40 days at 50°C is more pronounced than the effects seen over 160 days at 37 °C.

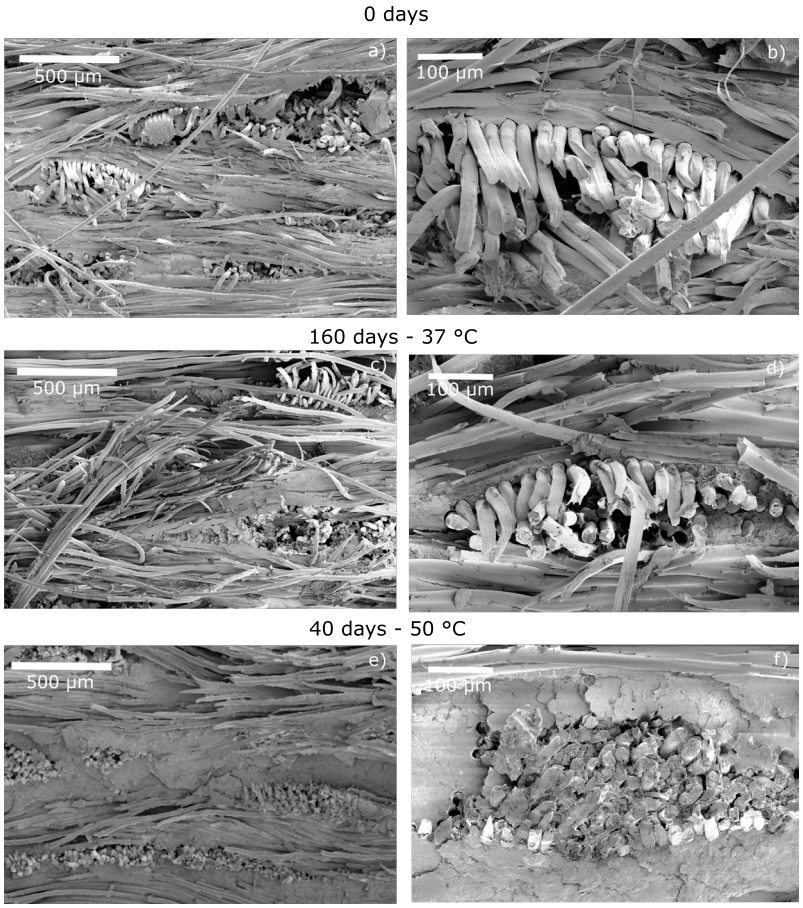


Figure 5.20: Fracture surfaces SEM images of the self-reinforced PLA laminates with different magnifications: a) and b) at 0 days degradation, c) and d) after 160 days degradation at 37°C, and e) and f) after 40 days degradation at 50°C.

Considering its properties, this material is not suitable for applications involving tendons or ligaments due to its low strain at failure. However, its high modulus could make it applicable for small bones. However, it is worth noting that the maximum stress capacity is also limited. Adjustments are necessary to make them more viable for these applications. For instance, introducing PCL could enhance its flexibility, or altering the ratio of PLA in the reinforcement fibres could also be explored as a potential modification.

**Fracture toughness and failure mechanisms**

Considering the previous results, three samples of PLA self-reinforced material were selected to see the tensile fracture surfaces to identify damage modes. Thus, fracture surfaces of the laminates at 0 days degradation, after 160 days at 37°C and after 40 days at 50°C, Figure 5.20.

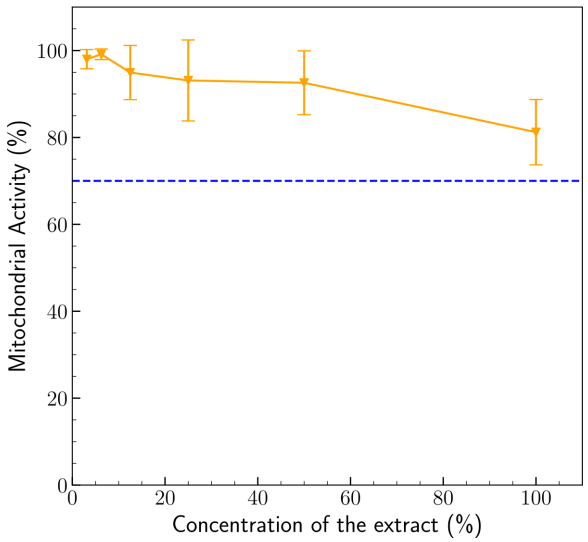


Figure 5.21: Mitochondrial activity as a function of the dilution of extracts from indirect tests in PLA-PLA composite. The dashed line represents the limit for the non-cytotoxic material (70%) according to the standard ISO 10993-5: 2009.

The post-tensile test observations in all images reveal bundled fibres being pulled from the surface. Visible holes on the opposing fracture surface confirm that this material behaves as a composite. Similarities are evident between the fracture surfaces of non-degraded samples, 0 days in Figure 5.20 a) and b), and those degraded for 160 days at 37°C, Figure 5.20 c) and d). The fibres appear more debonded, displaying significant fibre pull-out, indicating the energy dissipation from cracks successfully detaching the matrix from the fibres. Comparatively, samples degraded for 40 days at 50°C exhibit shorter fibre pull-out, suggesting less energy dissipation. The fracture surfaces in 5.20 e) and f), show much less pull-out indicating a higher degree of fibre degradation, even more so than those degraded for 160 days at 37°C. These findings align with the tensile test results, indicating that samples with greater tensile strength and toughness exhibit more debonding and fibre pull-out.

### Composite Biocompatibility

The mitochondrial activity of in MC3T3-E1 preosteoblasts was examined indirectly using extracts from PLA-PLA composites, following the ISO 10993-5:2009 standard. The results of the dilution process are depicted in Figure 5.21. According to the standard, if the normalised mitochondrial activity exceeds 70 % compared to the control group, the tested material is considered non-cytotoxic.

The findings in Figure 5.21 demonstrate the biocompatibility for the pure extracts,

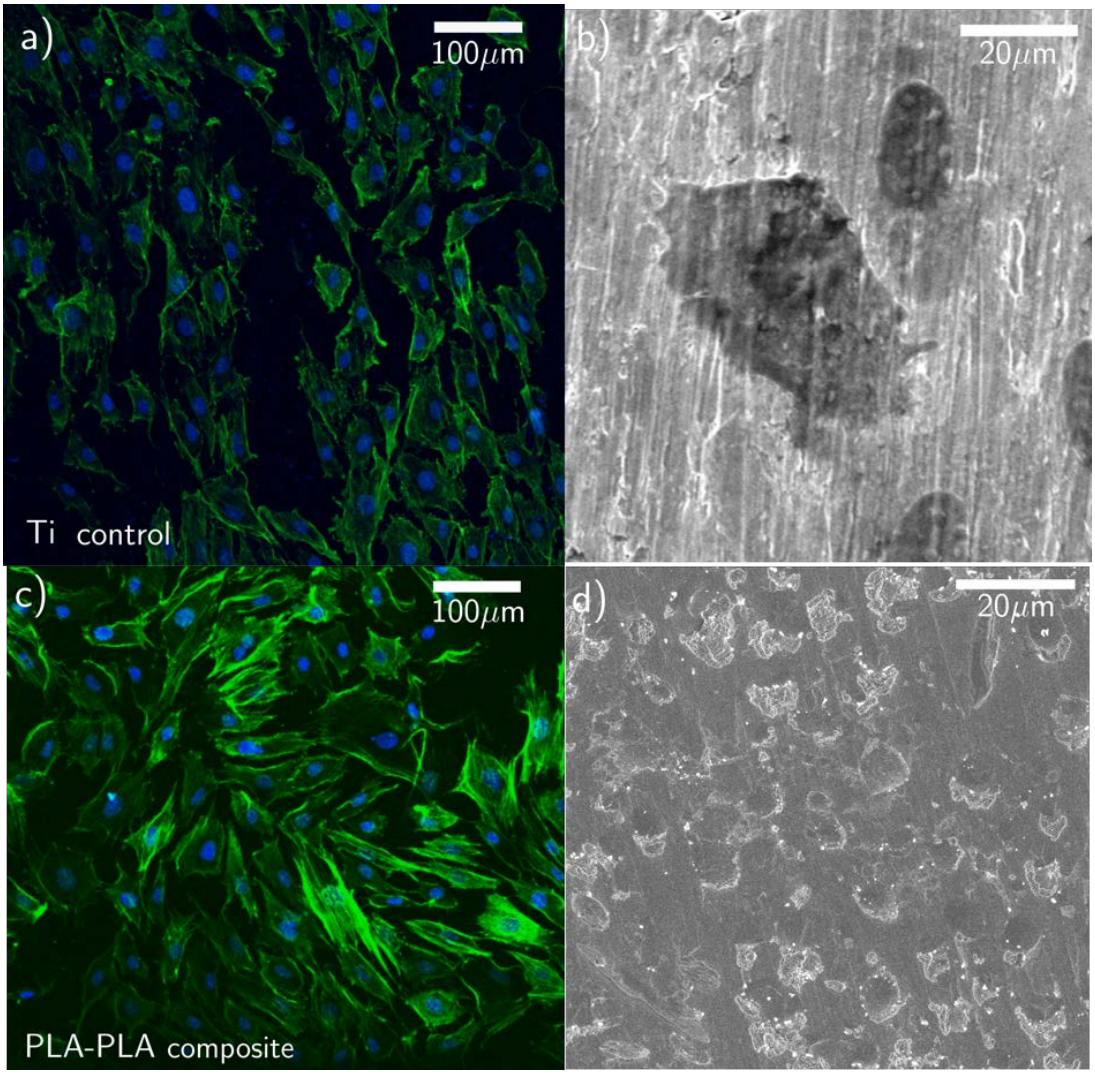


Figure 5.22: Confocal microscopy and SEM images of the interaction between MC3T3-E1 preosteoblasts and the surface of the samples,24h after seeding. a) and b) Ti control. c) and d) PLA/PLA composite.

averaging approximately $81 \pm 8\%$. The contact angle was measured in both water and culture medium, following the methodology outlined in section 3.2.3. The material displayed hydrophilic tendencies in both deionised water and culture medium, with a contact angle of $\Theta_L = 76 \pm 2°$, which decreased to $\Theta_L = 64 \pm 4°$ in the culture medium. Numerous studies have shown that cells exhibit enhanced attachment and spreading on surfaces possessing suitable hydrophilic properties compared to those with hydrophobic characteristics (166).

These findings were validated by a direct examination where confocal and scanning electron microscopy assessed the interaction between cells and the composite.

Fluorescence images in Figure 5.22 a) and c) showcase the Ti control and PLA-PLA composite, respectively. They reveal a well-defined monolayer of cells with triangular shapes adhering to the surface of the composite. Additionally, the SEM images depicted in Figure 5.22 b) and d) for the Ti control and PLA/PLA composite, respectively, showed several cells above the surface of the material, indicating their attachment to the material.

# Conclusions and future work 6

## 6.1 Conclusions

This thesis provides novel results on the application of commingling to manufacture woven textiles and composite materials of different biodegradable polymers to tailor the mechanical properties and degradation rate for repair and healing of connective tissue. The following conclusions are reached from the results presented in the thesis:

• Woven textiles of PLA-PCL and PLA-PLA were manufactured from commingled yarns of both polymers. It was shown that the mechanical properties could be controlled from the volume fraction and mechanical properties of each type of fiber in the commingled yarns, providing a large flexibility to tailor the stiffness, strength and tenacity of the textile. In particular, the properties of PLA-PCL were suitable for tendon ligaments for the high ductility.

• The degradation rate of the PLA-PCL and PLA-PLA woven textiles at 37°C in PBS was limited during the first 80 days of immersion and the reduction of the mechanical properties (that could be associated to the hydrolysis of the polymers chains) was noticeable after 160 days. These results indicate that these materials can be used for connective tissue implants because the average regeneration time for these tissues is around six months. Moreover, the link between the degradation mechanisms and the reduction in the mechanical properties with the variation in molecular weight and crystallinity of the different polymer fibers was established, opening the path to control the evolution of the properties of the textile through the use of different fibers.

• Composite plates manufactured from the PLA-PCL presented much higher stiffness and strength than the PLA-PCL woven textile while the ductility was maintained. Thus, consolidation by compression moulding provided another path to

tailor the mechanical properties of the material for different applications. However, compression moulding of the PLA-PLA woven textile only improved the stiffness and the strength but with a dramatic reduction in ductility. The properties of the PLA-PCL composite plates were suitable for the repair of various tendons.

• The degradation rate of the PLA-PCL and PLA-PLA composite plates by immersion in PBS at 37° was slower than that of the woven textiles very likely because of the lower porosity. The reduction in the mechanical properties after 160 days of immersion was limited. The degradation mechanisms were similar to those reported for the textile materials.

• The biocompatibility evaluation through biological tests confirmed that all materials were suitable for tissue engineering applications and that neither the processing route nor the microstructure impaired cell adhesion proliferation.

## 6.2 Future work

The future of Tissue Engineering holds immense potential to meet a wide range of medical needs. However, numerous steps and challenges must be addressed before a material can successfully enter the market for implantation. Areas for future work to address this gap are:

• One type of woven materials and composites were studied in this thesis. There is considerable room for a comprehensive optimization of materials by exploring the fiber type and volume fraction and the woven structure to meet the properties required for particular applications.

• Extension of the characterization of the mechanical properties to more realistic scenarios should be carried out before in vivo tests are planned. They included in vitro fatigue tests in different orientations.

• More detailed biological characterization (Live Dead assays and lactate dehydrogenase tests) would be necessary to establish the biological interaction between cells and materials.

# Bibliography


[1] L. N. Ramoshebi, T. N. Matsaba, J. Teare, L. Renton, J. Patton, and U. Ripamonti, "Tissue engineering: TGF-$\beta$ superfamily members and delivery systems in bone regeneration," pp. 1–11, 2002.

[2] A. E. Eldeeb, S. Salah, and N. A. Elkasabgy, "Biomaterials for tissue engineering applications and current updates in the field: A comprehensive review," *AAPS PharmSciTech*, 2022.

[3] R. Mhanna and A. Hasan, "Introduction to tissue engineering: Regenerative medicine, smart diagnostics and personalized medicine," *Tissue Engineering for Artificial Organs: Regenerative Medicine, Smart Diagnostics and Personalized Medicine*, pp. 1–34, 2017.

[4] B. R. Freedman and D. J. Mooney, "Biomaterials to Mimic and Heal Connective Tissues," *Advanced Materials*, pp. 1–53, 2019.

[5] I. Muntz, M. Fenu, G. J. V. M. van Osch, and G. H. Koenderink, "The role of cell-matrix interactions in connective tissue mechanics," *Physical Biology*, pp. 1–13, 2022.

[6] B. Wnek, *Encyclopedia of Biomaterials and Biomedical Engineering*. Andover, England, UK: Taylor & Francis, 2015.

[7] Y. Tang, Z. Wang, L. Xiang, Z. Zhao, and W. Cui, "Functional biomaterials for tendon/ligament repair and regeneration," *Regenerative Biomaterials*, pp. 1–19, 2022.

[8] C. Yilgor, P. Yilgor Huri, and G. Huri, "Tissue engineering strategies in ligament regeneration," *Stem Cells International*, pp. 1–9, 2012.

[9] C. Rinoldi, E. Kijenska-Gawronska, A. Khademhosseini, A. Tamayol, and Wojciech Swieszkowski, "Fibrous systems as potential solutions for tendon and ligament repair, healing, and regeneration," *Advanced Healthcare Materials*, pp. 1–26, 2021.

[10] Y. Jiao, C. Li, L. Liu, F. Wang, X. Liu, J. Mao, and L. Wang, "Construction and application of the textile-based tissue engineering scaffold: A review," *Biomaterials Science*, pp. 1–30, 2020.

[11] X. Zhu, C. Wang, H. Bai, J. Zhang, Z. Wang, Z. Li, X. Zhao, J. Wang, and H. Liu, "Functionalization of biomimetic mineralized collagen for bone tissue engineering," *Materials Today Bio*, pp. 1–21, 2023.

[12] "StatNano," Oct. 2023. [Online; accessed 2. Oct. 2023].

[13] U. Themes, "Tendons and Ligaments," *Musculoskeletal Key*, 2020.

[14] A. Sensini and L. Cristofolini, "Biofabrication of Electrospun Scaffolds for the Regeneration of Tendons and Ligaments," *Materials (Basel)*, pp. 1–43, 2018.

[15] A. V. Vasiliadis and K. Katakalos, "The Role of Scaffolds in Tendon Tissue Engineering," *Functional Biomaterials*, pp. 1–11, 2020.

[16] M. R. Citeroni, M. C. Ciardulli, V. Russo, G. D. Porta, A. Mauro, M. E. Khatib, M. Di Mattia, D. Galesso, C. Barbera, N. R. Forsyth, N. Maffulli, and B. Barboni, "In Vitro Innovation of Tendon Tissue Engineering Strategies," *Internacional Journal Molecular Science*, pp. 1–78, 2020.

[17] C.-Y. Lin and J.-H. Kang, "Mechanical Properties of Compact Bone Defined by the Stress-Strain Curve Measured Using Uniaxial Tensile Test: A Concise Review and Practical Guide," *Materials*, pp. 1–16, 2021.

[18] R. J. Hodgson, P. J. O'Connor, and A. J. Grainger, "Tendon and ligament imaging," *The British Journal of Radiology*, p. 1157–1172, 2012.

[19] R. B. Martin, D. B. Burr, N. A. Sharkey, and D. P. Fyhrie, *Skeletal Tissue Mechanics*. New York, NY, USA: Springer, 2015.

[20] P. Feng, J. Jia, M. Liu, S. Peng, Z. Zhao, and C. Shuai, "Degradation mechanisms and acceleration strategies of poly (lactic acid) scaffold for bone regeneration," *Materials Design*, pp. 1–18, 2021.

[21] J. R. Dias, A. Sousa, A. Augusto, P. J. Bártolo, and P. L. Granja, "Electrospun Polycaprolactone (PCL) Degradation: An In Vitro and In Vivo Study," *Polymers*, pp. 1–15, 2022.

[22] N. Abbasi, S. Hamlet, R. M. Love, and N.-T. Nguyen, "Porous scaffolds for bone regeneration," *Journal Science: Advanced Mateials and Devices*, pp. 1–9, 2020.

[23] M. Silva, S. Gomes, C. Correia, D. Peixoto, A. Vinhas, M. T. Rodrigues, M. E. Gomes, J. A. Covas, M. C. Paiva, and N. M. Alves, "Biocompatible 3D-Printed Tendon/Ligament Scaffolds Based on Polylactic Acid/Graphite Nanoplatelet Composites," *Nanomaterials*, pp. 1–23, 2023.

[24] L. Smith, Y. Xia, L. M. Galatz, G. M. Genin, and S. Thomopoulos, "Tissue-engineering strategies for the tendon/ligament-to-bone insertion," *Connective Tissue Research*, pp. 95–105, 2012.

[25] H. Ramakrishna, T. Li, T. He, J. Temple, M. W. King, and A. Spagnoli, "Tissue engineering a tendon-bone junction with biodegradable braided scaffolds," *Biomaterials Research*, pp. 1–12, 2019.

[26] S. Sahoo, J. G. Cho-Hong, and T. Siew-Lok, "Development of hybrid polymer scaffolds for potential applications in ligament and tendon tissue engineering," *Biomedical Materials*, pp. 169–173, 2007.

[27] O. Hakimi, P. A. Mouthuy, N. Zargar, E. Lostis, M. Morrey, and A. Carr, "A layered electrospun and woven surgical scaffold to enhance endogenous tendon repair," *Acta Biomaterialia*, pp. 124–35, 2015.

[28] D. C. Marshall, F. D. Silva, B. T. Goldenberg, D. Quintero, M. G. Baraga, and J. Jose, "Imaging Findings of Complications After Lateral Extra-Articular Tenodesis of the Knee: A Current Concepts Review," *Orthopaedic Journal of Sports Medicine*, pp. 1–14, 2022.

[29] A.-M. Pobloth, S. Checa, H. Razi, A. Petersen, and J. C. Weaver, "Mechanobiologically optimized 3D titanium-mesh scaffolds enhance bone regeneration in critical segmental defects in sheep," *Science Translational Medicine*, pp. 1–16.

[30] A. U. Daniels, M. K. Chang, and K. P. Andriano, "Mechanical properties of biodegradable polymers and composites proposed for internal fixation of

bone.," *Journal of applied biomaterials : an official journal of the Society for Biomaterials*, pp. 57–78, 1990.

[31] F. A. Barber, M. A. Herbert, and D. A. Coons, "Tendon augmentation grafts: biomechanical failure loads and failure patterns," *Arthroscopy*, pp. 534–538, 2006.

[32] B. Allan, R. Ruan, E. Landao-Bassonga, N. Gillman, T. Wang, J. Gao, Y. Ruan, Y. Xu, C. Lee, M. Goonewardene, and M. Zheng, "Collagen Membrane for Guided Bone Regeneration in Dental and Orthopedic Applications," *Tissue Engeneering Part A*, pp. 372–381, 2021.

[33] M. M. Murray, E. Magarian, D. Zurakowski, and B. C. Fleming, "Bone-to-bone Fixation Enhances Functional Healing of the Porcine Anterior Cruciate Ligament Using a Collagen-Platelet Composite," *Arthroscopy : the journal of arthroscopic & related surgery : official publication of the Arthroscopy Association of North America and the International Arthroscopy Association*, pp. 1–17, 2010.

[34] S. Leduc, L. Yahia, F. Boudreault, J. C. Fernandes, and N. Duval, "[Mechanical evaluation of a ligament fixation system for ACL reconstruction at the tibia in a canine cadaver model]," *Annales de Chirurgie*, pp. 735–741, 1999.

[35] K. Schindhelm, G. J. Rogers, B. K. Milthorpe, P. J. Hall, C. R. Howlett, R. Sekel, J. Goldberg, and W. Viglione, "Autograft and Leeds-Keio reconstructions of the ovine anterior cruciate ligament," *Clinical Orthopaedics*, pp. 278–293, 1991.

[36] "Tendon Repair Surgery, X-Repair Technology, Tendon Repair Technology," Sept. 2023. [Online; accessed 27. Sep. 2023].

[37] F. R. Noyes, L. E. Huser, D. Jurgensmeier, J. Walsh, and M. S. Levy, "Is an Anterolateral Ligament Reconstruction Required in ACL-Reconstructed Knees With Associated Injury to the Anterolateral Structures? A Robotic Analysis of Rotational Knee Stability," *American Journal of Sports Medicine*, pp. 1018–1027, 2017.

[38] B. Shiroud Heidari, R. Ruan, E. Vahabli, P. Chen, E. M. De-Juan-Pardo, M. Zheng, and B. Doyle, "Natural, synthetic and commercially-available

biopolymers used to regenerate tendons and ligaments," *Bioactive Materials*, pp. 179–197, 2023.

[39] W. L. Lim, L. L. Liau, M. H. Ng, S. R. Chowdhury, and J. X. Law, "Current Progress in Tendon and Ligament Tissue Engineering," *Tissue Engineering and Regenerative Medicine*, pp. 549–571, 2019.

[40] S. E. Kim, J. G. Kim, and K. Park, "Biomaterials for the Treatment of Tendon Injury," *Tissue Eng. Regen. Med.*, vol. 16, pp. 467–477, Oct. 2019.

[41] Y. J. No, M. Castilho, Y. Ramaswamy, and H. Zreiqat, "Role of Biomaterials and Controlled Architecture on Tendon/Ligament Repair and Regeneration," *Advanced Materials*, pp. 1–16, 2020.

[42] J. Fan, K. Abedi-Dorcheh, A. Sadat Vaziri, F. Kazemi-Aghdam, S. Rafieyan, M. Sohrabinejad, M. Ghorbani, F. Rastegar Adib, Z. Ghasemi, K. Klavins, and V. Jahed, "A Review of Recent Advances in Natural Polymer-Based Scaffolds for Musculoskeletal Tissue Engineering," *Polymers*, p. 2097, 2022.

[43] H. P. Felgueiras, M. D. M. Evans, and V. Migonney, "Contribution of fibronectin and vitronectin to the adhesion and morphology of MC3T3-E1 osteoblastic cells to poly(NaSS) grafted Ti6Al4V," *Acta Biomaterialia*, pp. 1–9, 2015.

[44] V. I. Sikavitsas, G. N. Bancroft, and A. G. Mikos, "Formation of three-dimensional cell/polymer constructs for bone tissue engineering in a spinner flask and a rotating wall vessel bioreactor," *Journal of Biomedical Materials Research: An Official Journal of The Society for Biomaterials, The Japanese Society for Biomaterials, and The Australian Society for Biomaterials and the Korean Society for Biomaterials*, pp. 136–148, 2002.

[45] Z. J. Wally, W. Van Grunsven, F. Claeyssens, R. Goodall, and G. C. Reilly, "Porous titanium for dental implant applications," *Metals*, pp. 1902–1920, 2015.

[46] A. Z. Kharazi, M. H. Fathi, and F. Bahmany, "Design of a textile composite bone plate using 3D-finite element method," *Materials and Design*, pp. 1468–1474, 2010.

[47] S. Ramakrishna, J. Mayer, E. Wintermantel, and K. W. Leong, "Biomedical applications of polymer-composite materials : a review," *Composites Science and Technology*, pp. 1189–1224, 2001.

[48] J. Li, L. Qin, K. Yang, Z. Ma, Y. Wang, L. Cheng, and D. Zhao, "Materials evolution of bone plates for internal fixation of bone fractures: A review," *Journal of Materials Science and Technology*, pp. 190–208, 2020.

[49] J. Malekani, B. Schmutz, and Y. Gu, "Biomaterials in orthopedic bone plates: a review," *Proceedings of the of the Annual International Conference on Materials Science, Metal and Manufacturing*, pp. 71–77, 2011.

[50] Y. Yun, Z. Dong, N. Lee, Y. Liu, D. Xue, X. Guo, J. Kuhlmann, A. Doepke, H. B. Halsall, and W. Heineman, "Revolutionizing biodegradable metals," *Materials Today*, pp. 22–32, 2009.

[51] M. Okamoto, "The role of scaffolds in tissue engineering," 2019.

[52] C. Li, C. Guo, V. Fitzpatrick, A. Ibrahim, M. J. Zwierstra, P. Hanna, A. Lechtig, A. Nazarian, S. J. Lin, and D. L. Kaplan, "Design of biodegradable, implantable devices towards clinical translation," *Nature Reviews Materials*, pp. 61–81, 2020.

[53] A. Tamayol, M. Akbari, N. Annabi, A. Paul, A. Khademhosseini, and D. Juncker, "Fiber-Based Tissue Engineering: Progress, Challenges, and Opportunities," *Biotechnology Advances*, pp. 669–687, 2013.

[54] N. A. Weir, F. J. Buchanan, J. F. Orr, and G. R. Dickson, "Degradation of poly-L-lactide. Part 1 in vitro and in vivo physiological temperature degradation," *Proceedings of the Institution Mechanical Engineers, Part H : Journal of Engineering in Medicine*, pp. 307–319, 2004.

[55] V. Ellä, T. Annala, S. Länsman, M. Nurminen, and M. Kellomäki, "Knitted polylactide 96/4 L/D structures and scaffolds for tissue engineering: shelf life, in vitro and in vivo studies.," *Biomatter*, pp. 102–113, 2011.

[56] A. Larrañaga and E. Lizundia, "A review on the thermomechanical properties and biodegradation behaviour of polyesters," in *European Polymer Journal*, pp. 1–58, 2019.

[57] S. Pina and J. M. Ferreira, "Bioresorbable plates and screws for clinical applications: A review," *Journal of Healthcare Engineering*, pp. 243–260, 2012.

[58] G. Buyle, L. Van der Schueren, J. Beauson, S. Goutianos, G. Schillani, and B. Madsen, "Self-reinforced biobased composites based on high stiffness PLA

yarns," *IOP Conference Series: Materials Science and Engineering*, pp. 1–6, 2018.

[59] O. Avinc and A. Khoddami, "Overview of Poly(lactic acid) (PLA) Fibre: Part I: Production, Properties, Performance, Environmental Impact, and End-use Applications of Poly(lactic acid) Fibres," *Fibre Chemistry*, pp. 455–482, 2009.

[60] G. G. Niederauer and K. A. Athanasiou, "Fabrication and Characterization of PLA-PGA Orthopedic Implants," *Tissue Engineering*, pp. 241–252, 1995.

[61] Z. M. Huang and K. Fujihara, "Stiffness and strength design of composite bone plates," *Composites Science and Technology*, pp. 73–85, 2005.

[62] L. Geddes, L. Carson, E. Themistou, and F. Buchanan, "A comparison of the increased temperature accelerated degradation of Poly( d , l -lactide- co -glycolide) and Poly( l - lactide- co -glycolide)," *Polymer testing*, pp. 1–14, 2020.

[63] Y. Hou, W. Wang, and P. Bartolo, "Investigation of polycaprolactone for bone tissue engineering scaffolds: In vitro degradation and biological studies," *Materials Design*, pp. 1–13.

[64] A. C. Vieira, J. C. Vieira, J. M. Ferra, F. D. Magalhães, R. M. Guedes, and A. T. Marques, "Mechanical study of PLA-PCL fibers during in vitro degradation," *Journal of Mechanical Behavior Biomedical Materials*, pp. 451–460, 2011.

[65] D. Łysik, P. Deptuła, S. Chmielewska, R. Bucki, and J. Mystkowska, "Degradation of Polylactide and Polycaprolactone as a Result of Biofilm Formation Assessed under Experimental Conditions Simulating the Oral Cavity Environment," *Materials (Basel)*, pp. 1–16, 2022.

[66] S. Goutianos, L. Van der Schueren, and J. Beauson, "Failure mechanisms in unidirectional self-reinforced biobased composites based on high stiffness PLA fibres," *Composites Part A*, pp. 169–179, 2019.

[67] B. Azimi, P. Nourpanah, M. Rabiee, and S. Arbab, "Poly ( $\epsilon$ -caprolactone) fiber : An overview," *Journal of Engineered Fibers and fabrics*, pp. 74–90, 2014.

[68] G. Narayanan, V. N. Vernekar, E. L. Kuyinu, and C. T. Laurencin, "Poly (lactic acid)-based biomaterials for orthopaedic regenerative engineering," *Advanced Drug Delivery Reviews*, pp. 247–276, 2016.

[69] R. Agarwal, K. M. Blum, A. Musgrave, E. A. Onwuka, T. Yi, J. W. Reinhardt, C. A. Best, and C. K. Breuer, "Degradation and in vivo evaluation of polycaprolactone, poly($\epsilon$-caprolactone-co-L-lactide), and poly-L-lactic acid as scaffold sealant polymers for murine tissue-engineered vascular grafts," *Regenerative Medicine*, pp. 627–637, 2019.

[70] F. J. v. Natta, J. W. Hill, and W. H. Carothers, "Studies of Polymerization and Ring Formation. XXIII.1 $\epsilon$-Caprolactone and its Polymers," *Journal of the American Chemical Society*, pp. 455–457, 1934.

[71] M. Bartnikowski, T. R. Dargaville, S. Ivanovski, and D. W. Hutmacher, "Degradation mechanisms of polycaprolactone in the context of chemistry, geometry and environment," *Progress in Polymer Science*, pp. 1–20, 2019.

[72] T. Meyhami, S. Hassanajili, N. Tanideh, and E. Taheri, "Three dimensional scaffolds of hybrid PLA/PCL/HA/silica nanocomposites for bone tissue engineering," *Polymer Bulletin*, pp. 1–29, 2023.

[73] S. Gautam, C. Sharma, S. D. Purohit, H. Singh, A. K. Dinda, P. D. Potdar, C.-F. Chou, and N. C. Mishra, "Gelatin-polycaprolactone-nanohydroxyapatite electrospun nanocomposite scaffold for bone tissue engineering," *Materials Science and Engineering: C*, pp. 1–14, 2021.

[74] A. A. Hassan, H. A. Radwan, S. A. Abdelaal, N. S. Al-Radadi, M. K. Ahmed, K. R. Shoueir, and M. A. Hady, "Polycaprolactone based electrospun matrices loaded with Ag/hydroxyapatite as wound dressings: Morphology, cell adhesion, and antibacterial activity," *International Journal of Pharmaceutics*, pp. 1–14, 2021.

[75] S. E. El-Habashy, H. M. Eltaher, A. Gaballah, E. I. Zaki, R. A. Mehanna, and A. H. El-Kamel, "Hybrid bioactive hydroxyapatite/polycaprolactone nanoparticles for enhanced osteogenesis," *Materials Science and Engineering: C*, pp. 1–16, 2021.

[76] E. Åkerlund, A. Diez-Escudero, A. Grzeszczak, and C. Persson, "The Effect of PCL Addition on 3D-Printable PLA/HA Composite Filaments for the Treatment of Bone Defects," *Polymers*, pp. 1–17, 2022.

[77] A. Kumar, S. M. Mir, I. Aldulijan, A. Mahajan, A. Anwar, C. H. Leon, A. Terracciano, X. Zhao, T.-L. Su, D. M. Kalyon, S. G. Kumbar, and X. Yu, "Load-bearing biodegradable PCL-PGA-beta TCP scaffolds for bone tissue regeneration," *Journal of Biomedical Materials Research Part B*, pp. 193–200, 2021.

[78] M. Fadaie, E. Mirzaei, B. Geramizadeh, and Z. Asvar, "Incorporation of nanofibrillated chitosan into electrospun PCL nanofibers makes scaffolds with enhanced mechanical and biological properties," *Carbohydrate Polymers*, pp. 628–640, 2018.

[79] Q. Yao, J. G. L. Cosme, T. Xu, J. M. Miszuk, P. H. S. Picciani, H. Fong, and H. Sun, "Three dimensional electrospun PCL/PLA blend nanofibrous scaffolds with significantly improved stem cells osteogenic differentiation and cranial bone formation," *Biomaterials*, pp. 115–127, 2017.

[80] M. E. Alemán-Domínguez, E. Giusto, Z. Ortega, M. Tamaddon, A. N. Benítez, and C. Liu, "Three-dimensional printed polycaprolactone-microcrystalline cellulose scaffolds," *Journal Biomedical Materials Resesearch Part B*, pp. 521–528, 2019.

[81] F. Alam, P. Verma, W. Mohammad, J. Teo, K. M. Varadarajan, and S. Kumar, "Architected poly(lactic acid)/poly($\epsilon$-caprolactone)/halloysite nanotube composite scaffolds enabled by 3D printing for biomedical applications," *Journal Material Science*, pp. 14070–14083, 2021.

[82] N. Svensson, R. Shishoo, and M. Gilchrist, "Manufacturing of Thermoplastic Composites from Commingled Yarns-A Review," *Journal of Thermoplastic Composite Materials*, pp. 22–56, 1998.

[83] R. Alagirusamy, "Hybrid yarns for thermoplastic composites," in *Technical Textile Yarns*, pp. 387–428, Buckingham, England, UK: Woodhead Publishing, 2010.

[84] N. V and B. Kandasubramanian, "Advanced polymeric composites via commingling for critical engineering applications," *Polymer Testing*, pp. 1–14, 2020.

[85] B. P. Chan and K. W. Leong, "Scaffolding in tissue engineering: General approaches and tissue-specific considerations," 2008.

[86] M. Kellomäki, K. Laine, V. Ellä, and T. Annala, *4 - Bioabsorbable fabrics for musculoskeletal scaffolds*, pp. 67–90. Woodhead Publishing Series in Biomaterials, Woodhead Publishing, 2015.

[87] L. Magnan, G. Labrunie, M. Fénelon, N. Dusserre, M.-P. Foulc, and M. Lafourcade, "Human Textiles: a cell-synthesized yarn as a truly "bio" material for tissue engineering applications.," *Acta biomaterialia*, pp. 111–120.

[88] S. D. McCullen, C. M. Haslauer, and E. Loboa, "Fiber-reinforced scaffolds for tissue engineering and regenerative medicine: use of traditional textile substrates to nanofibrous arrays," *Journal of Materials Chemistry*, pp. 3776–8788, 2010.

[89] A. Doersam, O. Tsigkou, and C. Jones, "A Review: Textile Technologies for Single and Multi-Layer Tubular Soft Tissue Engineering," *Advanced Materials Technologies*, pp. 1–28, 2022.

[90] B. A.-G. Bolagh, S. M. Mithieux, M. A. Hiob, Y. Wang, A. Chong, and A. S. Weiss, "Fabricated Tropoelastin-Silk Yarns and Woven Textiles for Diverse Tissue Engineering Applications," *Acta biomaterialia*, pp. 112–122, 2019.

[91] Y. Urita, H. Komuro, G. Chen, M. Shinya, R. Saihara, and M. Kaneko, "Evaluation of diaphragmatic hernia repair using PLGA mesh–collagen sponge hybrid scaffold: an experimental study in a rat model," *Springer Science*, pp. 1041–1045, 2008.

[92] F. S. Nolte, K. Hnnecke, K. Reimers, R. Schnabel, C. Allmeling, P. Vogt, J. Kuhbier, and U. Mirastschijski, "Biomechanics and Biocompatibility of Woven Spider Silk Meshes During Remodeling in a Rodent Fascia Replacement Model," *Annals of Surgery*, pp. 781–792, 2014.

[93] W. Dai, N. Kawazoe, X. Lin, J. Dong, and G. Chen, "The influence of structural design of PLGA/collagen hybrid scaffolds in cartilage tissue engineering," *Biomaterials Elsevier*, pp. 2141–2152, 2010.

[94] J. A. Cooper, J. S. Sahota, W. J. G. II, J. CArter, S. B. Doty, and C. T. LAurencin, "Biomimetic tissue-engineered anterior cruciate ligament replacement," *Proceedings of the National Academy of Sciences*, pp. 3049—-3054, 2007.

[95] E. Waris, N. Ashammakhi, M. Lehtimäki, R.-M. Tulamo, M. Kellomäki, P. Törmälä, and Y. T. Konttinen, "The use of biodegradable scaffold as an alternative to silicone implant arthroplasty for small joint reconstruction: An experimental study in minipigs," *Biomaterials Elsevier*, pp. 683–691, 2008.

[96] B. Gupta and N. Revagade, "Development and structural evaluation of poly(lactic acid) based knitted scaffold for human urinary bladder reconstruction," *Indian Journal of Fibre & Textile Research*, pp. 115–121, 2009.

[97] W. Xingang, L. Qiyin, H. Xinlei, M. Lie, Y. Huangang, Z. Yurong, S. Huafeng, H. Chunmao, and G. Changyou, "Fabrication and characterization of poly(L-lactide-co-glycolide) knitted mesh-reinforced collagen–chitosan hybrid scaffolds for dermal tissue engineering," *Journal of the mechanical behavior of the biomedical materials*, pp. 204–215, 2012.

[98] G. Matsumuro, N. Isayama, S. Matsuda, K. Taki, Y. Sakamoto, Y. Ikada, and K. Yamazaki, "Long-term results of cell-free biodegradable scaffolds for in situ tissue engineering of pulmonary artery in a canine model," *Biomaterials*, pp. 6422–6428, 2013.

[99] M. Laranjeira, R. M. A. Domingues, R. Costa-Almeida, R. L. Reis, and M. E. Gomes, "3D Mimicry of Native-Tissue-Fiber Architecture Guides Tendon-Derived Cells and Adipose Stem Cells into Artificial Tendon Constructs," *Small*, pp. 1–13, Aug. 2017.

[100] S. Kopf, D. Åkesson, and M. Skrifvars, "Textile fiber production of biopolymers–a review of spinning techniques for polyhydroxyalkanoates in biomedical applications," *Polymer Reviews*, pp. 200–245, 2023.

[101] F. T. Moutos, L. E. Freed, and F. Guilak, "A biomimetic three-dimensional woven composite scaffold for functional tissue engineering of cartilage," *Nature Materials*, pp. 162–167, 2007.

[102] C. K. Abrahamsson, F. Yang, H. Park, J. M. Brunger, P. Valonen, R. Langer, and J. Welter, "Chondrogenesis and mineralization during in vitro culture of

human mesenchymal stem cells on three-dimensional woven scaffolds," *Tissue Engineering: Part A*, pp. 3709–18, 2010.

[103] S. Wu, Y. Wang, P. N. Streubel, and B. Duan, "Living nanofiber yarn-based woven biotextiles for tendon tissue engineering using cell tri-culture and mechanical stimulation," *Acta Biomaterialia*, pp. 102–115, 2017.

[104] W. Jia, *Polylactic Acid Fibre Reinforced Biodegradable Composites*. PhD thesis, The University of Manchester, 2015.

[105] E. Karamuk, J. Mayer, and G. Raeber, "Tissue engineered composite of a woven fabric scaffold with tendon cells, response on mechanical simulation in vitro," *Composites Science and Technology*, pp. 885–891, 2004.

[106] X. Xie, J. Cai, Y. Yao, Y. Chen, A. u. R. Khan, J. Wu, and X. Mo, "A woven scaffold with continuous mineral gradients for tendon-to-bone tissue engineering," *Composites Part B*, pp. 1–12, 2021.

[107] F. Wang, E. Xie, X. Wang, P. Sun, Y. Ji, Y. Niu, D. Wang, F. Li, and J. Wei, "Polyetheretherketone fibers woven fabrics coated nanostructured silicon nitride and load EGCG as artificial ligaments for promoting ligament-bone integration," *Applied Materials Today*, pp. 1–12, 2022.

[108] T. G. Lang, D. Nuß, T. Gereke, G. Hoffmann, M. Wöltje, D. Aibibu, and C. Cherif, "Simulation-Based Development of Gradient Woven Fabrics for Biomimetic Implants to Restore Tendons and Ligaments," *Textiles*, pp. 336–348, 2022.

[109] L. Savić, E. M. Augustyniak, A. Kastensson, S. Snelling, R. E. Abhari, M. Baldwin, A. Price, W. Jackson, A. Carr, and P.-A. Mouthuy, "Early development of a polycaprolactone electrospun augment for anterior cruciate ligament reconstruction," *Materials Science and Engineering: C*, pp. 1–9, 2021.

[110] W. Jia, R. Gong, C. Soutis, and P. Hogg, "Biodegradable fibre reinforced composites composed of polylactic acid and polybutylene succinate," *Plastics, Rubber and Composites*, pp. 82–88, 2014.

[111] N. Wu, Y. Liang, K. Zhang, W. Xu, and L. Chen, "Preparation and bending properties of three dimensional braided single poly (lactic acid) composite," *Composites Part B*, pp. 106–113, 2013.

[112] B. Gareb, C. C. Roossien, N. B. van Bakelen, G. J. Verkerke, A. Vissink, R. R. M. Bos, and B. van Minnen, "Comparison of the mechanical properties of biodegradable and titanium osteosynthesis systems used in oral and maxillofacial surgery," *Scientific Reports*, pp. 1–18, 2020.

[113] J. E. Räihä, P. Axelson, K. Skutnabb, P. Rokkanen, and P. Törmälä, "Fixation of cancellous bone and physeal fractures with biodegradable rods of self-reinforced polylactic acid," *Journal of Small Animal Practice*, pp. 131–138, 1993.

[114] F. Mai, W. Tu, E. Bilotti, and T. Peijs, "Preparation and properties of self-reinforced poly(lactic acid) composites based on oriented tapes," *Composites Part A*, pp. 145–153, 2015.

[115] P. Törmälä, "Ultra-high strength, self-reinforced absorbable polymeric composites for applications in different disciplines of surgery," *Clinical Materials*, pp. 35–40, 1993.

[116] T. A. Turvey, R. B. Bell, T. J. Tejera, and W. R. Proffit, "The use of self-reinforced biodegradable bone plates and screws in orthognathic surgery," *Journal of Oral and Maxillofacial Surgery*, pp. 59–65, 2002.

[117] C. Ferretti, "A prospective trial of poly-L-lactic/polyglycolic acid co-polymer plates and screws for internal fixation of mandibular fractures," *International Journal of Oral and Maxillofacial Surgery*, pp. 242–248, 2008.

[118] L. A. Bregagnolo, P. F. Bertelli, M. C. Ribeiro, C. E. Sverzut, and A. E. Trivellato, "Evaluation of in vitro resistance of titanium and resorbable (poly-L-DL-lactic acid) fixation systems on the mandibular angle fracture," *International Journal of Oral and Maxillofacial Surgery*, pp. 316–321, 2011.

[119] T. Köhler, T. Gries, and G. Seide, "Development of bio-based self-reinforced PLA composites," in *Key Engineering Materials*, pp. 278–284, 2017.

[120] P. Törmäla, T. Pohjonen, and P. Rokkanen, "Ultrahigh-strength self-reinforced polylactide composites and their surgical applications," *Macromolecular Symposia*, pp. 123–131, 1997.

[121] R. Li and D. G. Yao, "Preparation of single poly(lactic acid) composites," *Journal of Applied Polymer Science - J APPL POLYM SCI*, pp. 2909–2916, 2008.

[122] L. Mészáros, B. Tatár, K. Toth, A. Földes, K. S. Nagy, A. Jedlovszky-Hajdu, T. Tóth, and K. Molnár, "Novel, injection molded all-polyethylene composites for potential biomedical implant applications," *Journal of Materials Research and Technology*, pp. 743–755, 2022.

[123] D. D. Wright, E. P. Lautenschlager, and J. L. Gilbert, "Bending and fracture toughness of woven self-reinforced composite poly(methyl methacrylate)," *Journal of Biomedical Materials Research*, pp. 441–453, 1997.

[124] R. Naseem, C. Tzivelekis, M. J. German, P. Gentile, A. M. Ferreira, and K. Dalgarno, "Strategies for Enhancing Polyester-Based Materials for Bone Fixation Applications," *Molecules*, pp. 1–19, 2021.

[125] Y. Fan, X. Miao, C. Hou, J. Wang, J. Lin, and F. Bian, "High tensile performance of PLA fiber-reinforced PCL composite via a synergistic process of strain and crystallization," *Polymer*, pp. 1–14, 2023.

[126] V. Guarino and L. Ambrosio, "The synergic effect of polylactide fiber and calcium phosphate particle reinforcement in poly $\epsilon$-caprolactone-based composite scaffolds," *Acta Biomaterialia*, pp. 1778–1787, 2008.

[127] D. Ju, L. Han, Z. Guo, J. Bian, F. Li, S. Chen, and L. Dong, "Effect of diameter of poly(lactic acid) fiber on the physical properties of poly($\varepsilon$-caprolactone)," *International Journal of Biological Macromolecules*, pp. 49–57, 2015.

[128] T. Tariverdian, F. Sefat, M. Gelinsky, and M. Mozafari, "Scaffold for bone tissue engineering," in *Handbook of Tissue Engineering Scaffolds: Volume One*, pp. 189–209, Buckingham, England, UK: Woodhead Publishing, 2019.

[129] J. C. H. Goh and S. Sahoo, "Scaffolds for tendon and ligament tissue engineering," in *Regenerative Medicine and Biomaterials for the Repair of Connective Tissues*, pp. 452–468, Buckingham, England, UK: Woodhead Publishing, 2010.

[130] SSM, "SSM- Air texturing."

[131] T. Köhler, K. Vonberg, B. Mohr, T. Gries, and G. Seide, "Development of Thermoplastic Composites for Visible Parts in Automotive," *Key Engineering Materials*, vol. 742, pp. 62–69, 2017.

[132] T. Köhler, K. Vonberg, G. Seide, and T. Gries, "New Self-reinforced Polymeric Composites Made of Biobased PLA Commingled Yarns," *3rd International Conference & Exhibiti on Thermoplastic Composites*, pp. 153–156, 2016.

[133] A. Long, ed., *Design and Manufacturing of textile Composites*. Cambridge England: Woodhead Publishing Limited, 2005.

[134] T. Gries, D. Viet, and B. Wulhorst, *Textile Technology An Introduction*. Munich: Hanser Publications, 2nd ed., 2015.

[135] S. Rana and R. Fangueiro, eds., *Advanced Composite Materials for Aerospace Engineering. Processing, Properties and Applications*. Matthew Deans, 2016.

[136] F. C. Campbell, ed., *Manufacturing Process for Advanced Composites*. Oxford, UK: Elsevier Ltd., 2004.

[137] W. Jia, R. H. Gong, and P. J. Hogg, "Poly(lactic-acid) fibre reinforced biodegradable composites," *Composites Part B: Engineering*, vol. 62, pp. 104–112, 2014.

[138] B. P. Van West, R. B. Pipes, and S. G. Advani, "The consolidation of commingled thermoplastic fabrics," *Polymer Composites*, pp. 417–427, 1991.

[139] "ISO/DIS 527-4:" Test conditions for isotropic an orthotropic fibre-reinforced plastic composites"," 2021.

[140] S. Farah, D. G. Anderson, and R. Langer, "Physical and mechanical properties of PLA, and their functions in widespread applications — A comprehensive review," *Advanced Drug Delivery Reviews journal*, pp. 367–392, 2016.

[141] T. Patrício and P. Bártolo, "Thermal stability of PCL/PLA blends produced by physical blending process," *Procedia Engineering*, pp. 292–297, 2013.

[142] "ISO 13934:Textiles — Tensile properties of fabrics," 2013.

[143] P. Väänänen, *Testing of Biodegradable Bone Fixation Implants In Vitro and Clinical Experiments*. PhD thesis, 2009.

[144] D. A. Brennan, A. A. Conte, G. Kanski, S. Turkula, X. Hu, M. T. Kleiner, and V. Beachley, "Mechanical Considerations for Electrospun Nanofibers in Tendon and Ligament Repair," *Advanced Healthcare Materials*, pp. 1–31, 2018.

[145] ASTM International, "F2902- Standard Guide for Assessment of Absorbable Polymeric Implants," tech. rep., 2016.

[146] D. Li and A. Neumann, "Contact angles on hydrophobic solid surfaces and their interpretation," *Journal of Colloid and Interface Science*, pp. 190–200, 1992.

[147] A. Kramschuster and L. S. Turng, *Fabrication of Tissue Engineering Scaffolds*. Elsevier, 2013.

[148] J. C. Middleton and A. J. Tipton, "Synthetic biodegradable polymers as orthopedic devices," *Biomaterials*, pp. 2335–2346, 2000.

[149] M. A. Woodruff and D. W. Hutmacher, "The return of a forgotten polymer - Polycaprolactone in the 21st century," *Progress in Polymer Science*, pp. 1217–1256, 2010.

[150] A. C. Vieira, J. C. Vieira, R. M. Guedes, and A. T. Marques, "Degradation and viscoelastic properties of PLA-PCL, PGA-PCL, PDO and PGA fibres," *Materials Science Forum*, pp. 825–832, 2010.

[151] N. A. Weir, F. J. Buchanan, J. F. Orr, D. F. Farrar, and G. R. Dickson, "Degradation of poly-l-lactide. part 2: Increased temperature accelerated degradation," *Proceedings of the Institution of Mechanical Engineers, Part H: Journal of Engineering in Medicine*, pp. 321–330, 2004.

[152] S. Li, "Hydrolytic degradation characteristics of aliphatic polyesters derived from lactic and glycolic acids," pp. 342–353, 1998.

[153] D. Hukins, A. Mahomed, and S. Kukureka, "Accelerated aging for testing polymeric biomaterials and medical devices," pp. 1270–1274, 2008.

[154] K. Polak-Kraśna, A. R. Abaei, R. N. Shirazi, E. Parle, O. Carroll, W. Ronan, and T. J. Vaughan, "Physical and mechanical degradation behaviour of semi-crystalline plla for bioresorbable stent applications," *Journal of the Mechanical Behavior of Biomedical Materials*, pp. 1–11, 2021.

[155] Y. J. No, M. Castilho, Y. Ramaswamy, and H. Zreiqat, "Role of biomaterials and controlled architecture on tendon/ligament repair and regeneration," *Advanced materials*, vol. 32, pp. 1–16, 2019.

[156] M. Silva, F. N. Ferreira, N. M. Alves, and M. C. Paiva, "Biodegradable polymer nanocomposites for ligament/tendon tissue engineering," *Journal of Nanobiotechnology*, pp. 1–33, 2020.

[157] D. da Silva, M. Kaduri, M. Poley, O. Adir, N. Krinsky, J. Shainsky-Roitman, and A. Schroeder, "Biocompatibility, biodegradation and excretion of polylactic acid (PLA) in medical implants and theranostic systems," *Chemical Engineering Journal*, pp. 9–14, 2018.

[158] Y.-T. Hsieh, S. Nozaki, M. Kido, K. Kamitani, K. Kojio, and A. Takahara, "Crystal polymorphism of polylactide and its composites by X-ray diffraction study," *Polymer Journal*, pp. 755–763, 2020.

[159] R. M. Felfel, K. M. Z. Hossain, A. J. Parsons, C. D. Rudd, and I. Ahmed, "Accelerated in vitro degradation properties of polylactic acid/phosphate glass fibre composites," *Journal Material Science*, pp. 3942–3955, 2015.

[160] C. Fiuza, K. Polak-Kraśna, L. Antonini, L. Petrini, O. Carroll, W. Ronan, and T. J. Vaughan, "An experimental investigation into the physical, thermal and mechanical degradation of a polymeric bioresorbable scaffold," *Journal of the Mechanical Behavior of Biomedical Materials*, pp. 1–14, 2022.

[161] E. Díaz, I. Sandonis, and M. B. Valle, "In Vitro Degradation of Poly(caprolactone)/nHA Composites," *Journal of Nanomaterials*, pp. 427–446, 2014.

[162] G. Yang, B. B. Rothrauff, and R. S. Tuan, "Tendon and ligament regeneration and repair: Clinical relevance and developmental paradigm," *Birth Defects Research Part C*, pp. 203–222, 2013.

[163] S. Hassanajili, A. Karami-Pour, A. Oryan, and T. Talaei-Khozani, "Preparation and characterization of PLA/PCL/HA composite scaffolds using indirect 3D printing for bone tissue engineering," *Materials Science and Engineering: C*, pp. 1–13, 2019.

[164] M. Karamanlıoğlu and Ü. Alkan, "Influence of Time and Room Temperature on Mechanical and Thermal Degradation of Poly(lactic) Acid," *Vinca inst nuclear*, pp. 1–9, 2019.

[165] T. Niemelä, "Effect of $\beta$-tricalcium phosphate addition on the in vitro degradation of self-reinforced poly-l,d-lactide," *Polymer Degradation and Stability*, pp. 492–500, 2005.

[166] K. Webb, V. Hlady, and P. A. Tresco, "Relative importance of surface wettability and charged functional groups on NIH 3T3 fibroblast attachment, spreading, and cytoskeletal organization," *J Biomed Mater Res*, vol. 41, p. 422, Sept. 1998.